LOAN DOCUMENT

DTIC ACCESSION NUMBER

LEVEL

INVENTORY

0

Digital Terrain Modeling And Distributed soil Erosion---

DOCUMENT IDENTIFICATION

Feb 2000

DISTRIBUTION STATEMENT A
Approved for Public Release
Distribution Unlimited

DISTRIBUTION STATEMENT

H
A
N
D
L
E

W
I
T
H

C
A
R
E

ACCESSION FOR

NTIS	GRA&I
DTIC	TRAC
UNANNOUNCED	
JUSTIFICATION	

BY

DISTRIBUTION/

AVAILABILITY CODES

DISTRIBUTION	AVAILABILITY AND/OR SPECIAL

A-1

DISTRIBUTION STAMP

DATE ACCESSIONED

DATE RETURNED

DTIS QUALITY INSPECTED 4

20000720 094

DATE RECEIVED IN DTIC

REGISTERED OR CERTIFIED NUMBER

PHOTOGRAPH THIS SHEET AND RETURN TO DTIC-FDAC

DTIC FORM 70A
JUN 90

DOCUMENT PROCESSING SHEET

PREVIOUS EDITIONS MAY BE USED UNTIL
STOCK IS EXHAUSTED.

LOAN DOCUMENT

THE CENTER
for Ecological Management of Military Lands

S.D. Warren, H. Mitasova, M.R. Jourdan, W.M. Brown,
B.E. Johnson, D.M. Johnston, P.Y. Julien, L. Mitas,
D.K. Molnar and C.C. Watson

Colorado
State

REPORT DOCUMENTATION PAGE

Public reporting burden for this collection of information is estimated to average 1 hour per response, including the time for reviewing instructions, searching existing data sources, gathering and maintaining the data needed, and completing and reviewing this collection of information. Send comments regarding this burden estimate or any other aspect of this collection of information, including suggestions for reducing this burden to Washington Headquarters Services, Directorate for Information Operations and Reports, 1215 Jefferson Davis Highway, Suite 1204, Arlington, VA 22202-4302, and to the Office of Management and Budget, Paperwork Reduction Project (0704-0188), Washington, DC 20503

1. AGENCY USE ONLY (Leave blank)	2. REPORT DATE February 2000	3. REPORT TYPE AND DATES COVERED Final Report	

4. TITLE AND SUBTITLE
Digital Terrain Modeling and Distributed Soil Erosion Simulation/Measurement for Minimizing Environmental Impacts of Military Training (CS-752)

5. FUNDING NUMBERS
N/A

6. AUTHOR(S)
S.D. Warren, H. Mitasova, M.R. Jourdan, W.M. Brown, B.E. Johnson, D.M. Johnston, P.Y. Julien, L. Mitas, D.K. Molnar and C.C. Watson

7. PERFORMING ORGANIZATION NAME(S) AND ADDRESS(ES)

Center for Ecological Management of Military Lands, Department of Forest Sciences, Colorado State University, Fort Collins, CO 80523

8. PERFORMING ORGANIZATION REPORT NUMBER
N/A

9. SPONSORING / MONITORING AGENCY NAME(S) AND ADDRESS(ES)
SERDP
901 North Stuart St. Suite 303
Arlington, VA 22203

10. SPONSORING / MONITORING AGENCY REPORT NUMBER
N/A

11. SUPPLEMENTARY NOTES
No copyright is asserted in the United States under Title 17, U.S. code. The U.S. Government has a royalty-free license to exercise all rights under the copyright claimed herein for Government purposes. All other rights are reserved by the copyright owner.

12a. DISTRIBUTION / AVAILABILITY STATEMENT
Approved for public release: distribution is unlimited.

12b. DISTRIBUTION CODE
A

13. ABSTRACT *(Maximum 200 Words)*

In recognition of the negative repercussions that soil erosion and sediment deposition can have on military preparedness and the environment, the Strategic Environmental Research and Development Program (SERDP) funded a research effort between Fiscal Years 1993 and 1998 to develop geographic information system (GIS) tools and methods to enhance the accuracy, spatial prediction and visual representation of erosion and deposition on military lands. Because of the variability in the quality and availability of data to support erosion/deposition modeling efforts, the project sought to enhance both relatively simple empirical models and more data-intensive process-based models. In addition, the project addressed the demands for long-term average annual estimates of erosion/deposition and single event-based predictions.

14. SUBJECT TERMS
SERDP, SERDP Collection, soil erosion, sediment deposition, The Unit Stream Power Erosion and Deposition (USPED)

15. NUMBER OF PAGES
73

16. PRICE CODE
N/A

17. SECURITY CLASSIFICATION OF REPORT unclass	18. SECURITY CLASSIFICATION OF THIS PAGE unclass	19. SECURITY CLASSIFICATION OF ABSTRACT unclass	20. LIMITATION OF ABSTRACT UL

NSN 7540-01-280-5500

Digital Terrain Modeling and Distributed Soil Erosion Simulation/Measurement for Minimizing Environmental Impacts of Military Training (CS-752)

S.D. Warren[1], H. Mitasova[2], M.R. Jourdan[3], W.M. Brown[2], B.E. Johnson[3], D.M. Johnston[2], P.Y. Julien[4], L. Mitas[2], D.K. Molnar[4] and C.C. Watson[4]

[1]Center for Ecological Management of Military Lands, Colorado State University, Fort Collins, CO 80523
[2]Geographic Modeling and Systems Laboratory, University of Illinois, Urbana, IL 61801
[3]US Army Waterways Experiment Station, Vicksburg, MS 39180
[4]Department of Civil Engineering, Colorado State University, Fort Collins, CO 80523

ABSTRACT

In recognition of the negative repercussions that soil erosion and sediment deposition can have on military preparedness and the environment, the Strategic Environmental Research and Development Program (SERDP) funded a research effort between Fiscal Years 1993 and 1998 to develop geographic information system (GIS) tools and methods to enhance the accuracy, spatial prediction and visual representation of erosion and deposition on military lands. Because of the variability in the quality and availability of data to support erosion/deposition modeling efforts, the project sought to enhance both relatively simple empirical models and more data-intensive process-based models. In addition, the project addressed the demands for long-term average annual estimates of erosion/deposition and single event-based predictions.

The Unit Stream Power Erosion and Deposition (USPED) model was developed as a modification of the Universal Soil Loss Equation (USLE). Whereas the USLE is a 1-dimensional empirical model, the USPED model is 2-dimensional, considering upslope contributing area, as well as profile and tangential curvatures. The spatial patterns of erosion, as predicted by the USPED model, are much more accurate than the traditional USLE, particularly in areas of complex topography. In addition, whereas the USLE predicts only erosion, the USPED model predicts the spatial distribution of sediment deposition. The CASC2D model, originally developed to simulate the volume and distribution of runoff for single rainfall events, was modified to include an upland erosion algorithm. In tests at the Goodwin Creek watershed in Mississippi and the Henson Creek watershed at Fort Hood, Texas, the CASC2D-SED model produced remarkably accurate runoff hydrographs. Predictions of sediment discharge were less accurate, but fell within a reasonable range (-50% to +200%). The process-based SIMulated Water Erosion (SIMWE) model was developed as a multi-dimensional alternative to the Water Erosion Prediction Project (WEPP) model developed by the US Agricultural Research Service. It borrows from the detachment/transport theory of the WEPP model, but solves the underlying continuity equations by Green's function Monte Carlo methods to provide the robustness necessary for spatially variable conditions and high resolutions. It is a landscape scale bivariate model of erosion and deposition by overland flow designed for spatially complex terrain, soil and cover conditions.

EXECUTIVE SUMMARY

Soil erosion and the consequent siltation of waterways have long been major environmental concerns on military installations. In recognition of the negative repercussions that soil erosion and deposition have on military preparedness and the environment, the Strategic Environmental Research and Development Program (SERDP) funded this project from Fiscal Year 1993 to Fiscal Year 1998 to develop geographic information system (GIS) tools and methods to enhance the accuracy of soil erosion and deposition modeling on military lands and to facilitate improved visual representation of model results. The models developed and enhanced during this effort provide significantly improved capability to estimate erosion/deposition potential as an input for choosing optimal land use management and rehabilitation programs. More accurate modeling of erosion and deposition assists land managers and trainers in optimizing the training schedules, delineating training areas, and monitoring changes over time. The models also assist in maximizing availability of military lands with minimal impact to natural resources, especially to soil and vegetation. The overall net result of this research is improved ability to manage military lands and reduce land maintenance costs.

To achieve maximum effectiveness in large areas of complex terrain, integration of erosion and deposition models with GIS is essential. Often, high resolution digital elevation models (DEMs) required by erosion/deposition models must be interpolated from coarser resolution DEMs, scattered point data, or topographic contours. For this project, a method of interpolation by regularized spline with tension was enhanced for the purpose of deriving high resolution DEMs. The method supports the combination of data from various sources with different accuracies, with the resulting surfaces passing the closest to the most accurate data and allowing deviation from the less accurate data. When compared with other methods of interpolation, the resulting DEM provides a much more accurate representation of the actual terrain.

The Universal Soil Loss Equation (USLE) and its revision (RUSLE) are the most widely accepted erosion models in the world. They are lumped-parameter semi-empirical models developed to predict long-term average annual soil erosion on agricultural fields. The models account for topography by the use of a parameter that incorporates only slope length and steepness. Such a simplistic approach cannot account for convergence and divergence of slope or for concavities, convexities and other irregularities that affect erosion and deposition processes. With SERDP funding, the topographic parameter of these models was replaced with an analog that incorporates upslope contributing area rather than slope length. With this simple modification, the USLE better reflects the impact of concentrated flow on soil erosion. Further enhancement of the USLE resulted in the Unit Stream Power Erosion and Deposition (USPED) model which is applicable to complex slope geometries. The USPED model is most appropriately applied in situations where soil erosion is limited only by the ability of runoff to transport sediment, whereas the USLE model is best applied where erosion is limited by the ability of runoff to detach soil particles. The USPED model accurately predicts greater erosion on slope shoulders than on downslope positions. Furthermore, by measuring the change in sediment transport capacity across a GIS grid cell, it also predicts sediment deposition.

CASC2D is a 2-dimensional, physically based rainfall-runoff model that simulates spatially variable surface runoff for individual rainfall events. As a result of SERDP funding, the model was applied to simulate watershed responses to military training scenarios. In addition, an upland erosion algorithm (CASC2D-SED) was added to the model by merging the physically based CASC2D model with the empirical USLE model. In tests at the Goodwin Creek watershed in Mississippi and the Henson Creek watershed at Fort Hood, Texas, the CASC2D-SED model produced remarkably accurate runoff hydrographs. Predictions of sediment discharge were less accurate, but fell within a reasonable range (-50% to +200%).

Over the past decade, several process-based models have been developed with the hope of completely replacing the older empirical models. While these models incorporate the impact of soil, cover and manage-

ment practices in great detail, the description of topography is overly simplified. To overcome these short-comings, the SIMulated Water Erosion (SIMWE) model was developed with SERDP funding. The SIMWE model is based on the solution of the continuity equation which describes the flow of sediment over the landscape, depending on a steady state water flow, detachment and transport capacities, and properties of soil and cover. It is a landscape scale, bivariate model of erosion and deposition by overland flow designed for spatially complex terrain, soil and cover conditions. The underlying continuity equations are solved by Green's function Monte Carlo methods to provide the robustness necessary for spatially variable conditions and high resolutions. Tests show that soil erosion and deposition estimates provided by the SIMWE model were spatially and quantitatively accurate. In addition, investigations conducted to determine if the SIMWE model can be used to predict the consequences of common erosion and sediment control practices were promising.

In conjunction with the development and enhancement of the erosion and deposition models, numerous GIS tools were developed and implemented to assist in the visualization of the model results.

TABLE OF CONTENTS

LIST OF TABLES

LIST OF FIGURES

1. INTRODUCTION

1.1 Background

Soil erosion and the consequent siltation of waterways have long been major environmental concerns on military installations. Accelerated soil erosion results from and ultimately jeopardizes military training and testing. Among the research and development priorities for Department of Defense lands, abatement of soil erosion ranks second only to threatened and endangered species concerns (Andrulis Research Corporation 1994). It has been variously estimated that the cost to restore damaged Army lands to tolerable levels of soil erosion could range from $100M to $200M per year for up to a decade. Annual maintenance costs to keep soil erosion at an acceptable level have been estimated around $40M using existing technology. In an era of declining budgets, the Department of Defense simply cannot afford such expenditures. It is paramount that more cost-effective measures be developed to plan and implement erosion control.

Numerous erosion and sediment control technologies are readily available to military installations. These include revegetation, construction of earthen features such as sediment retention ponds and terraces, and the use of a wide variety of commercially available erosion control products. Unfortunately, it is not always clear which techniques to use, where they should be placed, what size they should be, or when the optimal time occurs for implementation. As a result, projects are often over- or under-engineered. In addition, land managers often address the symptoms of a problem (*e.g.*, an area of intensive erosion) while failing to consider the ultimate source of the problem (*e.g.*, the source of excessive runoff). Cost-effectiveness of land reclamation practices can be maximized as we better understand and model landscape processes that affect soil erosion. With adequate understanding and modeling capability, it is possible to intervene at the appropriate times and places and with the appropriate techniques to achieve maximum benefit with the least expenditure of human energy and financial resources.

Until recently, most approaches to erosion and sediment modeling relied on lumped-parameter semi-empirical relationships developed for agricultural lands. The most widely accepted and used model is the Universal Soil Loss Equation (USLE) (Wischmeier and Smith 1978) and its Revised form (RUSLE) (Renard *et al.* 1997). These equations estimate long-term average annual soil loss as the product of factors representing rainfall erosivity, inherent soil erodibility, the length and steepness of slope, plant cover and conservation support practices. While these models are helpful in predicting average annual soil erosion over relatively homogenous parcels of land, they provide little insight into the landscape processes governing soil erosion, and they are incapable of accurately predicting erosion on complex terrain. In addition, they cannot predict the extent or spatial distribution of sediment deposition.

Over the last decade, there has been a move to replace the empirical models with more complex process-based models such as the Water Erosion Prediction Project (WEPP) (Flanagan and Nearing 1995). While still developmental and not widely accepted, these models have improved the understanding of erosional processes and provide the basis for dramatic improvements in the accuracy of erosion and sediment modeling.

A major drawback of existing empirical and process-based models has been the 1-dimensional approach used to derive them. Landscapes have generally been assumed to be homogenous, planar features. Average erosion rates have been determined and assigned to entire hillslopes and watersheds, thus providing no information regarding the sources and sinks of eroded materials. Alternatively, complex landscapes have been computationally divided into a series of semi-homogenous planes, and erosion has been calculated for each plane. Neither approach provides adequate spatially distributed information on erosion and deposition to

effectively optimize erosion control efforts. Only through integration with a geographic information system (GIS) is it possible to model erosion, sediment transport and sediment deposition in an environment that can account for heterogenous landscapes, *i.e.*, convergence, divergence, concavity and convexity of slopes, variable land uses and conditions, heterogenous soil types, etc.

Geographic information systems represent variability in terrain with digital elevation models (DEMs), where elevation is recorded for each pixel or grid cell in a map. DEMs are generally derived from scattered elevation data or topographic maps. Interpolation of elevation data from known points to all pixels in a map is generally required. While numerous methods are available, some are more accurate than others. Given the importance of topography in erosion modeling, the best possible method of interpolation should be used.

With an adequate DEM, various aspects of the hydrologic cycle can be modeled. These include rainfall infiltration, runoff, soil detachment, sediment transport and sediment deposition. Military land managers are required to make a variety of decisions related to short- and long-term planning of military training and testing operations, and the need for, timing and placement of land reclamation activities. The most appropriate hydrologic model for one application may be unsuitable or overkill for another application. Therefore, a variety of models should be available to meet the various data requirements. In addition, there is a great need to develop the capability within these models to predict the hydrologic consequences of various land reclamation practices.

The phrase "a picture is worth a thousand words" holds true for hydrologic models. No amount of text or numerical output can replace the value of a picture that illustrates the spatial distribution of erosion and deposition. Such depictions, as well as 3-dimensional visualization of soil profiles, watershed cross-sections, etc. can be invaluable for planning and placing erosion and sediment control projects. While multi-dimensional visualization is common for many applications, it has been problematic in natural resource GIS applications where data at a variety of scales may need to be combined (*e.g.*, terrain surface features are generally mapped at a scale of meters while soil profile features are measured in centimeters).

1.2 Objectives

Given the deficiencies identified in erosion and deposition models, as well as the methodologies to process digital elevation data and graphically represent the spatial and temporal distribution of natural resources data to support erosion/deposition models, the following objectives were established:

1. Develop multivariate spline interpolation methods and topographic analysis tools to support terrain modeling and processing of field data (Section 2).

2. Enhance visualization techniques supporting the design and communication of dynamic erosion and sediment transport model results (Section 3).

3. Based on upslope contributing area and the unit stream power theory, modify the Universal Soil Loss Equation (USLE) to improve prediction of erosion, add prediction of deposition, and allow application of the model in complex topography (Section 4).

4. Add an upland erosion module (CASC2D-SED) to the CASC2D rainfall-runoff model to allow event-based erosion/deposition prediction (Section 5).

5. Develop the SIMulated Water Erosion (SIMWE) model as a multi-dimensional application of the detachment/transport capacity theory approach to erosion and sediment prediction as contained in the Water Erosion Prediction Project (WEPP) (Section 6).

The U.S. Army Corps of Engineers Waterways Experiment Station in Vicksburg, Mississippi was responsible for Objective 4. The remaining objectives were addressed in a collaborative effort between the U.S. Army Corps of Engineers Construction Engineering Laboratory in Champaign, Illinois and the University of Illinois.

1.3 Products

Each of the objectives listed above was completed and the corresponding products were placed in the public domain. In addition to this and other periodic reports to the SERDP office, this project has contributed significantly to the scientific literature. As a result of efforts related to this project, the authors have produced over 40 professional journal articles, book chapters, conference proceedings, professional presentations and trade journal articles. These are listed in Appendix A.

2. DIGITAL LANDSCAPE CHARACTERIZATION AND ANALYSIS

To model soil erosion/deposition using a GIS, an adequate discrete representation of terrain, soil and cover properties, and climatic phenomena must be created in a GIS database. These phenomena are usually measured at irregularly distributed points or digitized from isoline maps. In order to be useful for most erosion/deposition modeling applications, such data need to be converted to raster or grid format through a process of interpolation. This task can be difficult to perform especially for geoscientific data due to a variety of reasons: (1) surfaces are complex, and the complexity is spatially heterogeneous, (2) the spatial distribution of data points is often heterogeneous and inadequate, (3) data sets are often very large, thus creating computational complexity, and (4) data are often noisy.

2.1 Multivariate spline interpolation

Various methods have been developed to solve the problems of interpolation (Mitas and Mitasova 1999), although a general solution giving perfect results for all data sets does not exist. An illustration of the results obtained by various methods available in GIS is given in Figure 1. Significant improvement in the interpolation of digital elevation models and other scattered data has been achieved by new spline interpolation and approximation methods. Spline methods are based on the assumption that the approximation function should pass as closely as possible to the given data points and should be as smooth as possible. These two requirements can be combined into a single condition of minimizing the deviation from the measured points and the smoothness seminorm of the function. The solution to this problem can be expressed as a sum of two components (Talmi and Gilat 1977): a *trend* function and a *radial basis* function with an explicit form that depends on the choice of the smooth seminorm. For our choice of the smooth seminorm (Mitasova and Mitas 1993), the *trend* function is a constant and the general form of the *radial basis* function for a d-variate case (Mitasova *et al.* 1995) includes an incomplete *gamma* function (Abramowitz and Stegun 1964). We call this function Regularized Spline with Tension (RST). For the special 2D case, the radial basis function can be expressed through a logarithmic and exponential integral function (Abramowitz and Stegun, 1964). The explicit form for the function for 3D (volume) and 4D (volume in time) data has been presented by Mitasova and Mitas (1993) and Mitasova *et al.* (1995). The coefficients of the interpolation function are obtained by solving the system of N linear equations, where N is the number of given points.

In addition to high accuracy (Mitasova and Mitas 1993, McCauley and Engel 1995, Rohling *et al.* 1998), the RST has several other useful properties. The generalized tension parameter controls the distance over which a given point influences the resulting surface. For the bivariate (2D) case, tuning the tension can be interpreted as tuning the character of the resulting surface between a membrane and a thin plate. The smoothing parameter can be used to interpolate smooth surfaces from noisy data. This parameter can be spatially variable depending on the noise/accuracy for each data point. The proper choice of smoothing and tension parameters is important for successful interpolation or approximation. By tuning the tension and smoothing it is possible to minimize the overshoots (Mitasova and Mitas 1993), artificial pits, and the banding effect of the elevation values around contour lines as observed for the less general forms of splines such as the thin plate spline or thin plate spline with fixed tension. GIS implementation of this function provides several tools for controlling the quality of resulting DEMs, such as computation of deviations, predictive errors based on ordinary cross-validation procedures, and computation of curvatures useful for detecting artificial waves around contours caused by improperly chosen tension parameters. An optimal smoothing parameter can be found by ordinary or general cross-validation schemes (Wahba 1990, Mitasova *et al.* 1995).
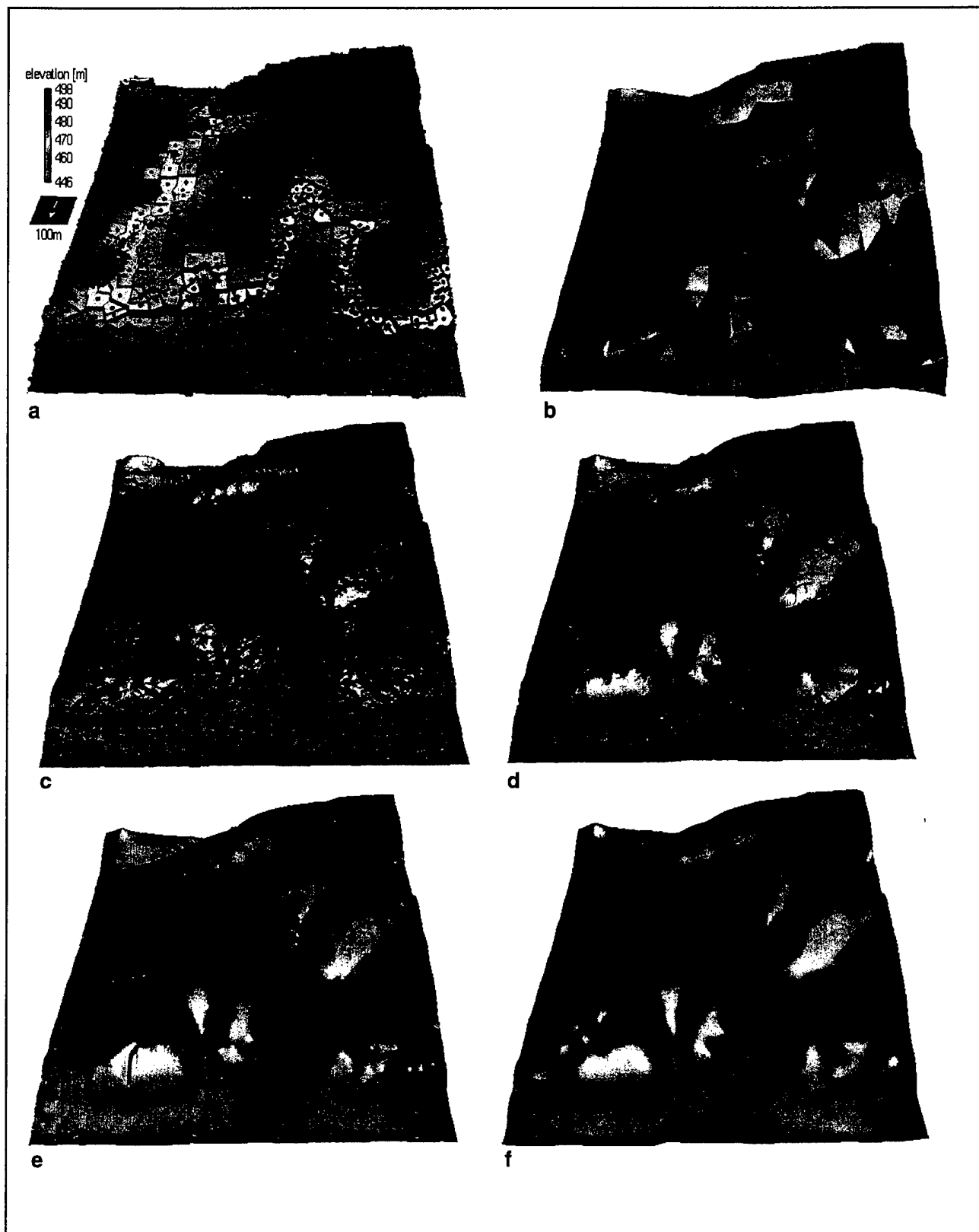
Figure 1. Interpolation of a digital elevation model (DEM) from scattered data points using methods available in geographic information systems (GIS): (a) Voronoi polygons, (b) triangulated irregular network (TIN) based linear interpolation, (c) inverse distance weighting, (d) ordinary kriging, (e) spline with tension and stream reinforcement with ArcInfo TOPOGRID, and (f) regularized spline with tension and smoothing. Data are from the Scheyern Experimental Farm, Germany courtesy of Dr. Karl Auerswald.

Due to the solution of systems of linear equations, the computational demands for the presented method are proportional to N^3 and their application to large data sets becomes problematic. A solution to interpolation of large data sets using an explicit interpolation function was proposed by Franke (1982) and further developed and applied in geosciences by Mitasova and Mitas (1993). The approach is based on the division of a given region into rectangular segments and the computation of an interpolation function for each segment using the data points from this segment and from its neighborhood. Because the method works with equally sized segments, the approach is not very efficient for strongly heterogeneous data like digitized contours or clustered drill hole data. A more effective approach to decomposition of a given region with heterogeneous spatial distribution of data into segments with approximately the same number of points for each segment has been designed with quadtrees (Mitasova *et al.* 1995). The interpolation function is then computed for each segment using the points from this segment and the points located in the window which adjusts its size to the density of points in the neighborhood of each segment. The segmentation is sensitive to tension; for very low tension parameters used in flat areas, the number of points needed for smooth connection of segments can be very large. In certain extreme situations where a flat segment is adjacent to a segment with rapidly changing terrain, additional smoothing may be necessary. To improve the performance of the program for such situations the segmentation procedure was further enhanced by using an automatically adjustable number of data points dependent on the size of each segment.

2.2 Topographic analysis

Topographic parameters needed for erosion modeling include parameters describing the local geometry of the surface, *i.e.*, slope, aspect, curvatures, upslope contributing area, and slope length (Figure 2). RST has been specially designed to meet the demands of topographic analysis. It has continuous derivatives of all orders allowing the use of these derivatives to compute slope, aspect and curvatures simultaneously with interpolation.

2.2.1 Local geometry parameters. Regularized spline with tension (RST) was specially designed to support direct computation of topographic parameters which are functions of first and second order derivatives. Using the partial derivatives of the RST function, *slope* angle is computed as the arctangent of the magnitude of the elevation surface gradient, and *aspect* angle is computed as arctangent of the direction of minus gradient (Mitasova and Hofierka 1993). Computation of *curvatures* is more complicated because, in general, the surface has different curvatures in different directions. A determination of which curvatures are important is dependent on the type of processes under study. For applications in geosciences, curvature in the primary gradient direction (*profile curvature*) is important because it reflects the change in slope angle and thus controls the change of velocity of water flowing down along the slope curve. The curvature in a direction perpendicular to the gradient reflects the change in aspect angle and influences the divergence/convergence of water flow. This curvature is usually measured in the horizontal plane as the curvature of contours and is called plan curvature (Zevenbergen and Thorne 1987, Moore *et al.* 1991). However, for the study of flow divergence/convergence, it is more appropriate to introduce a curvature measured in the normal plane in the direction perpendicular to gradient (Krcho 1991). This curvature is called *tangential curvature* because the direction perpendicular to gradient is, in fact, the direction of a tangent to a contour at a given point. Equations for these curvatures can be derived using the general equation for curvature of a plane section through a point on a surface as described by Mitasova and Hofierka (1993). The positive and negative values of profile and tangential curvature can be combined to define the basic geometric relief forms (Krcho 1991, Dikau 1990). Each form has a different type of flow. Convex and concave forms in the gradient direction have accelerated and decelerated flow, respectively; convex and concave forms in tangential direction have converging and diverging flow, respectively.

2.2.2 Flow-related parameters. Derivation of flow-related parameters, such as upslope contributing area and slope length requires implementation of an effective flow-tracing algorithm. Standard algorithms for flow
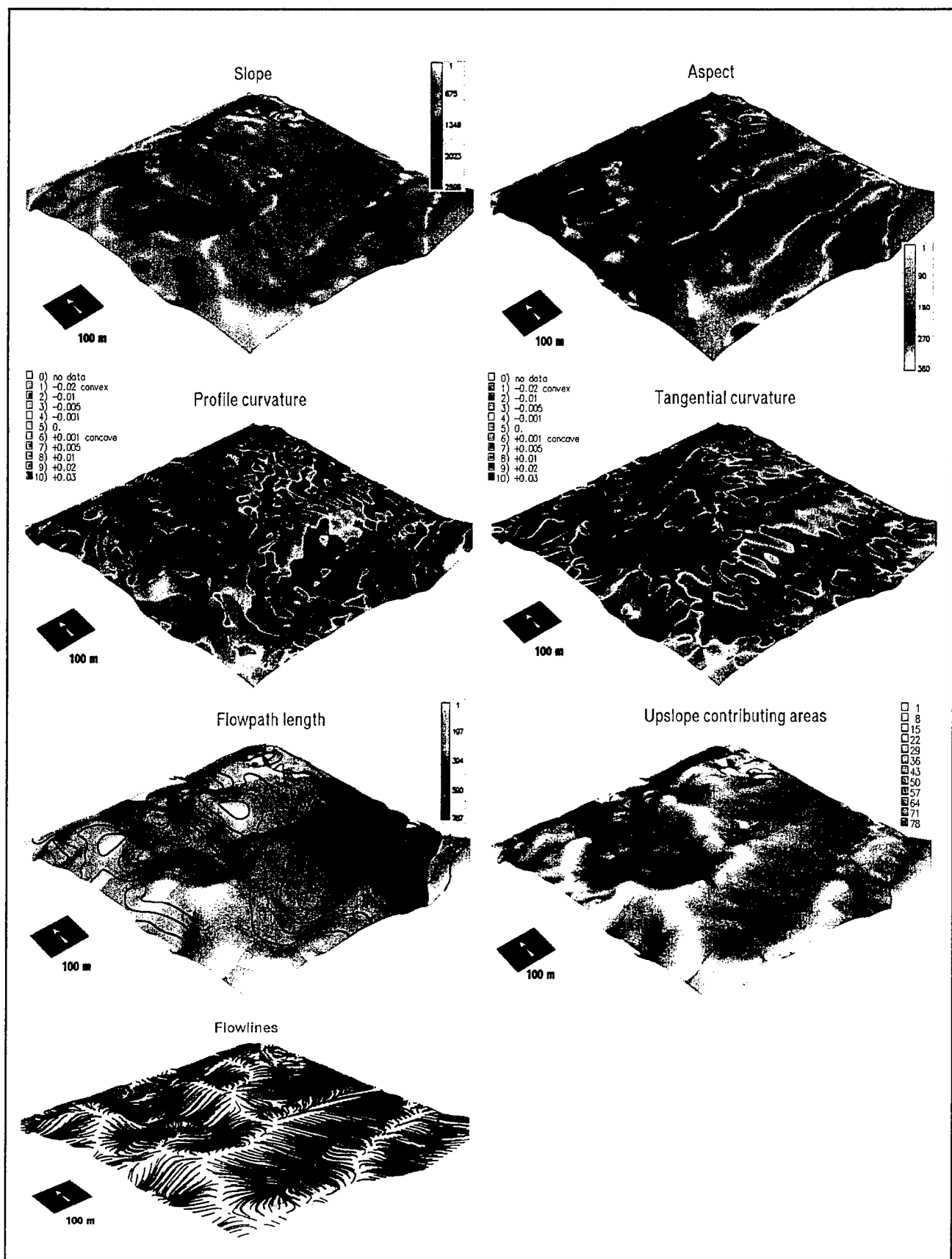
Figure 2. Topographic parameters describing the local geometry (slope, aspect and curvatures) and flow over the terrain surface (flowpath length, upslope contributing area and flowlines).

tracing, which use only a limited number of flow directions (most often 8) from each grid cell, can lead to various unrealistic situations, such as prevailing flow in the direction parallel to x or y axes or diagonals (Fairfield and Leymarie 1991). Several new algorithms for flow tracing help to overcome deficiencies of standard algorithms by using the random eight node approach (Fairfield and Leymarie 1991), multiple nearest neighbor nodes (Freeman 1991), and by using 360 directions of flow with the vector-grid algorithm (Mitasova and Hofierka 1993, Mitasova *et al.* 1996).

2.2.2.1 Flow path length. Flow path length is used in the standard form of USLE/RUSLE and is appropriate for hillslopes with negligible water flow convergence/divergence. For the computation of flow path length, flow lines are generated *uphill* from each grid cell in the gradient direction until they reach a boundary line, singular point, barrier, or a grid cell with the slope lower than the specified minimum. Flow path length for each grid cell is then computed from the coordinates of points of their intersection with grid cells. Uphill flow lines converge on ridgetops.

2.2.2.2 Upslope contributing area. Upslope contributing area is the entire area that contributes runoff into a given grid cell. The upslope contributing area for any given grid cell is computed as the sum of the area comprised by all grid cells which contribute runoff into the cell of concern (Moore *et al.* 1991). This approximation is acceptable if the DEM is interpolated with adequate resolution. Our experience, supported by several recent studies (*e.g.*, Zhang and Montgomery 1994), is that 2 m to 20 m resolution is appropriate for models using upslope contributing areas in regions with complex terrain. For the computation of the number of cells draining into each grid cell, flow lines are constructed *downhill* from each grid cell in the minus gradient direction, until they reach a boundary line, singular point, barrier (*e.g.*, road), or a cell with a slope lower than the specified minimum. An improved algorithm for the construction of flow lines based on vector-grid approach (Mitasova and Hofierka 1993) is used. Flow lines constructed by this algorithm are represented in vector format. The points defining the flow line are computed as the points of intersection of a line constructed in the flow direction given by aspect angle and the grid cell edges. Downhill flow lines merge in valleys and can also be used to define the location of channels (Jenson and Domingue 1988).

2.3 GIS implementation of interpolation and topographic analysis

2.3.1 Geographic Resources Analysis Support System (GRASS). RST for bivariate interpolation was first released with GRASS4.1 as the command *s.surf.tps*. The original program has been completely redesigned and enhanced for the GRASS5.0 produced by Baylor University. The new version of the RST interpolation program was renamed to *s.surf.rst* (Appendix B). The most important enhancements include (1) output of floating point rasters representing elevation, slope, aspect, profile and tangential curvatures as well as first and second order partial derivatives of the modeled surface, (2) output of a site file with deviations in given points, (3) enhanced segmentation including an option to output the quadtree segments, (4) spatially variable smoothing to support the approximation of surfaces from data with heterogeneous accuracy, and (5) easier to modify source code. If a raster DEM is available, local geometry parameters (slope, aspect, curvatures) can be computed in GRASS5.0 with *r.slope.aspect* (Appendix B). The enhancements include support for floating point, computation of curvatures and estimation of partial derivatives. A vector-grid flowtracing algorithm for computation of upslope contributing area, hillslope length and flowlines was implemented as *r.flow* (Appendix B).

2.3.2 ARC/INFO, ArcView. Spatial interpolation can be performed by *TOPOGRID*, which is a different version of thin plate spline with tension, developed by Hutchinson (1989). The DEM derived by *TOPOGRID* should be used with caution for erosion/deposition modeling, because it tends to create waves along contours leading to artificial spatial patterns. Thin plate spline with tension and regularized spline developed by Mitas and Mitasova (1988) are available in ARCGRID and ArcView Spatial Analyst as the *SPLINE* command. These functions do not include smoothing capabilities or topographic analysis. These must be performed

separately after the surface is interpolated, using the functions *SLOPE, ASPECT, CURVATURE* command functions. *FLOWACCUMULATION* and *FLOWLENGTH* are derived using functions based on the D8 algorithm (Jenson and Domingue 1988). This algorithm works well for low resolution data, but at high resolutions it tends to create artificial flow patterns biased towards grid cell diagonals.

3. MULTIDIMENSIONAL DYNAMIC VISUALIZATION

Implementation of landscape process simulation tools within a GIS has stimulated integration of GIS and computer cartography with scientific visualization (Brown and Gerdes 1992, Brown and Astley 1995, Brown *et al.* 1995, Mitasova *et al. 1994*). Scientific visualization is used as both a process of research and discovery and a method of communicating measured or modeled geographic phenomena. As a process of discovery, the visualization process is cyclical in nature, with immediate interactive visualizations feeding a refinement of the model. We have found that effective visualization of intermediate results during model development is vital for confirming modeled phenomena with measured results, and encourages more rigorous testing and evaluation of the model. Combinations of various graphical representations of raster, vector, and point data displayed simultaneously allow researchers to study and query all of their spatial data in 3D space. At the same time, visual analysis of data requires the capability to distort this spatial data by changing vertical scale, separating surfaces, performing simple transformations on point or vector data for scenario development, etc.

Our visualization software tools provide methods and tools for creating dynamic cartographic models representing landscape phenomena and processes. These tools display multiple dynamic surfaces and isosurfaces, together with draped raster, vector and point data in an appropriate projection of 3D space with selectable parameters of the visualization environment.

For interactive viewer positioning, scaling, zooming, etc., we use custom graphical user interface (GUI) widgets and a "fast display mode" where only wire mesh representations of the data are drawn. When rendering a scene, the user may select various preset resolutions for better control over rendering time. For positioning we also chose to use a paradigm of a moving viewer rather than a moving object because we think it is more intuitive when modeling the reality of generally immobile geography. As a result, the user feels as though they are flying around the geographic space, rather than holding it in their hand and rotating it. Horizons are kept level, resulting in less disorientation and fewer unnatural viewing angles. To focus on a particular object, the user simply clicks on the object to set a new center of view.

Initially, tools were implemented on the Silicon Graphics platform using a proprietary graphics library, IRIS GL. While the chosen interface language, Tcl, is publicly available for use on multiple platforms, the underlying graphics routines needed to be converted to OpenGL, a widely available graphic standard. Most of the tools have now been converted to use the OpenGL graphics API. Implementation resulted in the creation of several specialized visualization applications and utilities, a multi-purpose viewer application, several application programmer interface libraries (APIs) (see Appendix B), and enhancements to existing open source software.

GRASS GIS, as an open system with a full range of GIS capabilities, has provided a sound basis for testbed development of visualization tools. Each GRASS data type (raster, vector, and site) plus our own 3D grid format may be used for visualization in a single 3D space. In our implementation, there are four object types and various ways to represent each.

Surfaces. A surface requires at least one raster data set to represent topography and may use other raster data sets to represent attributes of color, transparency, masking, and shininess. These data sets may have been derived from vector (*e.g.,* contour) or scattered point data using tools within the GIS. Users are allowed to use a constant value in the place of any raster data set to produce, for example, a flat surface for reference purposes or a constant color surface.

Vector sets. 3D vector sets are not currently supported, so in order to display 2D vector sets in 3 dimensions, they must be associated with one or more surfaces. The 2D vector sets are then draped over any of these surfaces.

Site Objects. Point data is represented by 3D solid glyphs. Attributes from the database may be used to define the color, size, and shape of the glyphs. 2D site data must be associated with one or more surfaces, and 3D site data may be associated with a surface (*e.g.*, sampling sites measured as depth below terrain).

Volumes. 3D grid data may be represented by isosurfaces or cross sections at user-defined intervals. Color of the isosurfaces may be determined by threshold value or by draping color representing a second 3D grid data set over the isosurfaces. Implementation and initial testing of a 3D grid data file format for managing volumetric spatial data was completed. The storage format and programmer's interface routines we developed allow random access to compressed floating point double precision 3D data with caching. It is fully integrated within the GIS, using the established database hierarchy for header and data files. The resulting library was used to write several utility applications such as *r3.in.ascii, r3.out.ascii, r3.in.grid3, r3.mask, r3.null, r3.info,* and *g3.region*. In addition, a program *r3.mkdspf* reads the 3D grid data and creates a "display" file containing geometry for drawing isosurfaces to represent the data for visualization purposes. Future work will incorporate the 3D grid file and display file formats for use within visualization tools. The specification and design documents for our 3D grid API, and the function prototypes may be found at:

> http://www2.gis.uiuc.edu:2280/modviz/htdoc/g3d/specification.html
> http://www2.gis.uiuc.edu:2280/modviz/htdoc/g3d/protos.html

For visualization purposes, point data is often used to derive an artificial surface or a volume from which isosurfaces may be calculated; for modeling purposes such derived data is used as input for models that work with grids or volumes. When interpolating terrain from point data, it is easy to see undershoots or overshoots by displaying measured sites as spheres and seeing how the interpolated surface passes over, under, or through the spheres. Parameters of the model are then adjusted and the surface is re-interpolated until satisfactory results are obtained. Similarly, a mis-measured point is easy to spot when visualized by 3D position and color. While statistical tools are helpful in analyzing data validity, we find that many erroneous data points that are well within reasonable range and may otherwise be considered valid are easy to detect using spatial-temporal visualization tools.

Qualitative pre-selection of raw data points can help eliminate data with low certainty. We developed tools (*d.siter*, Appendix B) that allow selection and visualization of subsets of data directly within the GIS in the native multi-attribute site format. From data consisting of soil cores we were able to quickly sort out cores with a particular range of particle size at specific depth ranges, or desired color characteristics, helping us to verify soil horizons.

Visualization tools have been improved to allow multiple attributes/dimensions of point data to determine the shape, size, color and orientation of solid 3D markers as well as the 3D position (SG3d Upgrades, Appendix B). Given a value for an attribute of the data at a particular site, visualization is accomplished by mapping the value to one or more characteristics of the marker. In the case of color, three attributes (representing red, green, and blue components) may be used to map a single characteristic, color. For each data attribute, the 3D viewer allows a transformation consisting of an *addvalue* and a *multiplyvalue* which converts the data value to visualization units, preventing duplication of data in the database solely for the purpose of visualization and allowing the researcher to more freely explore visualization combinations.

Variable shape is accomplished by having an "alternative" size field which is used to scale the marker vertically. Plans to allow scaling the marker differently in each dimension according to attributes of the site data will further enhance the variability of shape. Using time stamps representing data measurement times, it is possible to visualize data collection sites and measured values in compressed time, drawing the site markers at intervals proportionally representing the time of measurement, and perhaps using derived data as a background surface. Such methods may highlight, for example, a measurement interval in which instruments

were improperly calibrated, a period of sparse measurement, inadvertent influence due to spatial measurement patterns, or dramatic change that would need to be investigated further. In such cases, much of the dataset may be found to be useful and valid and only the bad data may be discarded, where otherwise the conclusion may have been that the entire dataset was unusable.

Scripting is used to create animations from series of data, automatically loading the data sets and rendering frames for the animation. Animation is useful for representation of change in time, change in a modeling parameter (Ehlschlaeger and Goodchild 1994), change in viewer position (fly-bys) or change in visible data. A keyframe technique is used to generate animations when there is no change in data, *e.g.*, to create fly-bys or show a series of isosurfaces in volumetric data. (Mitasova *et al.* 1994, Brown *et al.* 1995) (Also see nviz Tutorial in Appendix B). Figure 3a shows several frames from an animation where a fence cut is moved through data to better view underlying surface structure. We implemented animation capabilities in both 2D (*xganim*, Figure 3b and Appendix B, *r.out.mpeg*, Appendix B) and 3D (NVIZ, Appendix B) tools.

Producing an animation of the data involves redrawing the scene repeatedly with slightly changing data or viewpoint, saving each resulting image, and then combining them into a movie using multimedia tools. Our scripting mechanism records the actions of the user while also allowing the use of loops. An integrated tool in the GUI provides methods for building the script, including functions such as Open Loop, Close Loop, Open File Sequence Loop, and Close File Sequence Loop, which help in the creation of animations by allowing a sequence of actions to be applied to a sequence of data files. Similarly, a File Sequence Tool allows iteration of data associated with the raster, vector, and site maps for producing the most common type of data visualization animation, where data has been precalculated to represent a timestep or change in modeling parameter and there will be no change in viewer position. This tool also makes it easy to add a somewhat constant dataset such as roads for better spatial reference. For more details on the use of animations for erosion modeling see Mitas *et al.* 1997.

Multiple surfaces have proven useful to visualize boundaries of layers when examining soil core data and soil horizon cross-sections. Achieving intuitive visual representations of these horizons presents a technical challenge in terms of dimensional scale, as demonstrated by Figure 4. The vertical dimension is often quite small relative to the other two (*e.g.*, soil depth of a few meters vs. region dimensions of several kilometers), so is often exaggerated when a single surface is displayed. This exaggeration is usually adequate to add relief to an otherwise featureless surface, but in order to separate close stratified layers, the required exaggeration grossly distorts the modeled layers. If vertical translation of a surface is used to separate surfaces enough that they may be viewed separately, intersections between horizons and relative distances are misrepresented. This is unacceptable since these may actually be the features we are interested in viewing. To study differences between two similar surfaces, we use a scaled difference approach where only the spatial distance between surfaces is exaggerated, maintaining correct surface intersections.

Querying a 2D data set displayed as a raster image can be thought of as a scale operation and a translation operation. When a user clicks on a pixel, the relative position in the image is scaled by the resolution of a pixel and the north and east offsets are added to obtain the geographical position. When displaying surfaces in 3D space with perspective, however, clicking on a pixel on the image of the surface really represents a ray through 3D space. The point being queried is the intersection of this ray with the closest visible and unmasked part of one of the objects in the display. One method for 3D querying provided by some graphics libraries is a "selection" method, where objects are "redrawn" without actually drawing to the screen, and any objects drawn at the query point are returned as the "selected" objects. This method is slow and at best the returned object is a polygon rather than a specific point on the polygon.

When evaluating surfaces made up of relatively large polygons or irregular triangular meshes, the extent of a queried polygon may overlap or encompass several measured points, or the polygon may be textured by points derived from a related dataset consisting of higher resolution data. Therefore a more precise 3D querying mechanism became necessary.
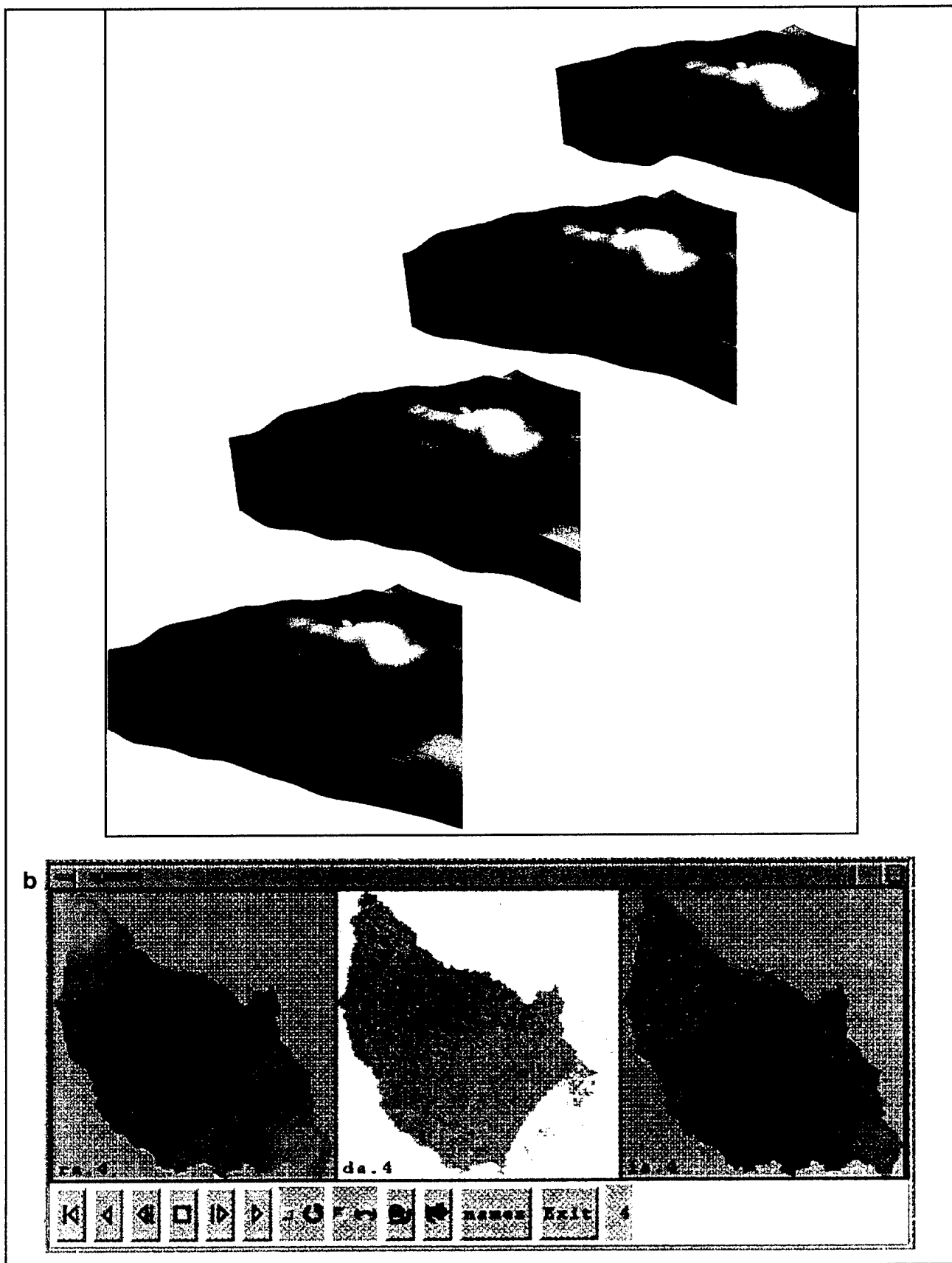
Figure 3. Animation methods: (a) moving a cutting plane through a group of surfaces to examine underlying spatial relationships, and (b) *xganim* application allows up to 4 series of raster data to be animated simultaneously while examining spatial and temporal relationships in the data.
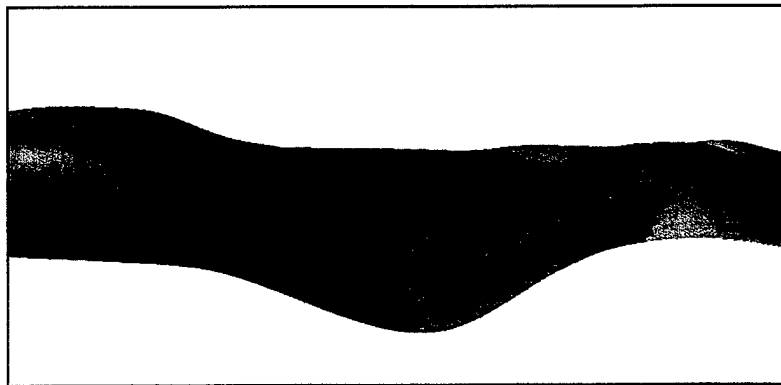
No exaggeration yields little information about spatial differences between surfaces.
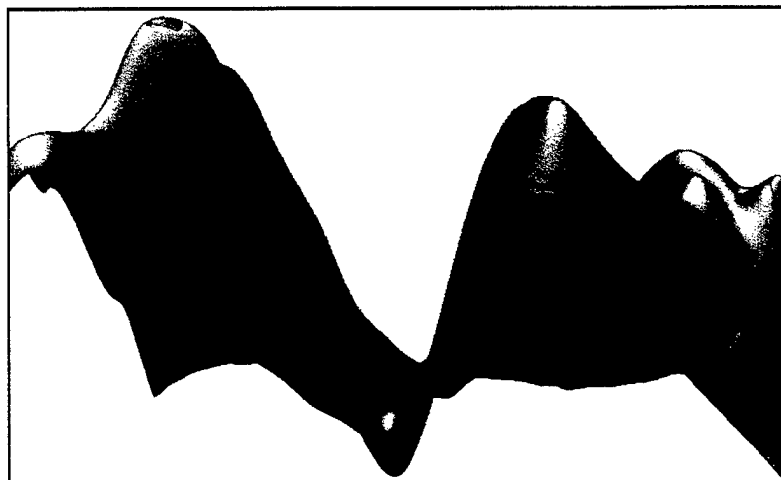
Uniform 10X exaggeration overly distorts surfaces.
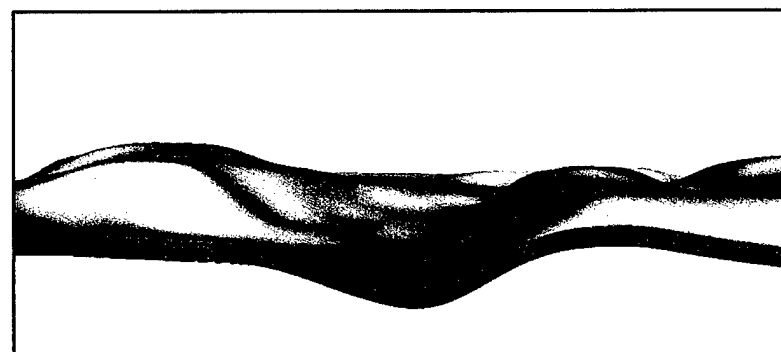
No exaggeration, surfaces separated – surface intersections are lost.
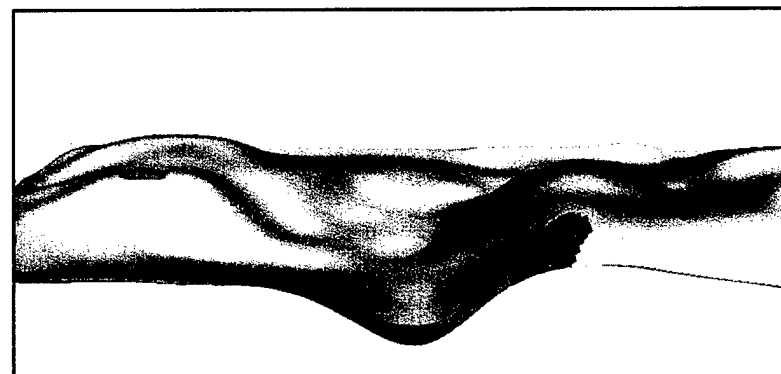
10X exaggeration of difference between surfaces yields better visualization of relative differences.

Figure 4. Visualization of two similar surfaces using the scaled difference approach results in better representation of surface iterations.

To solve the general problem of querying multi-resolution data in 3D space, we require the user to specify the type of data they are querying (surface, point, or vector) and then use our knowledge of the geometry of that data to perform a geometric query in 3D. Figure 5 shows that using cutting planes can allow the user to query a specific location on a surface that is covered by another surface. This specialized point-on-surface algorithm can be outlined as follows: (1) transform point on view plane to a view ray, (2) intersect view ray with convex polyhedron defined by the intersection of the parallelepiped view region with any user defined cutting planes, (3) if ray enters this polyhedron, trace ray to find any intersections with visible and unmasked parts of any surfaces, and (4) choose closest intersection to viewer (or return an ordered list). Such point-on-surface functionality is useful for 3D data querying, setting center of view and setting center of rotation for vector transformations.
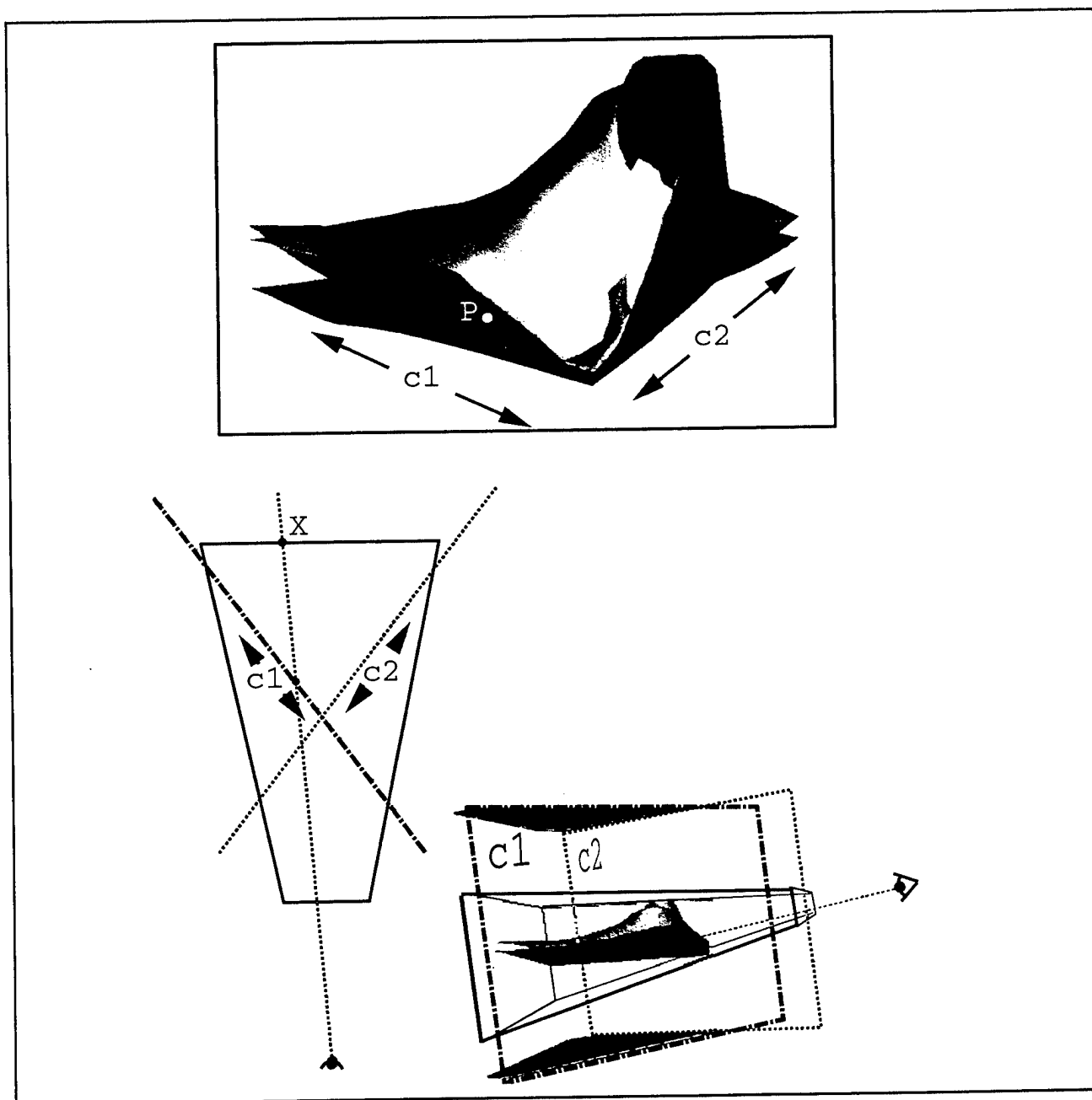
Figure 5. Querying multiple surfaces. A view of surfaces as seen by the user (above). Two cutting planes, c1 and c2, are used to see lower surfaces better. When the user queries the image at point P, the view ray intersects with the visible space enclosed by the convex polyhedron V at points E and X. The resulting line is then traced for intersections with surfaces and the intersection nearest the viewing position is used to query the database.

4. ENHANCEMENTS TO THE UNIVERSAL SOIL LOSS EQUATION

4.1 Enhanced computation of the effects of topography

The Universal Soil Loss Equation is an empirical model designed for the computation of soil erosion in agricultural fields. This equation was developed for fields with negligible curvature and no deposition, and where erosion is limited primarily by the ability of rainfall and runoff to detach soil particles (*i.e.*, detachment limited) as opposed to situations where erosion is determined primarily by the capacity of runoff to transport sediment (*i.e.*, transport limited). The equation has the form

$$E = RKLSCP \tag{1}$$

where average annual soil erosion (E) is computed as the product of factors representing the erosivity of rainfall and runoff (R), inherent soil erodibility (K), slope length and steepness (LS), plant cover (C) and conservation support practices (P) (Wischmeier and Smith 1978, Renard *et al.* 1991). Various modifications of this equation are often applied to the estimation of soil loss using GIS.

The topographic factor for USLE has been recently improved by segmenting irregular slopes to incorporate of the influence of profile convexity/concavity and by improving the empirical equations for the computation of LS factor (Foster and Wischmeier 1974, Desmet and Govers 1996, Renard *et al.* 1991). To incorporate the impact of flow convergence, the slope length factor (L) was replaced by upslope contributing area (Moore and Burch 1996, Desmet and Govers 1996). A modified equation for computation of the LS factor in finite difference form for applications in GIS was derived by Desmet and Govers (1996). A simpler, continuous form of the equation for computation of the LS factor at any given point on a hillslope was developed by Mitasova *et al.* (1996) as part of the SERDP effort. It has the form

$$LS(r) = (m+1) [A(r)/22.13]^m [\sin\beta (r)/0.0896]^n \tag{2}$$

where r represents the point location (x,y), A is the upslope contributing area, β is the slope angle, and m and n are constants. It has been shown that the values of m=0.6 and n=1.3 give results consistent with RUSLE LS factor for the slope lengths <100m and the slope angles <14 deg with negligible tangential curvature (Moore and Wilson 1992).

The impact of replacing the slope length by upslope area is illustrated in Figure 6 which shows that upslope area better reflects the impact of concentrated flow on increased erosion. However, both the USLE and RUSLE consider erosion only along the flow line without the full influence of flow convergence/divergence, and both the standard and modified equations can be properly applied only to areas experiencing net erosion (*e.g.*, Desmet and Govers 1995). Because these equations are incapable of predicting sediment deposition, depositional areas must be excluded from the analysis. Therefore, direct application of USLE/RUSLE to complex terrain within GIS is rather restricted.

4.2 The Unit Stream Power-based Erosion and Deposition (USPED) model

As part of the SERDP effort, the Unit Stream Power-based Erosion and Deposition (USPED) model was developed as a further enhancement to the USLE. It predicts the spatial distribution of erosion and
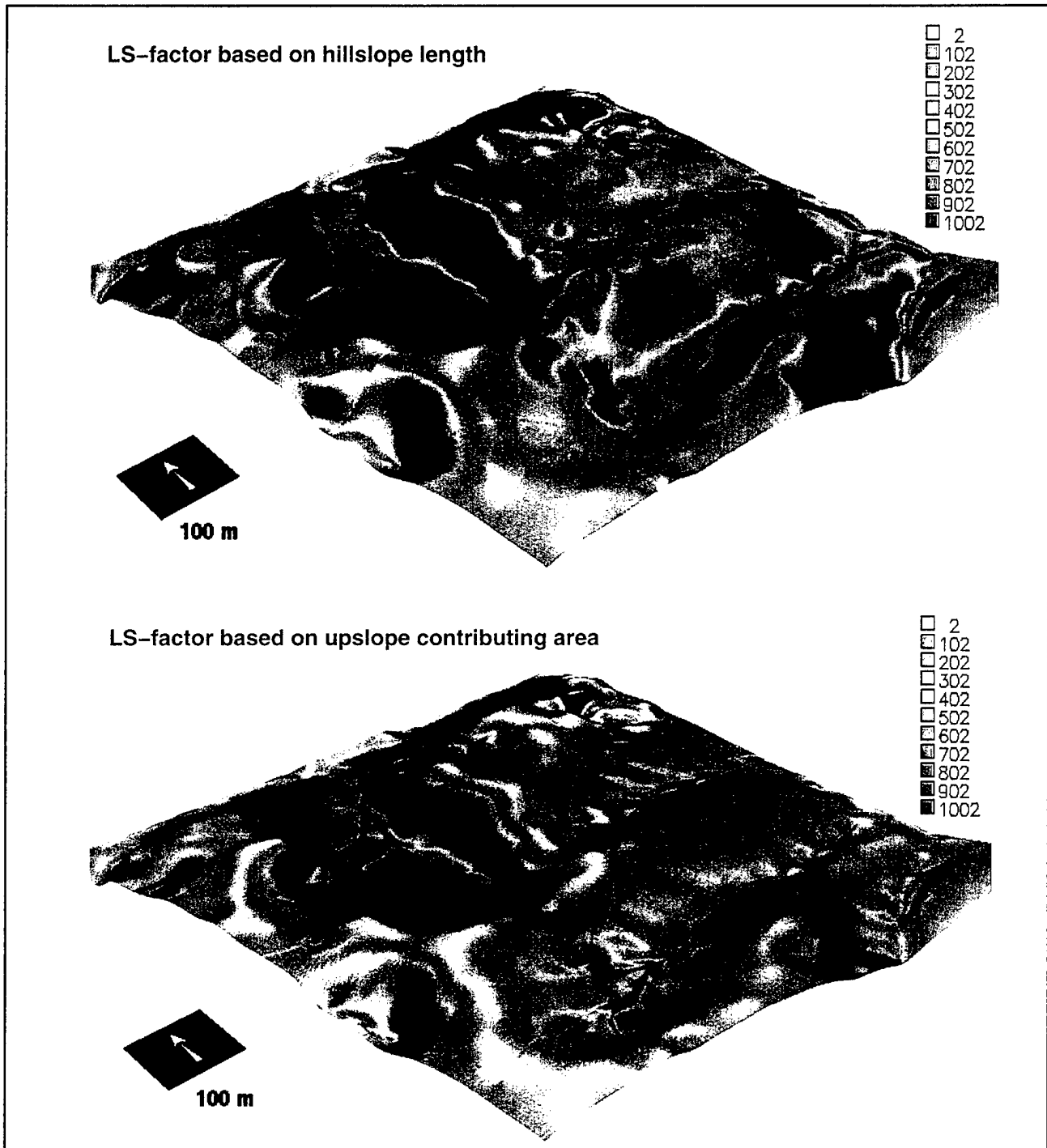
Figure 6. Comparison of LS-factors computed using hillslope length and upslope contributing area.

deposition rates assuming steady state overland flow with uniform rainfall excess conditions. The equation is applicable to situations where erosion is limited by the ability of runoff to transport sediment (*i.e.*, detachment capacity exceeds transport capacity). With this formulation, water flow q(r) and sediment flow $q_s(r)$ are represented by a bivariate vector field q(r), $q_s(r)$. Water flow can be expressed as a function of upslope contributing area (A)

$$|q(r)| = A(r) \ i(r) \qquad (3)$$

where A is the upslope contributing area and *i* is rainfall intensity. The model assumes that critical shear stress is negligible and that the sediment flow rate is equal to sediment transport capacity $T(r)$. Sediment transport

capacity is, in turn, approximated by a power function of slope (r), water flow q(r) and a transportability coefficient K_t(r) which is dependent on soil and cover (Julien and Simons 1985). The equation is computed as

$$|q_s(r)| = T(r) = K_t(r)|q(r)|^m \sin\beta(r)^n \qquad (4)$$

where m, n are constants that depend on the type of flow and soil properties. For situations where rill erosion dominates, these parameters are usually set to $m=1.6$ and $n=1.3$; where sheet erosion prevails, they are set to $m=n=1.0$ (Moore and Wilson 1992, Foster 1994). The transportability coefficient K_t is assumed to be approximately equivalent to the product of the soil erodibility (K), cover (C) and conservation support practice (P) parameters of the USLE; the rainfall coefficient (i^m) is assumed to approximate the rainfall (R) parameter. Hence the equation can be rewritten as

$$T = i^m \, K \, [A^m(\sin\beta)^n] \, CP \qquad (5)$$

where $LS = A^m (\sin\beta^n)$. It is important to note the difference in the computation of LS in this formulation as compared to the modified USLE discussed earlier in this section.

Net erosion/deposition (ED) is estimated as the divergence of the sediment flow

$$ED(r) = \text{div } q_s(r) = KCP\{[\text{grad } h(r) \bullet s(r)] \sin\beta(r) - h(r) [k_p(r) + k_t(r)] \} \qquad (6)$$

where $h(r)$ is water depth, $s(r)$ is the unit vector in the steepest slope direction, $k_p(r)$ is the profile curvature (terrain curvature in the direction of the steepest slope), and $k_t(r)$ is the tangential curvature (curvature in the direction perpendicular to the profile curvature). The topographic parameters $s(r)$, $k_p(r)$, $k_t(r)$ are computed from the first and second order derivatives of terrain surface approximated by the RST (Mitasova and Mitas 1993, Mitasova and Hofierka 1993, Krcho 1991, see also Section 2.1).

The spatial distribution of erosion/deposition is controlled by the change in the overland flow depth (first term) and by the local geometry of terrain (second term), including both profile and tangential curvatures. The local acceleration of flow in both the gradient and tangential directions (related to the profile and tangential curvatures) play equally important roles in spatial distribution of erosion/deposition. The impact of the tangential curvature $k_t(r)$ is therefore twofold. First, $k_t(r)$ influences the water depth $h(r)$ through its control of water flow convergence/divergence, with tangential concavity leading to rapid increase in water depth and an increase in the potential for erosion. Second, $k_t(r)$ causes a local change in sediment flow velocity which for tangential concavity has an opposite effect (reduction in sediment transport), thus creating potential for deposition. The *interplay* between the magnitude of water flow change and both terrain curvatures reflected in the bivariate formulation therefore determines whether erosion or deposition will occur. The bivariate solution provides a sound theoretical explanation for the results of field experiments reported by several authors (*e.g.*, Busacca *et al.* 1993, Quine *et al.* 1994, Sutherland 1991) where the highest erosion was observed on divergent shoulder elements and deposition on convergent footslope elements.

A functionally equivalent but computationally simpler formulation of the equation for net erosion/deposition (ED) is

$$ED = div(T \bullet s) = \frac{d(T \cos a)}{dx} + \frac{d(T \sin a)}{dy} \qquad (7)$$

where a is the aspect or direction of the steepest slope, reported in degrees.

GIS implementation of the USPED equation is rather simple, using the tools developed for this project and implemented in GRASS5.0. A step by step tutorial is available at www2.gis.uiuc.edu:2280/modviz/erosion/usped.html. It is important to note that the algorithms available in ArcView and ArcGrid for interpolation and topographic analysis are less sophisticated that those in GRASS, therefore to obtain acceptable result more attention should be paid to the proper selection of resolution and to the quality of DEM.

5. CASC2D-SED MODEL

The CASC2D model was originally developed as a 2-dimensional (2D) physically based rainfall-runoff model to simulate spatially variable surface runoff from single rainfall events (Julien *et al.* 1995). It is fully integrated with GIS. The model uses the Green and Ampt method to model infiltration, a 2D diffusive wave formulation of the Saint Venant equations for overland flow, and a 1D solution of the diffusive wave formulation for channel flow routing. Outputs include runoff hydrographs and maps of infiltration depth, surface moisture, surface runoff depth, channel runoff depth, and rate of infiltration.

With SERDP funding the CASC2D model was modified to include an upland erosion algorithm. The approach is based on a sediment transport equation developed by Kilinc and Richardson (1973) who experimentally examined soil erosion from overland flow generated by simulated rainfall. They developed a sediment transport equation for sheet and rill erosion for bare sandy soil:

$$q_s = 25500 \, q_o^{2.035} \, S_o^{1.664} \tag{8}$$

where unit sediment discharge (q_s) is calculated in the units of (tons/m s) as a function of runoff discharge (q_o) and bed slope (S_o). This equation was further modified by incorporating parameters from the USLE to accomodate various soil types, vegetation cropping management factors, and conservation practices (Julien *et al.* 1995):

$$q_s = 25500 q_o^{2.035} S_o^{1.664} \frac{K}{0.15} CP \tag{9}$$

The numerical formulation for surface runoff calculations stems from CASC2D (Julien *et al.* 1995). The algorithm for the continuity equation on elements (j,k) is:

$$h^{t+\Delta t}(j,k) = h^t(j,k) + i_e \Delta t - [\frac{q_x^t(k,k+1) - q_x^t(k-1,k)}{W} + \frac{q_y^t(j,j+1) - q_y^t(j-1,j)}{W}]\Delta t \tag{10}$$

where h^t(j,k) and h^{t+t}(j,k) denote flow depths at the element (j,k) at times t and t+ t, respectively; i_e is the average excess rainfall rate over one time step beginning from time t; q^t_x(k,k+1) and q^t_x(k-1,k) describe unit flow rates in the x-direction at time t, from (j,k) to (j,k+1), and from (j,k-1) to (j,k) consecutively; likewise q^t_y(j,j+1), q^t_y(j-1,j) denotes unit flow rates in the y-direction at time t, from (j,k) to (j+1,k), and from (j-1,k) to (j,k) respectively; and W is the grid size.

The momentum equations in the x and y directions are solved using the diffusive wave approximation. In the x-direction, the friction slope for the diffusive wave approximation is computed as:

$$S_{fx}^t(k-1,k) = S_{ox}(k-1,k) - \frac{h^t(j,k) - h^t(j,k-1)}{W} \tag{11}$$

in which the bed slope is given by:

$$S_{ox}(k-1,k) = \frac{E(j,k-1) - E(j,k)}{W}$$ (12)

where E represents the ground surface elevation of the element. Where the friction slope is greater than or equal to zero, the calculated unit discharge and unit sediment discharge for turbulent flow are given by:

$$q_x^t(k-1,k) = \frac{1}{n(j,k-1)}[h^t(j,k-1)]^{\frac{5}{3}}$$ (13)

and

$$q_{sx}^t(k-1,k) = e^{11.727} q_x^t(k-1,k)^{2.035} S_{ox}(k-1,k)^{1.664} \frac{K}{0.15} CP$$ (14)

respectively, where q_x implies unit discharge and q_{sx} implies unit sediment discharge in the x-direction at time t from (j,k-1) to (j,k).

Where the friction slope is less than zero, unit discharge and unit sediment discharge are calculated as:

$$q_x^t(k-1,k) = \frac{-1}{n(j,k)}[h^t(j,k)]^{\frac{5}{3}}$$ (15)

and

$$q_{sx}^t(k-1,k) = -e^{11.727} q_x^t(k-1,k)^{2.035} S_{ox}(k-1,k)^{1.664} \frac{K}{0.15} CP$$ (16)

respectively, thus producing negative values and implying that the flow direction is actually from (j,k) to (j,k-1).

The unit discharge and unit sediment discharge in the y-direction are similarly calculated based on the sign of the friction slope in the y-direction. Once the direction of flow and the unit sediment discharge have been computed, the upland erosion is broken down into three size fractions (sand, silt, and clay) and routed based upon how much sediment is in suspension, previous deposition, and how much sediment has been eroded from the soil surface. In determining how much sediment is transported from the outgoing cell, the model first gives priority to the volume of sediment in suspension, secondly to the volume of sediment in previous deposition, and lastly the remaining volume of sediment, is eroded from the soil surface. In order to determine how much sediment stays in suspension and how much is deposited on the receiving cell, the trap efficiency for each size fraction is computed using:

$$T_{Ei} = 1 - e^{\frac{-X\omega_i}{hV}}$$ (17)

where,

T_{Ei} = trap efficiency for each size fraction

X = longitudinal length

ω_i = fall velocity for each size fraction

h = flow depth

V = flow velocity

The trap efficiency indicates how much sediment deposit is on the receiving cell for each size fraction, thus the remaining volume of sediment $(1-T_{Ei})$ stays in suspension on the receiving cell.

  The CASC2D-SED model routes water and sediment from the upland areas to the watershed outlet. Sediment transport in channels for single storm-events assumes that the change in channel bed elevation and bank erosion processes are small compared to upland erosion processes. The model keeps track of the time changes in the following parameters: rainfall distribution, cumulative infiltration depth, surface runoff depth, suspended sediment volume, sediment flux, and net aggradation/degradation for each pixel.

6. PROCESS-BASED SIMULATION OF WATER EROSION MODEL (SIMWE)

Over the past decade, several process-based models have been developed with the hope of completely replacing the older empirical models. While these models incorporate the impact of soil, cover and management practices in great detail, the description of topography is overly simplified. To overcome these shortcomings, the SIMulated Water Erosion (SIMWE) model was developed with SERDP funding.

6.1 Model formulation

The methodological framework for the simulation of erosion/deposition processes within the SIMWE model (SIMulation of Water Erosion) is based on the description of water flow and sediment transport processes by first principles equations, a concept outlined previously, most often for a one dimensional case (Foster and Meyer 1972, Bennet 1974). Within our approach, inputs and outputs of the simulations are represented by multivariate functions (scalar or vector fields) rather than homogeneous hillslope segments. The underlying continuity equations are solved by a Green's function Monte Carlo method to provide the robustness necessary for spatially variable conditions and high resolutions. Detailed descriptions of equations used in this model are given by Mitas and Mitasova (1998).

Two-dimensional shallow water flow is described by the bivariate form of the Saint Venant equations (Julien *et al.* 1995) where the continuity of water flow relationship is coupled with the momentum conservation equation, and the hydraulic radius is approximated by the normal flow depth. The system of equations is closed using the Manning's relationship. For this effort, we assume that the solution of continuity and momentum equations for a steady state provides an adequate estimate of overland flow for land management applications (Flanagan and Nearing 1995). In addition, we assume that the flow is close to the kinematic wave approximation, but we include a diffusion-like term to include the impact of diffusive wave effects. The incorporation of diffusion in water flow simulation is not new; similar terms have been obtained in derivations of diffusion-advection equations for overland flow (*e.g.*, Lettenmeier and Wood 1992). In our reformulation, we simplify the diffusion coefficient to a constant and we use a modified diffusion term. The diffusion constant that we use is rather small (approximately one order of magnitude smaller than the reciprocal of Manning's coefficient) and therefore the resulting flow is close to the kinematic regime. However, the diffusion term improves the kinematic solution by overcoming small shallow pits common in digital elevation models (DEM) and by smoothing the flow over slope discontinuities or abrupt changes in Manning's coefficient (*e.g.*, due to roads or other anthropogenic changes in elevations or cover).

The basic relationship describing sediment transport by overland flow is the continuity of sediment mass, which relates the change in sediment storage over time, and the change in sediment flow rate along the hillslope to effective sources and sinks (Haan *et al.* 1994, Govindaraju and Kavvas 1991, Foster and Meyer 1972, Bennet 1974). The sediment flow rate is a function of water flow and sediment concentration. For shallow, gradually varied flow, the storage term can be neglected, leading to a steady state form of the continuity equation. The sources/sinks term is derived from the assumption that the erosion and deposition rates $ED(r)$ are proportional to the difference between the sediment transport capacity $T(r)$ and the actual sediment flow rate $|q_s(r)|$ (Foster and Meyer 1972)

$$ED(r) = c(r) \, [T(r) - |q_s(r)|] \tag{18}$$

with the first order reaction term $c(r)$ dependent on soil and cover properties. The $c(r)$ is obtained from the relationship (Foster and Meyer 1972)

$$ED(r)/D_m(r) + |q_s(r)|/T(r) = 1 \qquad (19)$$

which states that the ratio of erosion/deposition rate $ED(r)$ to the detachment capacity $D_m(r)$ plus the ratio of the sediment flow to the sediment transport capacity is a conserved quantity (unity). The sediment transport capacity and detachment capacity represent maximum potential sediment flow rate and maximum potential detachment rate, respectively, and are functions of a shear stress $t(r)$ (Foster and Meyer 1972)

$$t(r) = w\, h\,(r)\, \sin\beta(r) \qquad (20)$$

where w is the hydrostatic pressure of water with the unit height (h). Then the simplified equation for transport capacity is

$$T(r) = K_t(r)\, t(r)^p \qquad (21)$$

where $K_t(r)$ is the effective soil transportability coefficient and p is exponent dependent on the type of flow. Detachment capacity estimated as a function of shear stress can be expressed as

$$D_m(r) = K_d(r)\, [t(r)-t_s(r)]^q \qquad (22)$$

where $K_d(r)$ is the effective erodibility (detachment capacity coefficient), q is an exponent parameter and $t_s(r)$ is the critical shear stress. The parameters and adjustment factors for the estimation of detachment and transport capacity are functions of soil and cover properties. Typical values are being developed for the WEPP model for a wide range of soils, cover, agricultural and erosion prevention practices (Flanagan and Nearing 1995).

To solve the bivariate continuity equation, we introduce a small diffusion term (Mitas and Mitasova 1998) which represents local dispersion processes of the suspended flow (*e.g.*, the impact of small, local slope changes below the DEM resolution)(Bennet 1974). On the left hand side of the equation, the first term describes local diffusion, the second term is a drift driven by the water flow while the third term represents a velocity dependent 'potential' . The size of the diffusion constant is about one order of magnitude smaller than the reciprocal Manning's constant so that the impact of the diffusion term was relatively small.

The equations can be solved by projection methods (Rouhi and Wright 1995). An alternative is to interpret equations as a representations of stochastic processes with diffusion and drift components (Fokker-Planck equations) and then carry out the actual simulation of the underlying process utilizing stochastic methods (Gardiner 1985). This is very similar to Monte Carlo methods in computational fluid dynamics or to quantum Monte Carlo approaches for solving the Schrodinger equation (Hammond *et al.* 1994, Mitas 1996).

The Monte Carlo technique has several unique advantages which are becoming even more important due to new developments in computer technology. Perhaps one of the most significant Monte Carlo properties is robustness which enables us to solve the equations for complex cases, such as discontinuities in the coefficients of differential operators (in our case, abrupt slope or cover changes, etc). Also, rough solutions can be estimated rather quickly, allowing us to carry out preliminary quantitative studies or to rapidly extract qualitative trends by parameter scans. In addition, the stochastic methods are tailored to the new generation of computers (*i.e.*, they provide scalability from a single workstation to large parallel machines due to the independence of sampling points). Therefore, the methods are useful both for everyday exploratory work using a desktop computer and for large cutting-edge applications using high performance computing.

6.2 Model properties

Below we analyze the role of the SIMWE model parameters for complex terrain assuming spatially uniform rainfall excess, soil and cover properties.

The first-order reaction coefficient $c(r)$ is related to the soil detachability and transportability and controls the spatial extent of deposition. There are two limiting cases of erosion and sediment transport, ie., detachment limited and sediment transport capacity limited (Foster and Meyer 1972, Hairsine and Rose 1992). The first case occurs when $c(r)$ approaches 0, resulting in the net erosion being approximately equal to the detachment capacity. Therefore, for conditions when $c(r)<<1$, detachment limited erosion prevails. In this situation, almost all detached sediment is transported to the stream and deposition is restricted to small concave areas and channels. This case for a 1D hillslope is modeled by the Universal Soil Loss Equation (USLE). For the second limiting case represented by $c(r) > 1$, sediment flow approximates sediment transport capacity. In this case, net erosion/deposition is modeled as a divergence of the sediment transport flow, and the model predicts large areas with deposition. Such a behavior is close to the observed distribution of colluvial deposits, suggesting the prevailing influence of the transport capacity limited case on long term patterns of deposition. This case is modeled by the USPED model (Mitasova *et al.* 1996). Simulations in which the $c(r)$ values increase from 0.01 (fine soils) to 10.0 (sandy soils), assuming a rough cover (grass) with n=0.1, illustrate that c(r) has a dramatic effect on the spatial distribution of erosion and deposition over the landscape (Mitas and Mitasova 1998). As c(r) increases, depositional areas expand while the sediment flow rate in the streams decreases until the pattern typical for a transport capacity limiting case is reached. Because the $c(r)$ is dependent on the ratio between detachment capacity and sediment transport capacity, both erodibility and transportability coefficients influence the spatial extent of deposition. However, as we demonstrate in the next section, each of these coefficients has a different impact on the sediment loads in streams.

Erodibility, represented by the detachment capacity coefficient $K_d(r)$, is a measure of the susceptibility of soil to detachment by water flow (Flanagan and Nearing 1995). It is often defined as the increase in soil detachment per unit increase in shear stress of clear water flow. A change in the erodibility factor, while keeping the other parameters constant, changes the ratio between transport capacity and detachment capacity. This leads to the change in the character of erosion process. Detachment capacity limited erosion occurs when erodibility is significantly lower than transportability; transport capacity limited erosion occurs when erodibility is greater than transportability. Therefore, a change in erodibility will change the spatial pattern of erosion and deposition (Figure 7a-c). However, changes in erodibility have minimal impact on the amount of sediment load in the stream. This illustrates the problems associated with the use of in-stream sediment loads for making land management decisions.

Transportability, represented by the transport capacity coefficient $K_t(r)$, is a measure of the likelihood that soil particles will be transported by water flow. It depends on soil properties, but can be also influenced by vegetation. This coefficient is not directly measured and provided in the WEPP; rather it is estimated indirectly, making the proper determination of this parameter problematic. However, the parameter can be derived at least for some types of soils using the published values of first order reaction coefficient or using the procedure suggested by Finkner *et al.* (1989). Our simulations show that this parameter has a profound impact on the erosion process as it influences both spatial distribution and magnitude of sediment flow and erosion/deposition rates. Recently, the importance of transport capacity for overland flow erosion processes has been fully recognized and more experimental and theoretical work is being performed (Guy *et al.* 1991, Govers 1991, Nearing *et al.* 1997). Figures 8(a-c) 9illustrates how the change in transportability changes the erosion regime from detachment capacity limited to transport capacity limited while also reducing the magnitude of erosion rates.

Surface roughness is represented by the Manning's $n(r)$. It has a significant impact on the location and magnitude of deposition. For the same value of $c = 1.0$, the extent of deposition for smooth surfaces (bare soil with $n=0.01$) is smaller than for rough surfaces (grass with $n=0.1$). This also assumes an increase in detachability and transportability for bare soil as compared to grass.
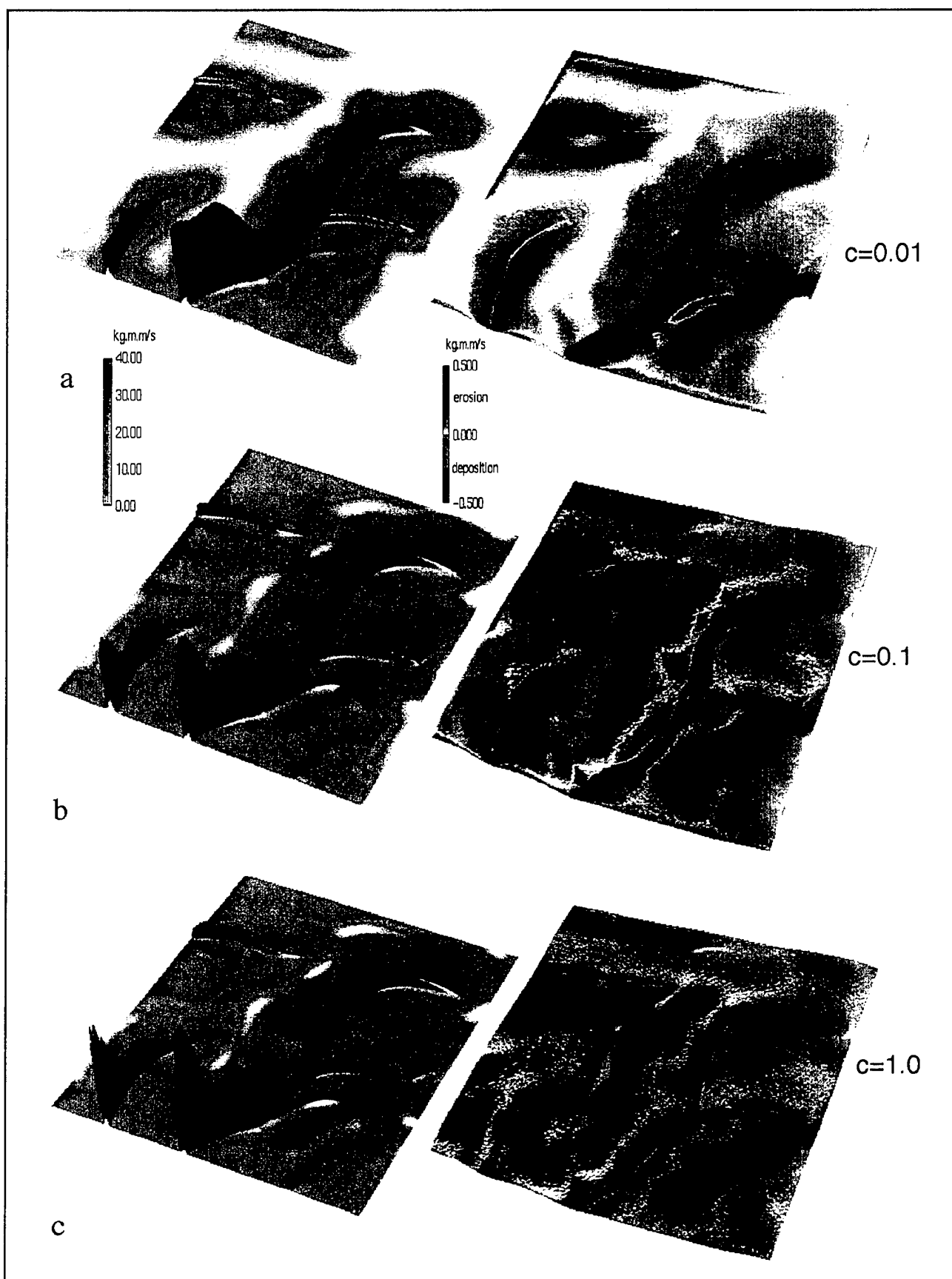
Figure 7. Changes in sediment flux (left) and erosion/deposition (right) as a result of a change in erodibility (K_d) when transportability (K_t) is held constant at 0.3 [(a) K_d=0.003, c=0.01; (b) K_d=0.03, c=0.1; (c) K_d=0.3, c=1.0].
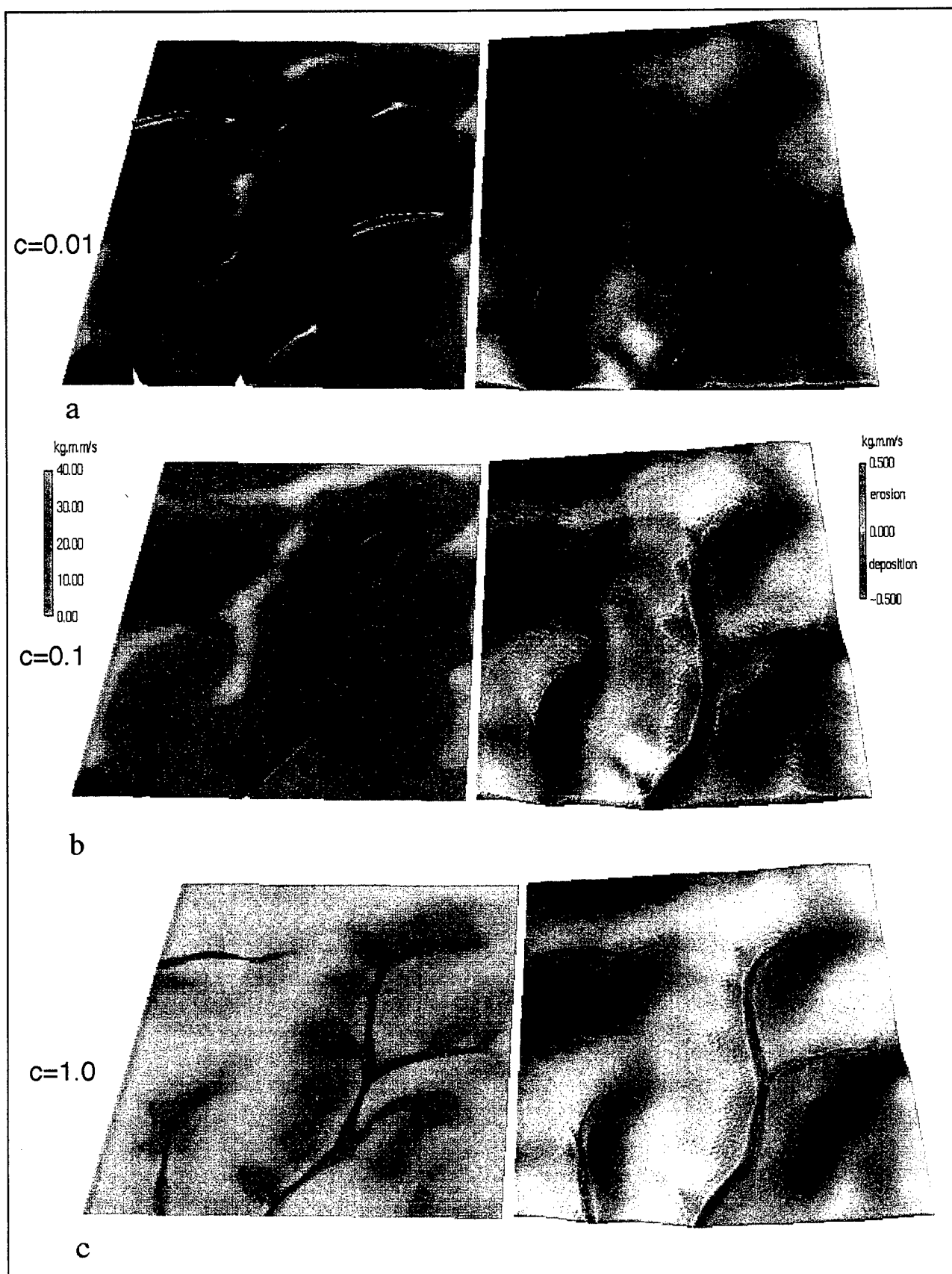
Figure 8. Changes in sediment flux (left) and erosion/deposition (right) as a result of a change in transportability (K_t) when erodibility (K_d) is held constant at 0.003 [(a) K_t=0.3, c=0.01; (b) K_t=0.03, c=0.1; (c) K_t=0.003, c=1.0)].

Rainfall excess I(r) is estimated as rainfall intensity minus infiltration rate. Rainfall excess can be estimated per unit time, as in a dynamic situation where rainfall intensity and infiltration rate vary with time, or as a constant where rainfall intensity and infiltration are assumed to be in a steady state. Rainfall excess influences the magnitude of erosion/deposition rates. When rainfall excess increases, erosion and deposition rates also increase. However the spatial pattern of erosion and deposition does not change.

Critical shear stress t_s(r) represents the soil's resistance to the shearing forces (shear stress) of flowing water. It depends on soil and cover properties. Typical values for many soils are available (Flanagan and Nearing 1995). If the shear stress of flowing water at the given location is lower than the critical shear stress of the soil, no soil is detached. This parameter, therefore, has an impact on erosion/deposition patterns. High values reduce the spatial extent of erosion. On the other hand, it can also increase the magnitude of erosion rates on steeper hillslopes and in areas with concentrated flow due to the fact that clean water has higher potential to transport the sediment.

It is important to note that the parameters do not act independently. They are interrelated, and it is their interaction that controls the pattern and magnitude of erosion. For example, the growth of vegetation reduces K_d and K_t, and increases n. The resulting erosion/deposition pattern depends on the interaction between the rates of this change. If both K_d and K_t change at the same rate, the spatial distribution of erosion/deposition stays the same and only the magnitude of rates changes. If vegetation growth reduces K_d faster than K_t, the erosion/deposition pattern will change from transport capacity limited towards detachment limited. The relationships between these parameters is an area ripe for additional research. There is a lack of systematic experimental and theoretical modeling work in this area.

The present analysis shows that for uniform soil and cover there is a generalized pattern of erosion and deposition. High erosion risk areas are located on upper convex parts of hillslopes and in hollows and centers of valleys with concentrated flow. Deposition occurs in valleys and concave lower parts of hillslopes. By varying soil and cover conditions uniformly across a hillslope, the position where deposition starts can move up or down slope. Spatial variability in soil and cover has a great impact on the basic pattern of erosion/deposition. Depending on the spatial distribution of soil and cover parameters, the distribution of erosion and deposition may change. In addition, the overall soil loss and sediment loads in streams may be altered. Transition zones between land covers types (*e.g.*, bare soil and dense grass) may cause abrupt changes in flow velocities, as well as transport and detachment capacities, creating effects important for erosion prevention.

Figure 9a illustrates this phenomenon at the Scheyern Experimental Farm in Germany. We performed a simulation with the parameters set for dense grass in the meadow area ($n=0.1$, $K_t = K_d = 0.0003$) and bare soil in the arable area ($n=0.01$, $K_t = K_d = 0.03$), and compared the results with the observed spatial patterns of erosion/deposition. The highest rates of both the net erosion and the net deposition are predicted in valleys with high concentrated sediment flow. Field measurements confirm that this area has the thickest layers of colluvial deposits with large linear erosion features observed after an unusually strong storm (Auerswald *et al.* 1996). Relatively high erosion rates were also predicted on bare upper parts of hillslopes. These predicted soil losses correlate well with the loss of radio-tracers and declines in crop productivity (Figure 10). High erosion was also predicted for narrow strips below the grass areas, where water accelerates after depositing the sediment and leaving the grass. This leads to an increase in the difference between the sediment transport capacity and the actual sediment flow, creating the conditions for higher net erosion.

Deposition is predicted at the lower, concave parts of hillslopes which is in agreement with the spatial distributions of colluvial deposits and radio-tracers (Figures 9a and 10). The sediment flow rate decreases sharply and eroded materials are deposited at the upper edges of grassed meadows, thus explaining why rilling ends abruptly at the border between the grassed and bare areas (Figure 9a). The influence of grass cover on flow velocity, transport and detachment capacities also explains the observed location of deposited material on the convex, upper part of the grassed hillslopes.
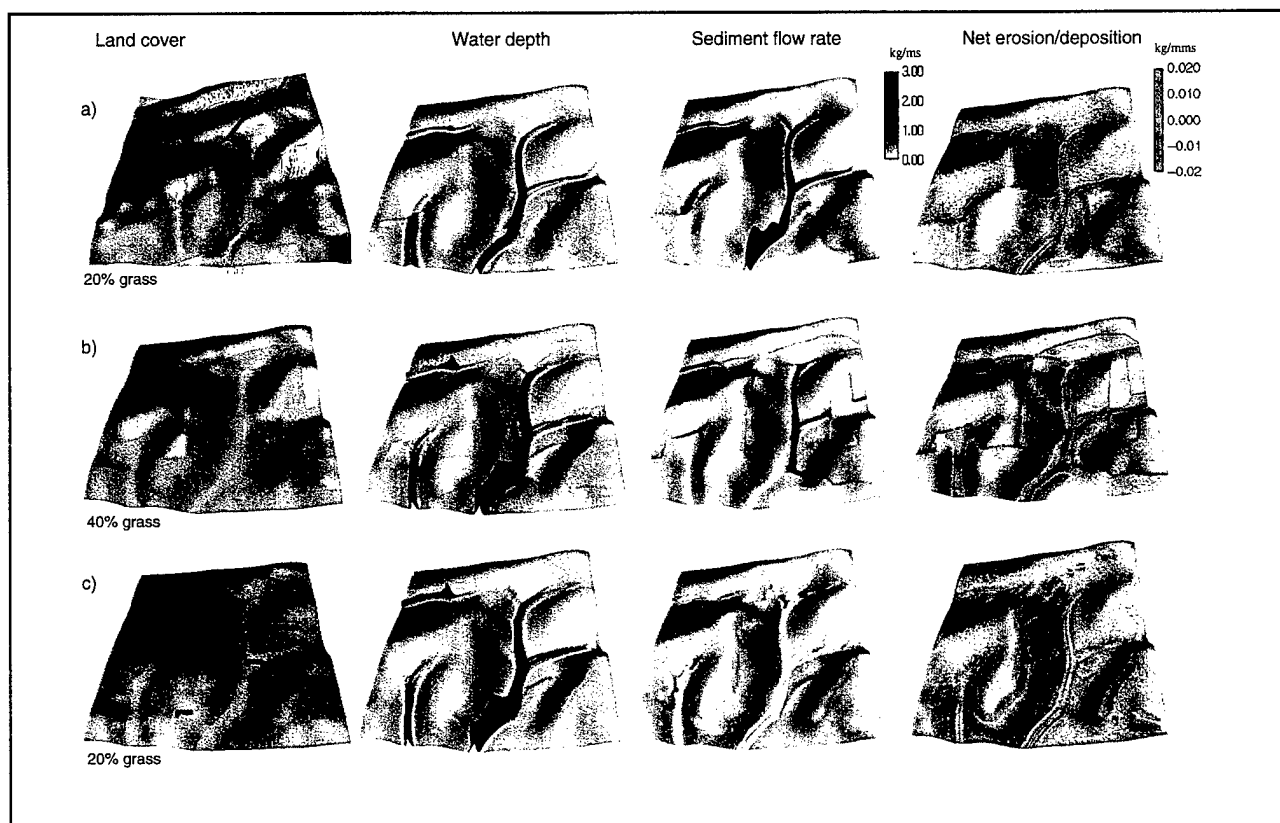
Figure 9. Simulation of runoff depth, sediment flow and net erosion/deposition for 3 different land management scenarios at the Scheyern Experimental Farm: (a) traditional land use, (b) "best management practices," and (c) computer designed scenario to minimize erosion.
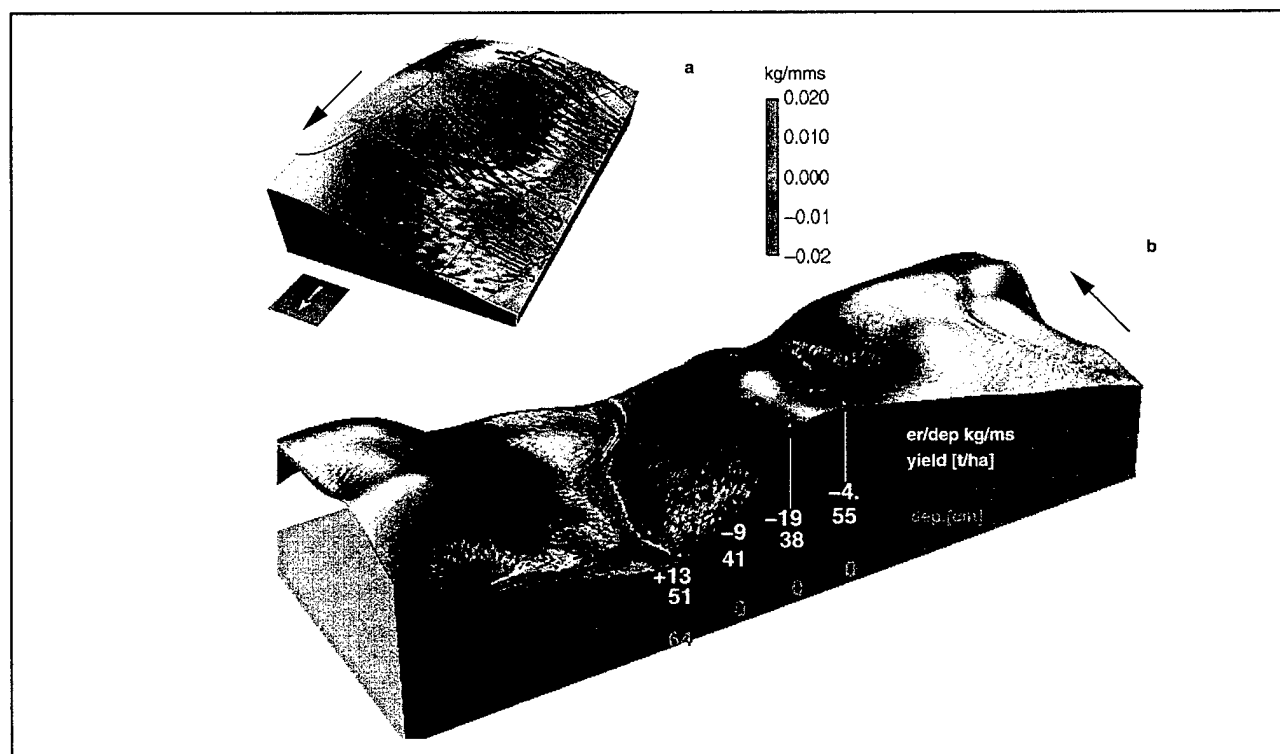
Figure10. Spatial distribution of net erosion and deposition predicted by the SIMWE model and compared with (a) rills observed after an intense rainstorm and (b) erosion/deposition estimates from radiotracer data, average crop yield, and measured colluvial deposits.

7. APPLICATIONS AND CASE STUDIES

One of the goals of this project was to develop methods and tools for erosion risk assessment and erosion prevention in support of military installations. This task poses a special challenge, because military installations often occupy large areas with terrains much more complex than typical agricultural regions for which most of the traditional erosion modeling tools were developed. In addition, the manner in which military installations are used often creates a mosaic of relatively well-preserved natural areas intermingled with landscapes exposed to high intensity disturbance. The principles of process-based erosion modeling developed for agriculture lands have to be significantly enhanced and new approaches have to be developed to meet this challenge. This section demonstrates that application of the new technologies to real world problems at several sites.

7.1 The effects of DEM resolution (Yakima Training Center, WA)

In the early stages of the project, we tested the reliability of using a standard U.S. Geological Survey (USGS) 30m DEM to predict topographic potential for erosion/deposition at the Yakima Training Center, Washington (Mitasova *et al.* 1996). We found that the conversion of USGS contour maps to digital elevation models with horizontal and vertical resolutions of 30 m and 1 m, respectively, resulted in systematic banding or artificial waves along the contours (Figure 11a). To improve the results, we used the regularized spline with tension (RST) method (see Section 2.1) to reinterpolate the elevations to the new DEM with 10m horizontal and 0.01m vertical resolution. Detailed analysis of the original and reinterpolated DEM, using 3 dimensional shaded views, curvatures and histograms, revealed that systematic bands or waves along the contours were significantly reduced but not eliminated (Mitasova *et al.* 1996). Profile curvature and histogram analysis proved that it was not possible to remove the waves completely. While resampling and smoothing improved the results, the USPED model still predicted waves of deposition along 20m contours (Figure 11b). To confirm that the wave patterns were artificial, we extracted 10m contours from the original grid DEM and interpolated a new DEM using the RST function with smoothing and tension. The new DEM had a root mean square error of 2.3m which is well within the vertical accuracy of the original data (given as 7m), and the banding effect around the contours disappeared (Figure 11c). A comparison of the results from the original, reinterpolated and recomputed DEMs demonstrates inadequacy of traditional 30m resolution USGS DEMs for erosion/deposition modeling. In the absence of higher resolution data, it is possible only to compute the topographic potential for detachment limited erosion which does not require the computation of deposition and is thus less sensitive to artifacts in DEM.

7.2 Analysis of topographic potential for erosion/deposition at Ft. McCoy, WI

Topographic potential for soil detachment, net erosion and deposition at Fort McCoy was estimated by the enhanced USLE and USPED models (Mitasova *et al.* 1996). Even with rather crude elevation data (30 m), it was possible to identify some areas with high topographic risk for soil erosion and deposition (Figure 12). The plateaus in low elevation areas due to the insufficient vertical resolution of 1m create an artificial pattern of steeper slopes along 1m contours and upslope contributing areas computed from the original 30m DEM by *r.flow* are underestimated. Pits and plateaus in the DEM cause problems in flowtracing with almost no flow generated in lower elevation areas and disrupted flow in valleys. The modified LS factor predicts
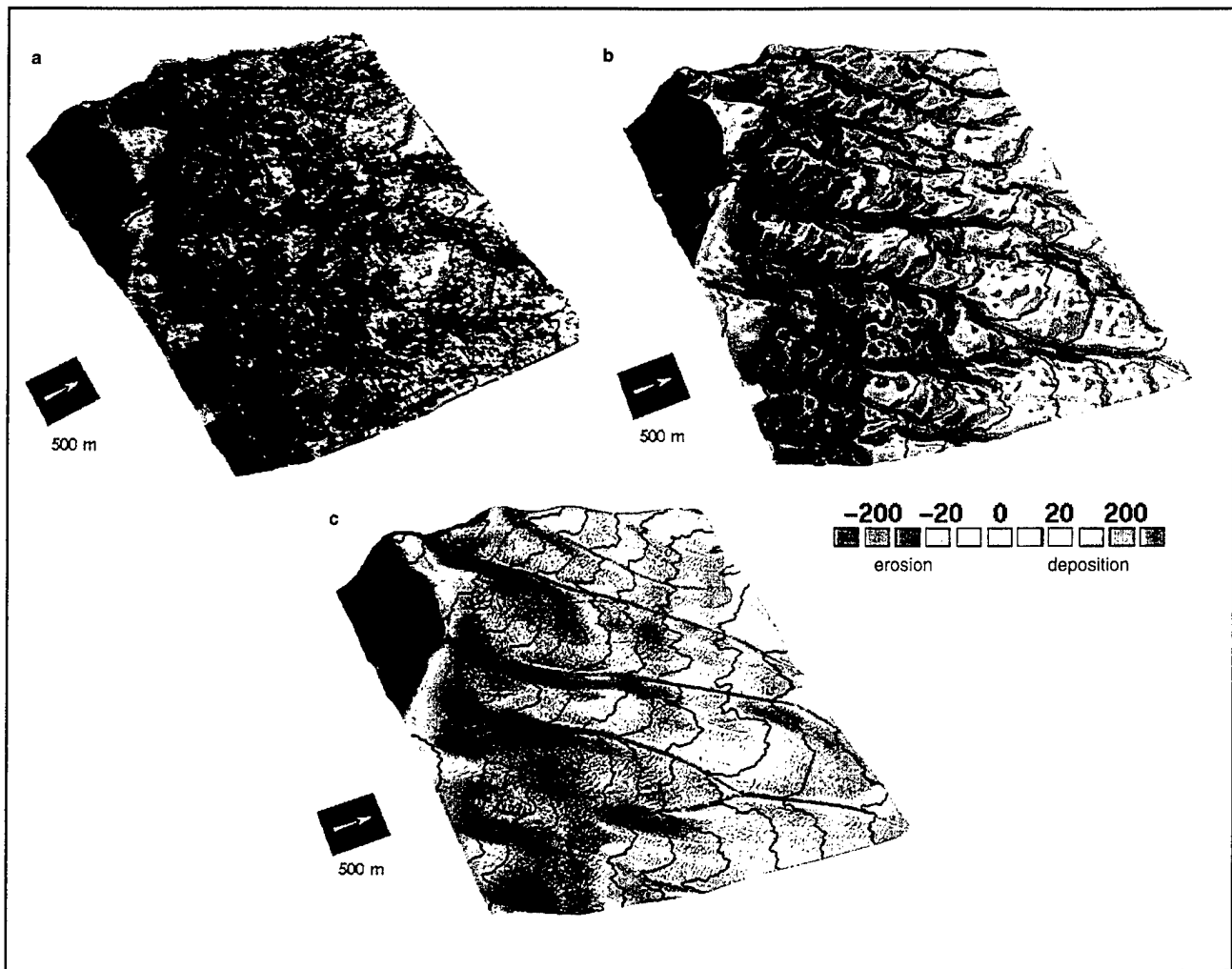
Figure11. Net erosion and deposition predicted by the USPED model using the original 30 m DEM (a), a resampled and smoothed DEM (b), and a DEM reinterpolated from contours (c).

well some areas of high potential for soil detachment, especially in hilly parts of the region. However, it does not predict the location of areas with concentrated flow with high potential for gully formation. Also, in lower elevation areas the artificial pattern of increased erosion is predicted along 1m contours. The net erosion/deposition map computed by the USPED model predicts high net erosion in hilly regions and on slopes along the streams. It also shows that a significant portion of the material eroded from hillslopes is deposited before it could reach the main streams. However, this map lacks the prediction of high erosion due to concentrated flow in valleys and shows artificial waves of erosion and deposition along the 1m contours in flatter areas.

To reduce the negative impact of the low resolution of the available elevation data, the DEM was reinterpolated to 10m horizontal and 0.01m vertical resolution using the RST method. Simultaneously with interpolation, maps of slope, aspect, profile and tangential curvatures were generated. Steady state water flow computed by $r.flow$ from the smoothed 10m DEM shows potential for channel formation in valleys and predicts water flow also in low elevation region (Figure 13). Flow in the two main streams is not adequately described because of lack of data, but it can be incorporated if stream data are available. Modified LS factors were computed from the 10m DEM using different exponents for the water flow term ($p=0.6$ and $p=1.5$). Value of this exponent is still a subject of research and discussion in erosion research community. The first result for $p=0.6$ puts more weight on the influence of slope and theoretically represents the detachment limited erosion (Figure 13). The second result with $p=1.5$ puts more weight on the influence of water flow and theoretically represents the sediment transport capacity limited erosion (Figure 13). Because the exponent depends on the conditions of water flow in a particular area it should be calibrated to reflect the type of flow
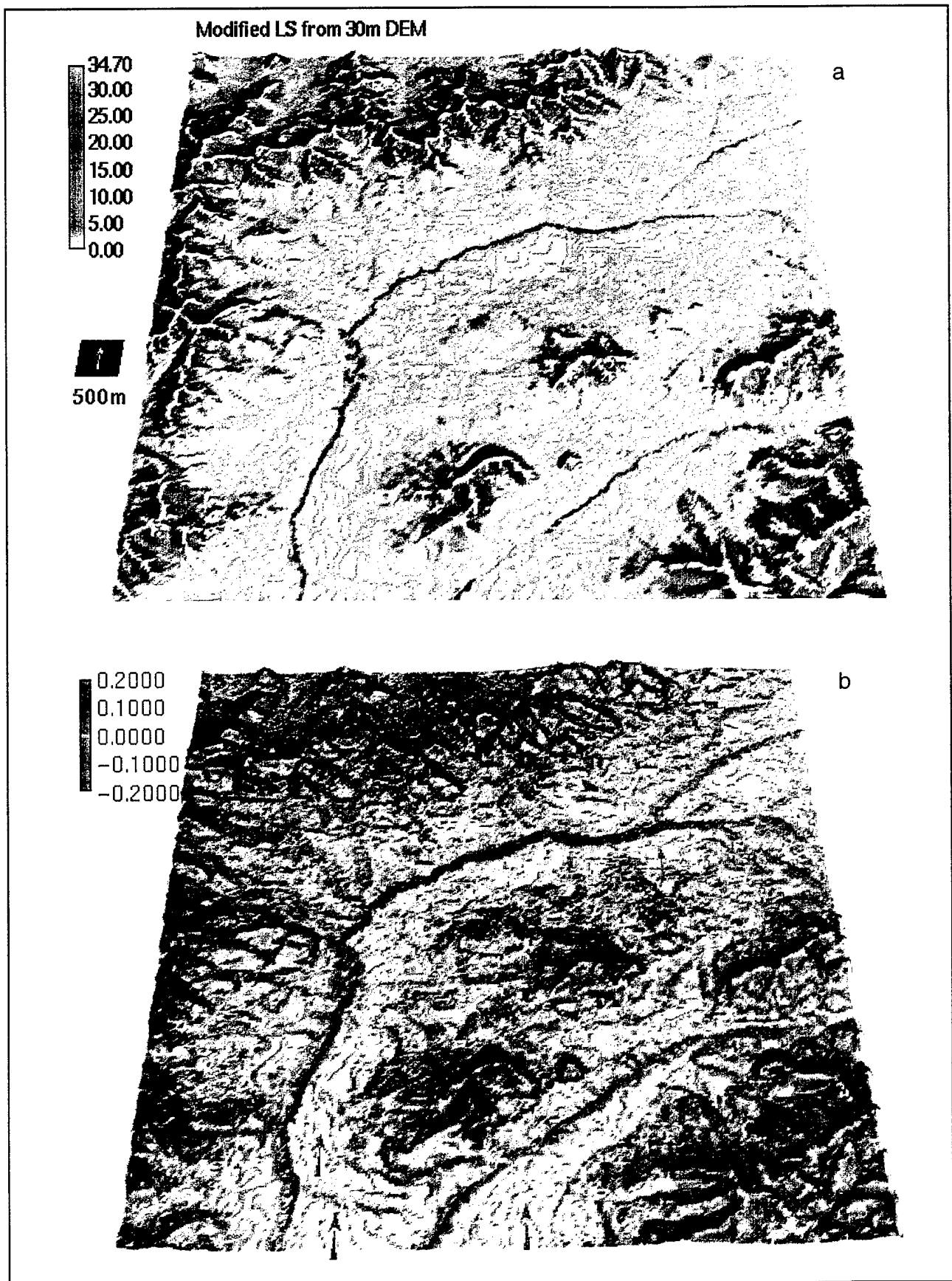
Figure12. Topographic potential for erosion as predicted by the enhanced USLE (a) and erosion/deposition as predicted by the USPED model (b) from a 30 m DEM. The arrows in b show artificial waves of deposition due to waves along the contours of the DEM.
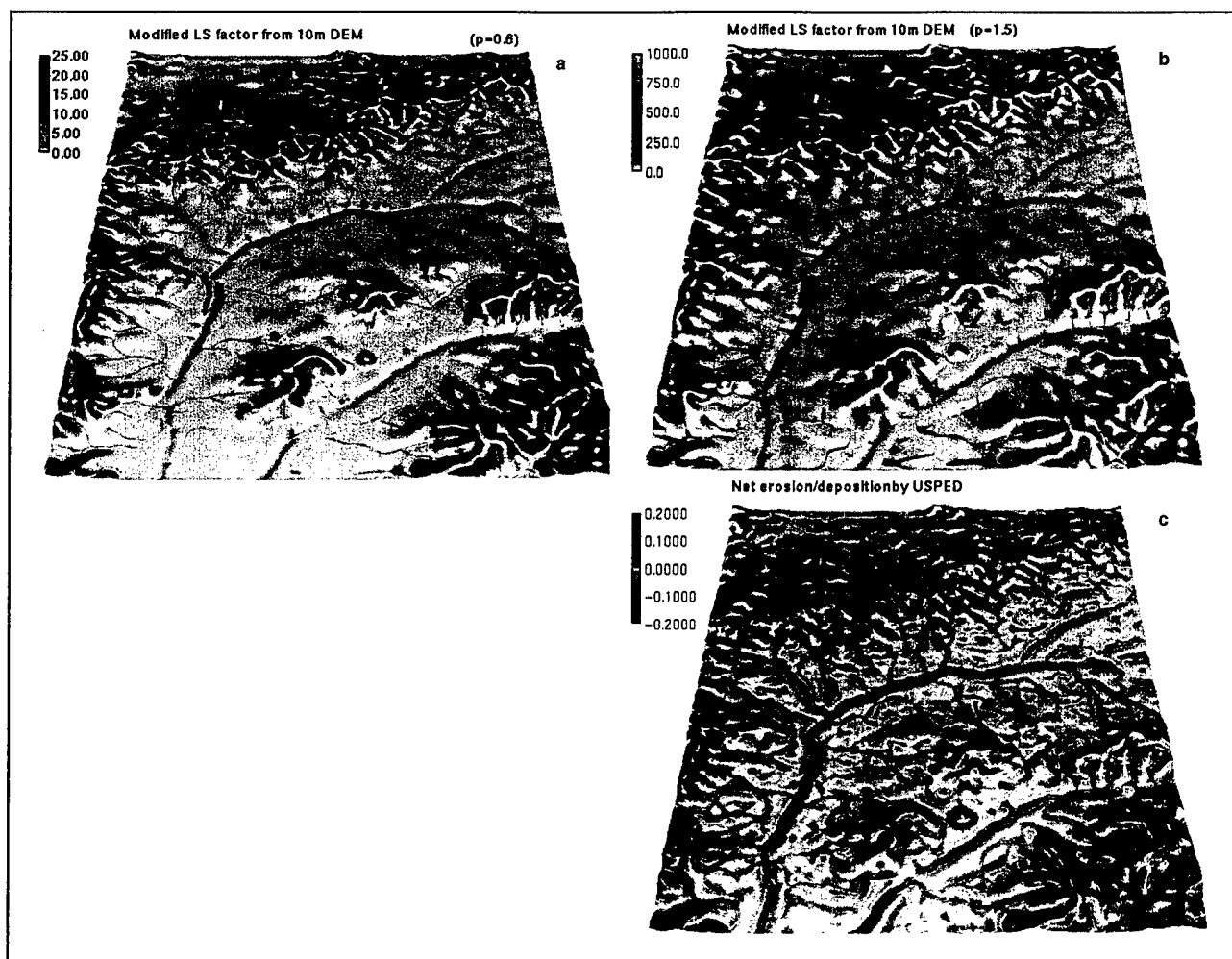
Figure 13. Results of erosion modeling based on a smoothed DEM that was resampled to 10 m resolution. (a) Enhanced USLE LS-factor with p=0.6, representing topographic potential for detachment limited erosion. (b) Sediment transport capacity estimated as a function of upslope area and slope with p=1.5. (c) Topographic potential for net erosion and deposition estimated as divergence of sediment flow with the USPED model where the magnitude of sediment flow is approximated by sediment transport capacity.

typical for the modeled area and time during the year. Topographic potential for net erosion/deposition was computed from the 10m DEM using the USPED model. Similarly as for the result of 30m DEM, the model shows high erosion in hilly area and along main streams and deposition in concave areas. It also indicates location of areas with concentrated flow which can reach streams.
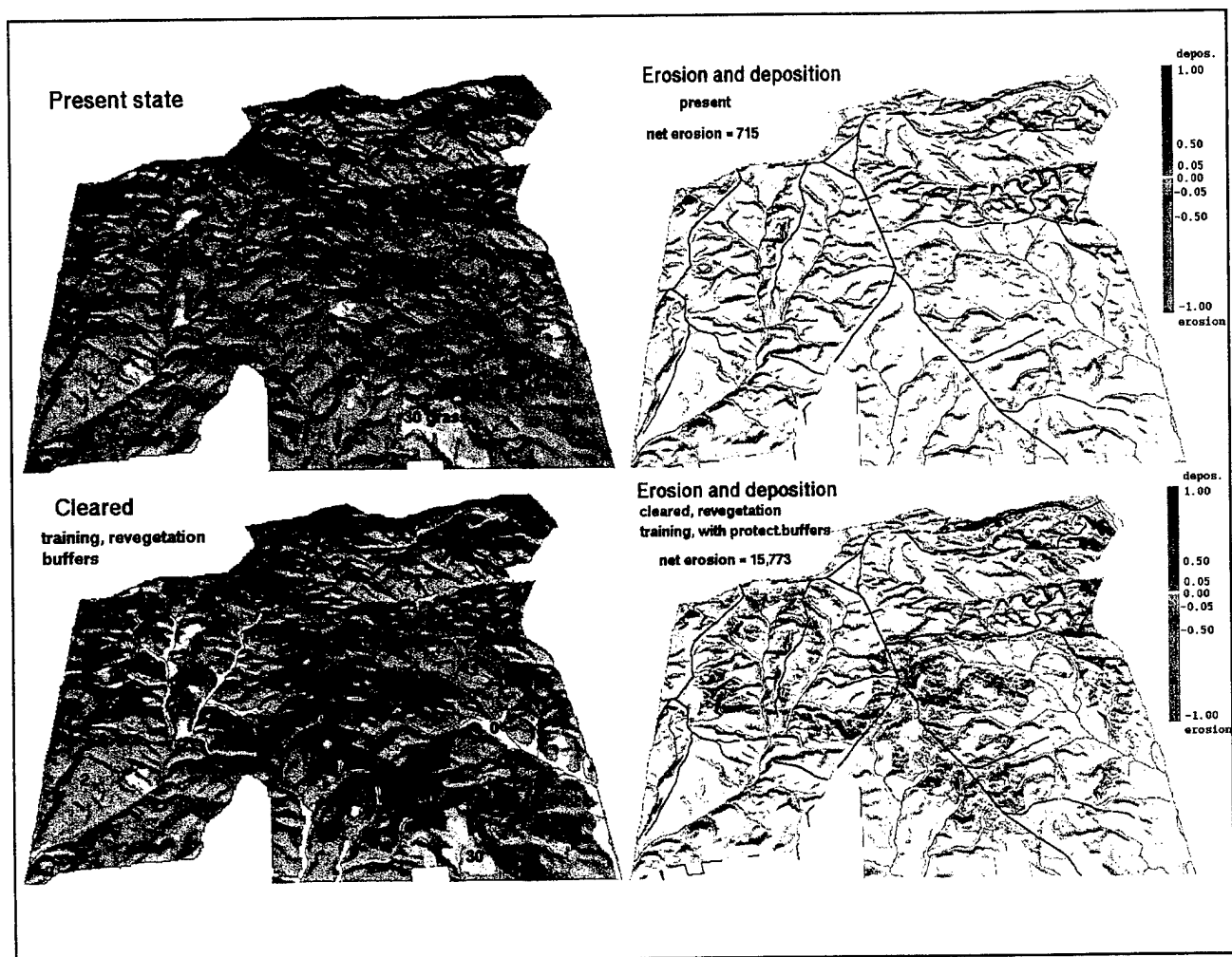
7.3 Impact of proposed land use change at Camp Shelby, MS

We used the USPED model to evaluate potential changes in the spatial distribution of erosion and deposition at Camp Shelby, Mississippi resulting from anticipated changes in land use patterns. Camp Shelby is largely wooded. In an attempt to open more area to military training, it was proposed that large areas be deforested and additional areas be selectively thinned to allow passage of tracked vehicles. A high resolution (5m) DEM with slope and aspect was created from digitized contours using regularized spline with tension (see Section 2.1). The upslope contributing area for each grid cell was computed by the vector-grid based flow tracing algorithm. A net erosion and deposition index was computed using the USPED model for the current undisturbed landuse and for several land use alternatives with a significant portion of the area exposed to intensive landuse during training. One alternative is shown in Figure 14. Calculations indicate that the

proposed scenario, if implemented without erosion protection measures, will lead to a 33-fold increase in average soil loss per acre. Use of protective stream buffers and exclusion slopes steeper than 10% from training could reduce potential erosion by about 40%, but it would still be 22 times greater than before clearing (Figure 14).

7.4 The effects of scale on erosion prediction (Fort Irwin, CA)

To illustrate the issues associated with simulations for large areas we use an example of a mountainous region at Fort Irwin, California. The standard 30m DEM available for the entire study area (3000 square km) represents 4 million grid cells, a challenging data set for currently available process-based simulation tools and workstations, at the resolution hardly sufficient for rough identification of high erosion risk areas. The DEM at 5m resolution required for more detailed modeling efforts would produce 121 million grid cells. Simulations would be prohibitively expensive, if not impossible, with the current computational resources. It is clear, that for such a large area, modeling at different scales and resolutions is needed, depending on the importance and complexity of the watersheds. It is important to note that our aim in this application is to

Figure 14. Impact of land use change on erosion and deposition: (a) original land use, (b) net erosion/deposition for the original land use, (c) proposed land use change including clearing, thinning, revegetation and stream buffers, and (d) USPED predicted net erosion/deposition for the proposed land use showing 20x increase in net erosion. Without the protective measures, the increase in net erosion would be 33x.

illustrate the possibility of using standard elevation data for erosion simulations in a large area. We do not take into account the variability in climate, soil and cover properties.

To demonstrate the impact of resolution, noise and systematic errors in standard elevation data, we computed tangential curvature for a part of Fort Irwin using the standard 30m DEM. The tangential curvature map was then draped over a terrain map. The tangential curvature showed acceptable structure in steeper mountainous areas but significant noise and systematic errors (stripes) in lowland areas (Figure 15a). After smoothing and resampling to 10m resolution using the RST interpolation method, the noise was reduced and the major topographic features became more visible (Figure 15b). The analysis clearly demonstrates that the need for precision and accuracy in elevation data is spatially variable. Areas of flat terrain are much more sensitive to noise and systematic errors in elevation data than mountains.
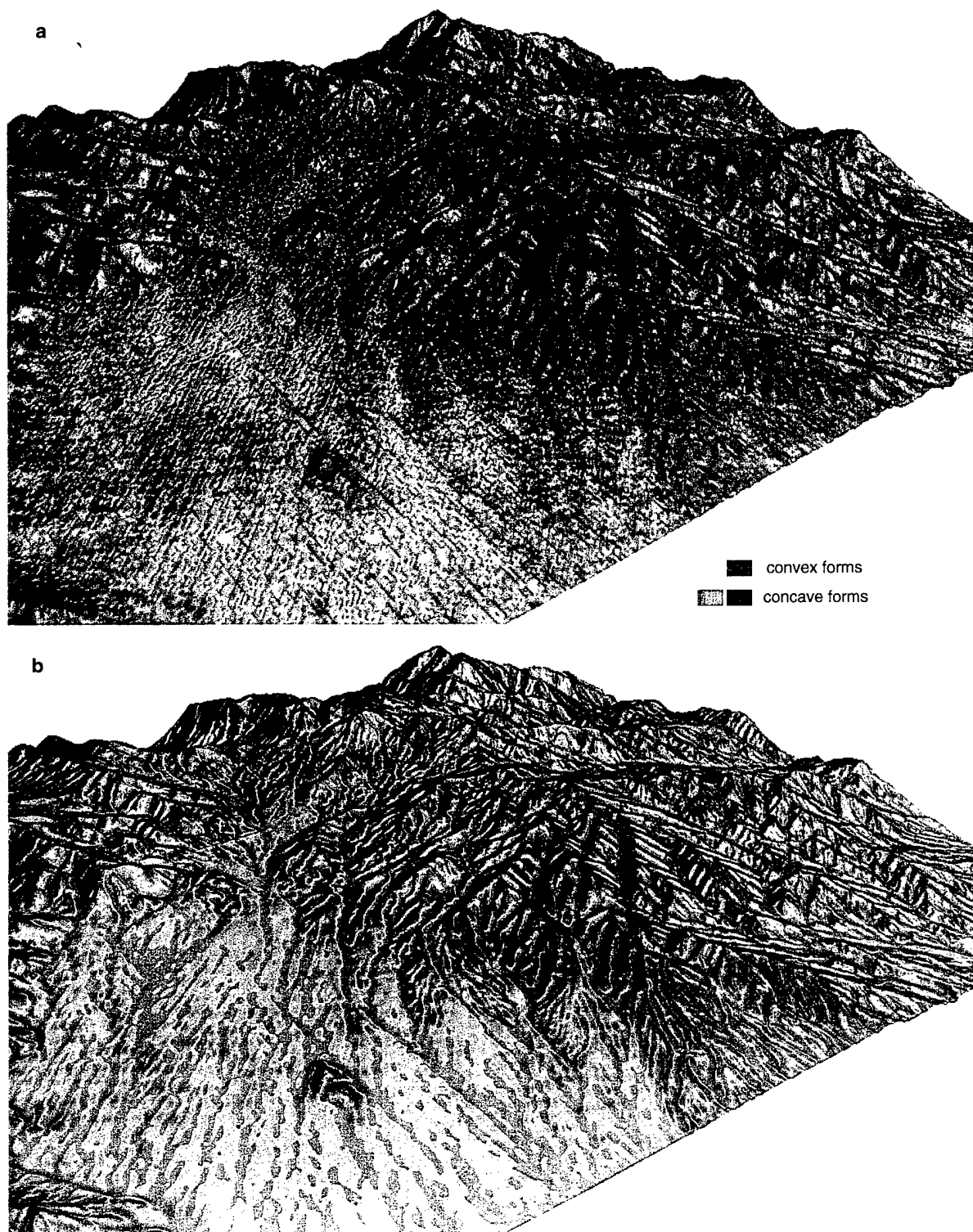
Topographic potential for detachment limited erosion and transport capacity limited erosion/deposition were estimated by the modified USLE (see Section 4.1) and the USPED models (see Section 4.2), respectively. To illustrate the impact of smoothing and resampling on erosion modeling, we computed the erosion estimates using DEMs at 90, 30 and 10m. The 90 and 10 m resolution DEMs were created by resampling the original 30 m DEM. To demonstrate the differences in detail that can be achieved at various resolutions, we display the results as color maps draped over the 10m resolution DEM for a 36 square km area (Figures 16 and 17). The results show that the 90m resolution DEM is inadequate for capturing the erosion by concentrated flow with the enhanced USLE (Figure 16) and does not allow the prediction of realistic net erosion/deposition patterns using USPED (Figure 17). The 30m resolution DEM starts to reveal the structure of erosion patterns, including the concentrated flow erosion in the valleys (Figure 16). However, it is not adequate for predicting net erosion/deposition patterns (Figure 17). The 10m resolution does not improve the accuracy of the original elevation model, but the smoothing reduces the noise in the data and the higher resolution allows better representation of terrain geometry, thus leading to more realistic results both for the detachment limited erosion (Figure 16) and net erosion/deposition (Figure 17).

To test the applicability of the SIMWE model to large areas, we computed the spatial distribution of steady state water flow, sediment flow and net erosion/deposition for a 36 square km area at Fort Irwin using the reinterpolated and smoothed 10m DEM (Figure 18). The water flow simulation captured the complex pattern of overland water flow, including the dispersal flow features typical for this area, which are difficult to predict by more traditional approaches (Figure 18a). Sediment flow rates were estimated by solution of continuity of mass equation predicting high sediment flow rates in centers of valleys with concentrated flow and dispersal of sediment flow with reduction of sediment loads in areas with alluvial fans (Figure 18b). Net erosion/deposition rates were estimated using a transport capacity limiting regime due to the prevailing sandy soils (Figure 18c). The simulation shows the formation of split gullies and their disappearance as the terrain flattens and the alluvial fans are formed.

This application demonstrates that processing of original elevation data by adequate tools, such as in our case the RST method and application of a robust, process-based model can lead to a more realistic prediction of a complex erosion/deposition pattern. This application also proved that the SIMWE model can be applied to large areas, in spite of its relatively complex formulation and computational demands.

7.5 Evaluation of CASC2D-SED (Goodwin Creek watershed, MS and Ft. Hood, TX)

The CASC2D-SED model was applied to Goodwin Creek watershed approximately 60 miles north of Memphis, Tennessee and the and the Henson Creek watershed at Fort Hood, Texas. The Goodwin Creek watershed is extensively gaged by the Agricultural Research Service (ARS) as a research watershed in the areas of upland erosion, in-stream sediment transport, and watershed hydrology. The watershed drains a total area of 8.26 square miles. Only 13% of the Goodwin Creek watershed is cultivated; the remainder is idle pasture or forestland. The predominant soil texture for Goodwin Creek watershed is silt loam with a small percent of sandy loam.

Figure 15. Tangential curvature draped over a DEM (a) derived from the original 30 m DEM and (b) derived from a smoothed and resampled DEM.
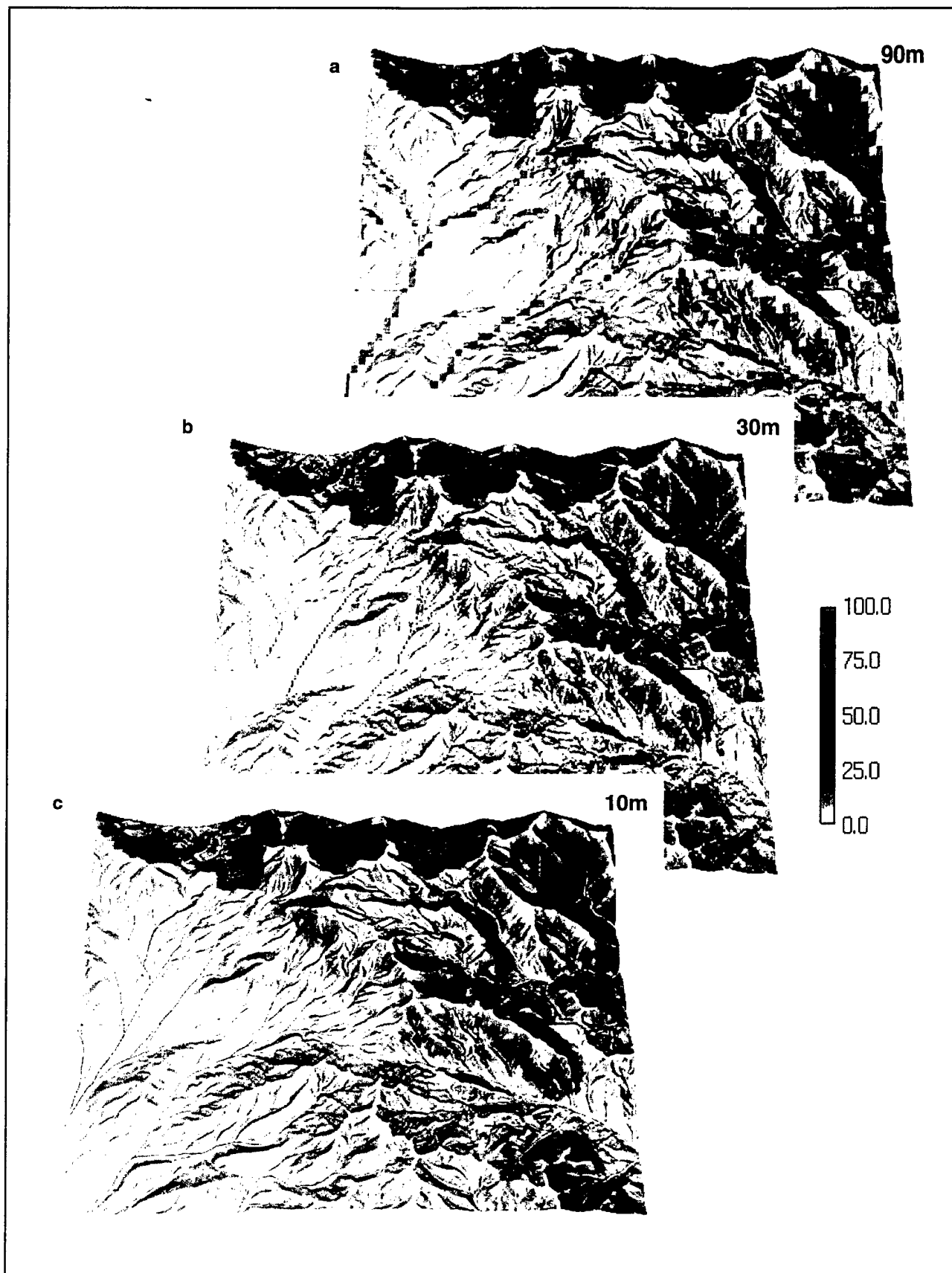
Figure 16. Topographic potential for detachment limited erosion estimated by the enhanced USLE for an area at Fort Irwin, California at resolutions of 90 m (a), 30 m (b) and 10 m (c).
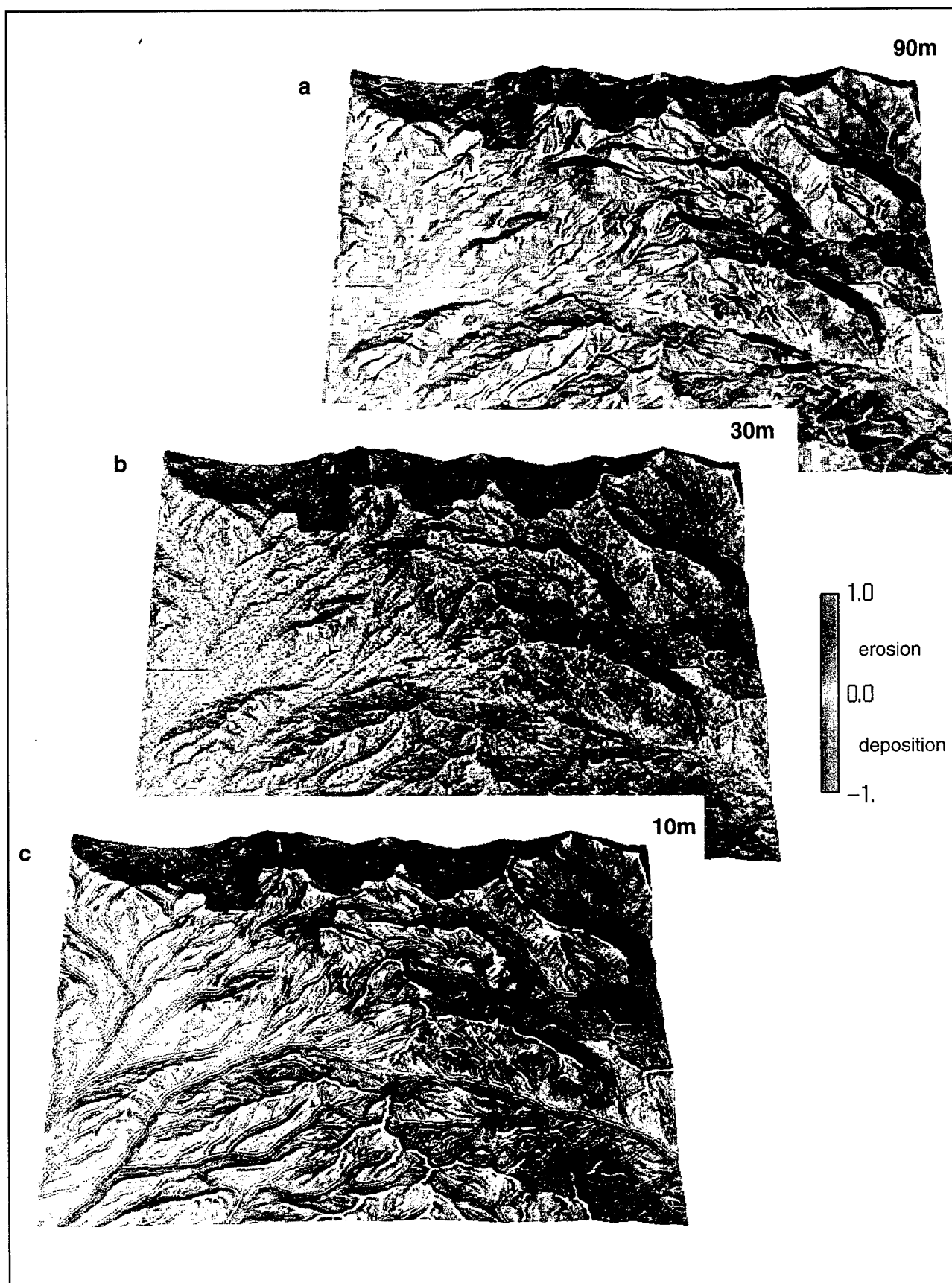
Figure 17. Erosion and deposition patterns estimated by the USPED model for an area at Fort Irwin, California at resolutions of 90 m (a), 30 m (b) and 10 m (c).
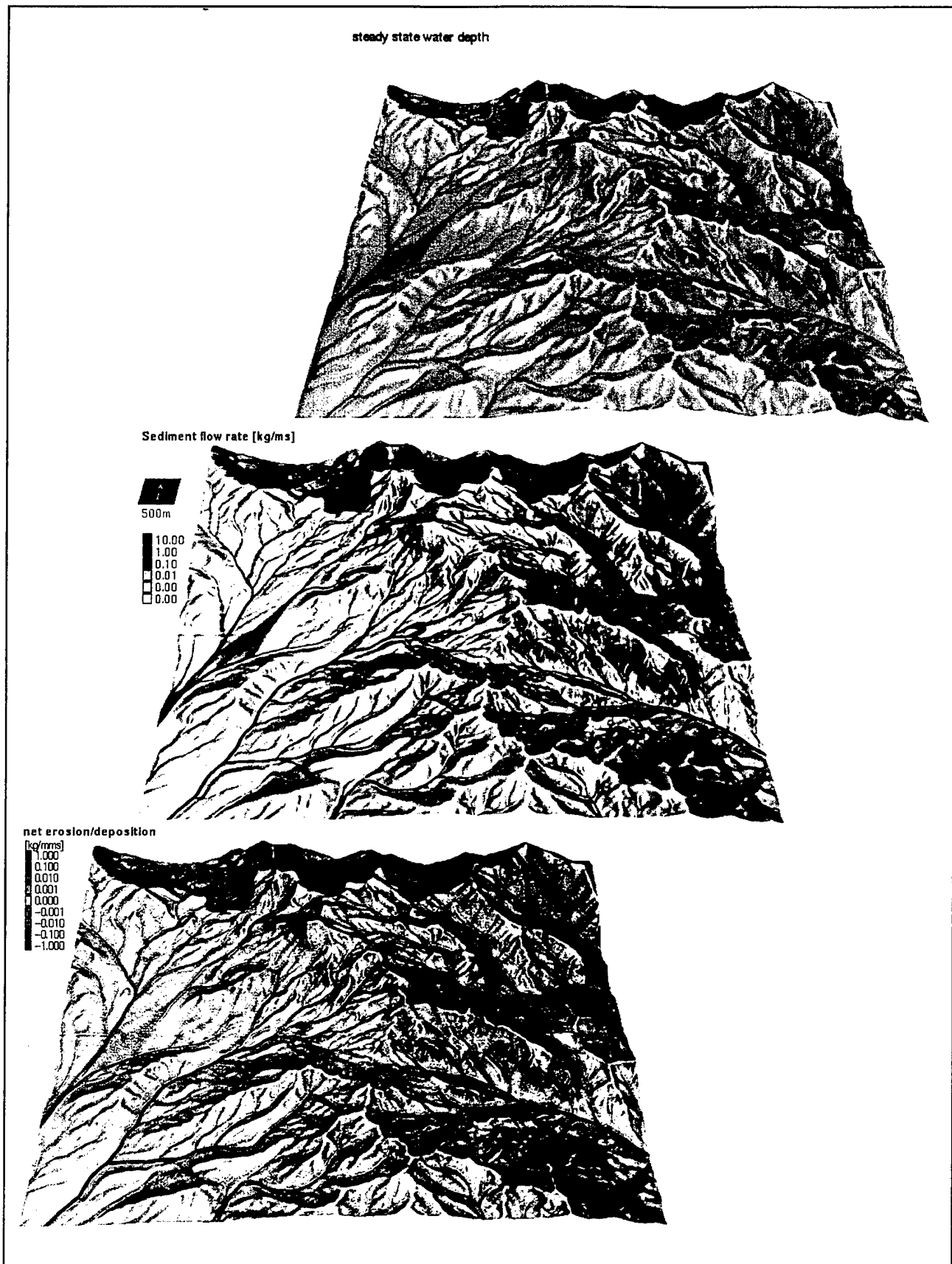
Figure 18. Runoff depth, sediment flow and erosion/deposition rates predicted by the SIMWE model from a 10 m resolution DEM smoothed with the regularized spline with tension (RST) method.

At the Goodwin Creek watershed, results of the CASC2D-SED simulations were compared with measured runoff and sediment discharge from the October 17-18, 1981 storm event. The storm event began at 9:19 pm and had a total rainfall duration of 3.5 hours with very little rainfall preceding this event. Across the watershed, the total rainfall for this event varied from 2.55 to 3.11 inches with an average value of 2.85 inches. A comparison of the hydrograph plots (Figures 19-21) show that CASC2D-SED was able to consistently simulate the overall shape and rate of rise. The time to peak was simulated within 3% at some places (gage 8 and gage 5), but was off by approximately 15% at gages 2 and 4. CASC2D-SED underestimated the total volume of runoff by approximately 20% across the watershed. A comparison of the sediment discharge plots (Figures 22-24) show that CASC2D-SED was able to predict upland erosion from the Goodwin Creek Watershed within an acceptable range of -50% to 200% of the actual upland erosion. This range (-50% to 200%) is generally considered by sedimentation engineers to be acceptable when comparing computed sediment yields versus actual sediment yields.

The Henson Creek watershed is contained almost completely within the boundaries of Fort Hood, Texas. Most of the watershed lies within the artillery impact area, parts of which are subjected to frequent use by military vehicles. Soils range from silty clay to clay loam; rock outcrops are common. Model application to the Henson Creek Watershed, Fort Hood, Texas, was performed using a single storm occurring between 0130 hrs on April 25 to 1800 hrs on April 27. Results indicate that CASC2D-SED provided reasonably accurate results (Figure 25).

For both watersheds, the CASC2D-SED model provided remarkably accurate estimates of runoff discharge. Sediment discharge estimates were less accurate, but generally within acceptable limits. The primary factor contributing to the errors in the prediction of sediment discharge appears to be the fact that the CASC2D-SED is not designed to predict bank failure and channel erosion. As much as 70% of the sediment discharged from the Goodwin Creek watershed has been attributable to those forms of erosion.

## 7.6 Design of erosion prevention measures (Scheyern Experimental Farm, Germany)

We first applied SIMWE to the Scheyern Experimental Farm in Germany to evaluate the erosional consequences of the traditional land use management scenario that was in use when we first began collaborative efforts with the farm prior to 1993 (Figure 9a). Approximately 80% of the area was tilled, while 20% was maintained in permanent grass cover. This land use resulted in severe erosion in the tilled areas when a large storm event occurred during the time when the agricultural fields were bare. The field data showed that the areas with the highest water and sediment flow potential were unprotected and that significant rilling and gully formation occurred. Simulations performed for these conditions confirm high potential for erosion on convex parts of the bare hillslopes and high sediment flows in the areas of concentrated water flow.

In response to the severe erosion, the farm implemented "best management practices" in 1993 to reduce erosion and enhance sustainable agriculture. The practices consisted of planting wide grassed buffers at the valley bottom. The new scenario consisted of approximately 40% grassed areas, with the remainder under cultivation. Based on SIMWE estimations, the improved land design altered the spatial patterns of erosion and deposition within the watershed and reduced the sediment load in the stream (Figure 9b).

We next used the SIMWE model to investigate the possibility of redesigning the land use patterns to minimize net soil loss and sediment loads. First, we used the model to identify locations with the highest erosion risk, assuming a uniform land use. Then, the original 20% protective grass cover was redistributed to the highest risk areas (Figure 9c). We performed a simulation with the new land use scenario to evaluate its effectiveness. The results demonstrate that the new design has the potential to dramatically reduce soil erosion and sediment transport (Figure 9c). The high sediment flow in the valley disappeared and was re-
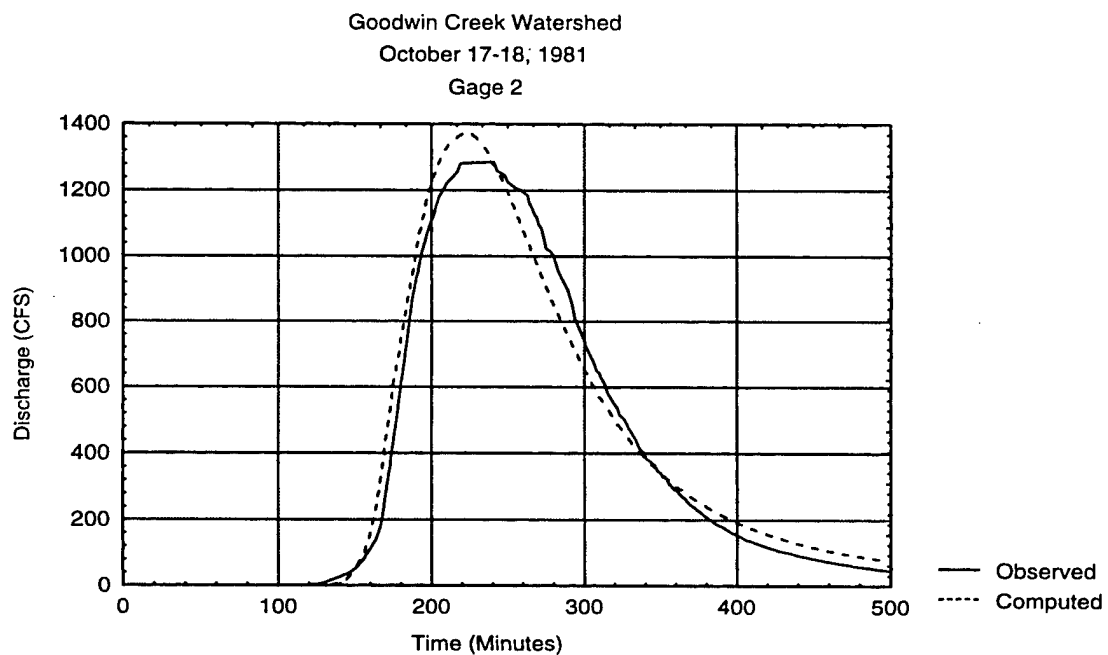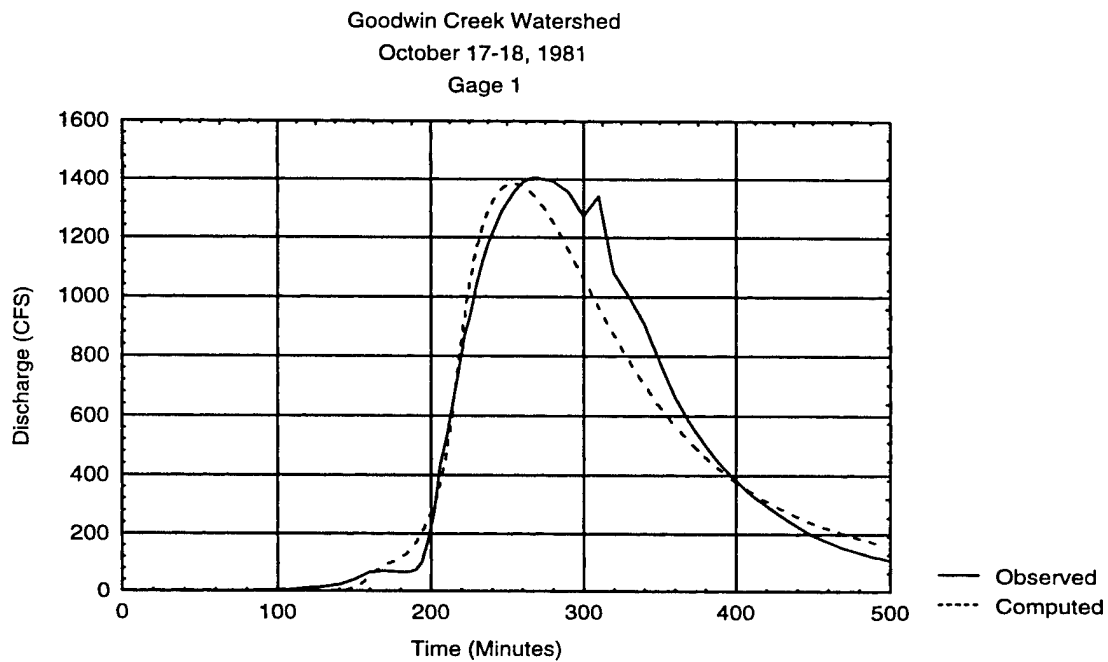
Figure 19. Actual and predicted runoff hydrograph for October 17-19, 1981 at gages 1 and 2 in the Goodwin Creek watershed, Mississippi.
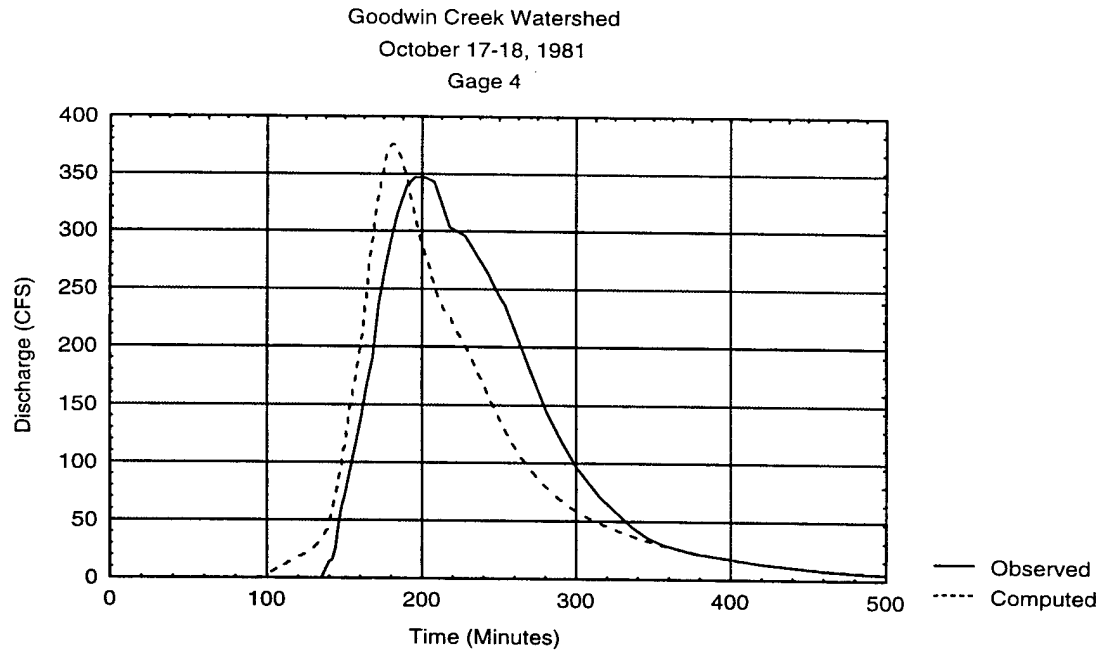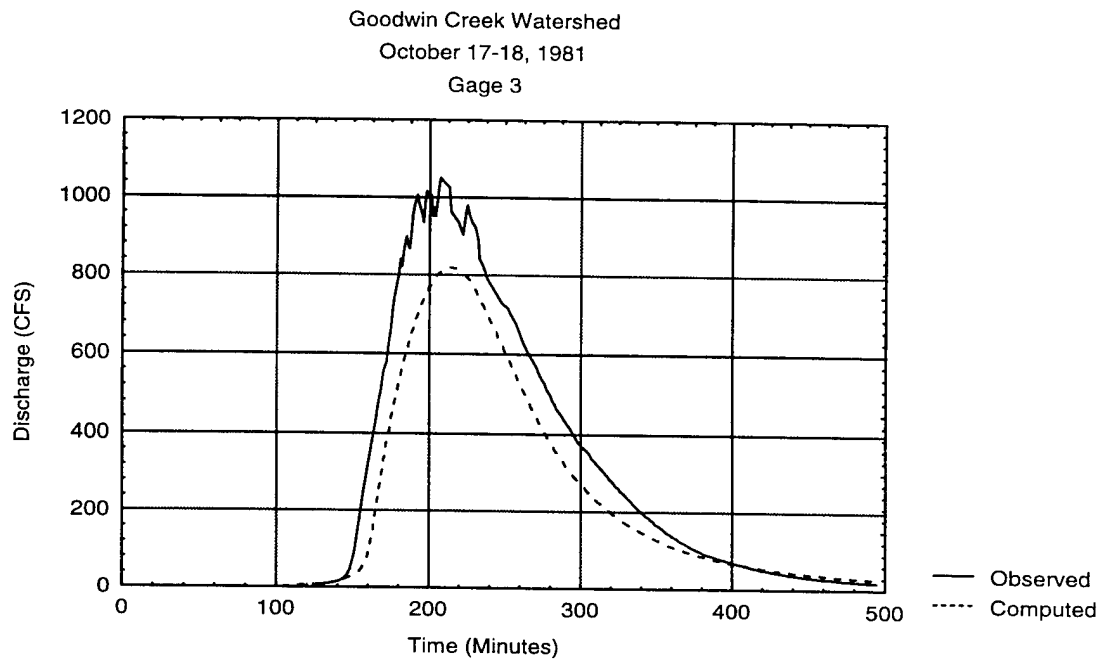
Figure 20. Actual and predicted runoff hydrographs for October 17-19, 1981 at gages 3 and 4 in the Goodwin Creek watershed, Mississippi.

Figure 21. Actual and predicted runoff hydrographs for October 17-19, 1981 at gages 5 and 8 in the Goodwin Creek watershed, Mississippi.

Figure 22. Actual and predicted sediment discharge for October 17-19, 1981 at gages 1 and 2 in the Goodwin Creek watershed, Mississippi.
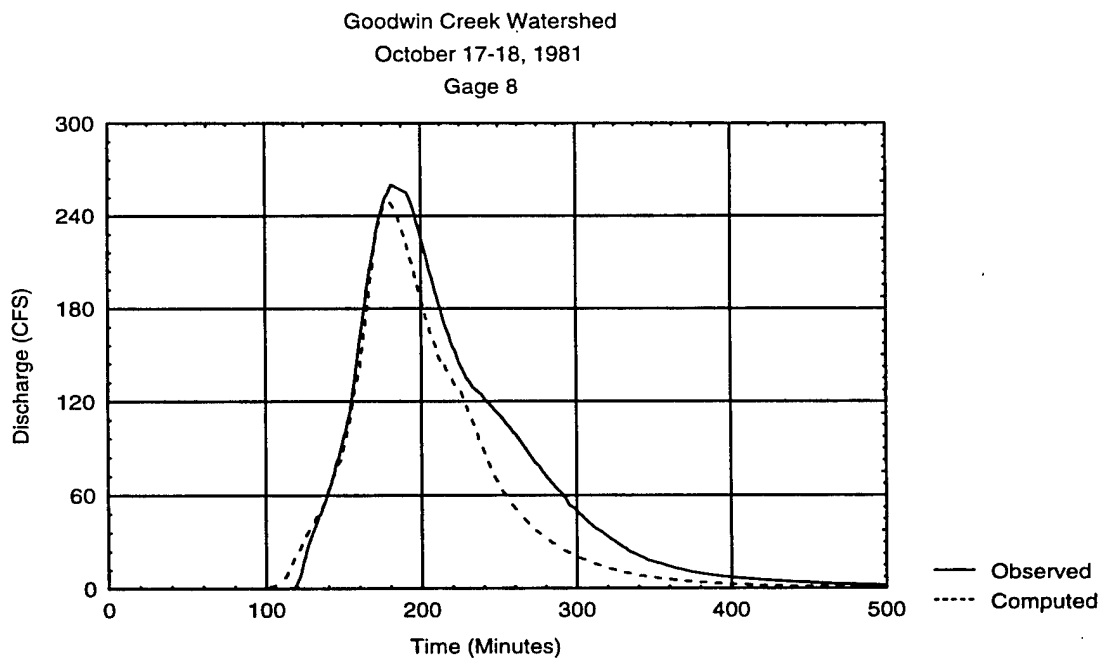
Figure 23. Actual and predicted sediment discharge for October 17-19, 1981 at gages 3 and 4 in the Goodwin Creek watershed, Mississippi.
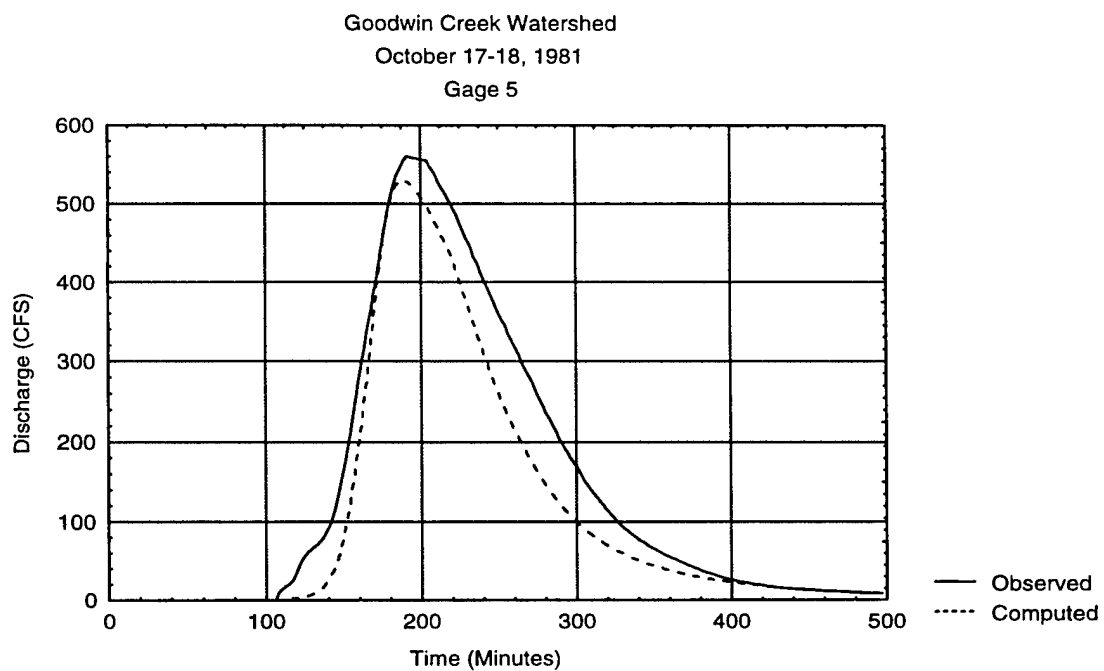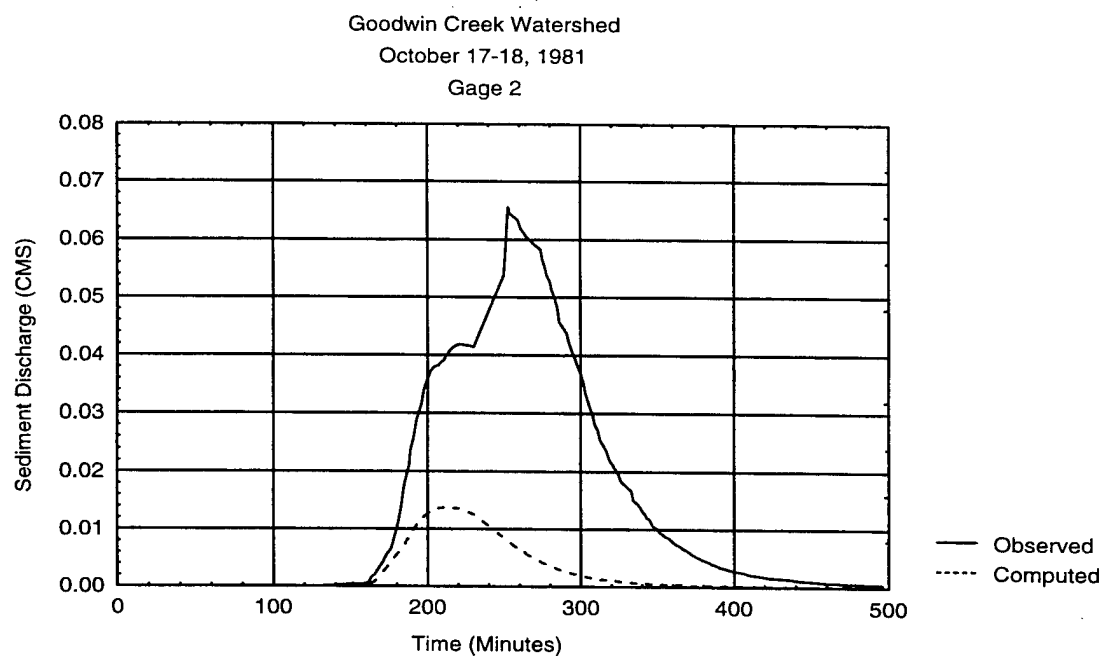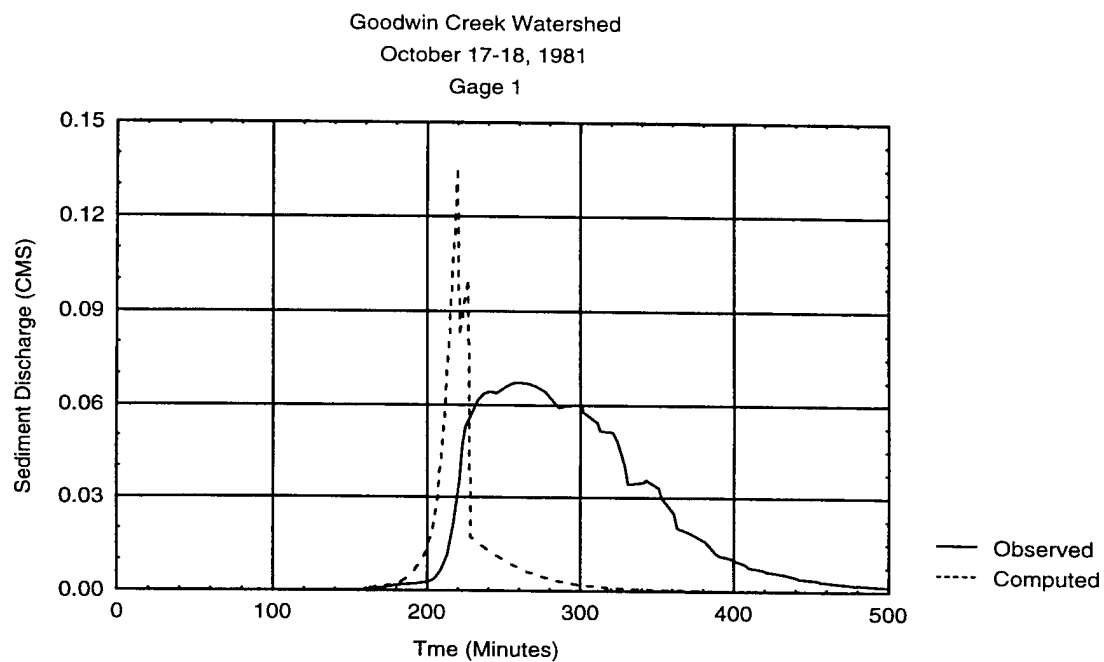
Figure 24. Actual and predicted sediment discharge for October 17-18, 1981 at gages 5 and 8 on the Goodwin Creek watershed, Mississippi.
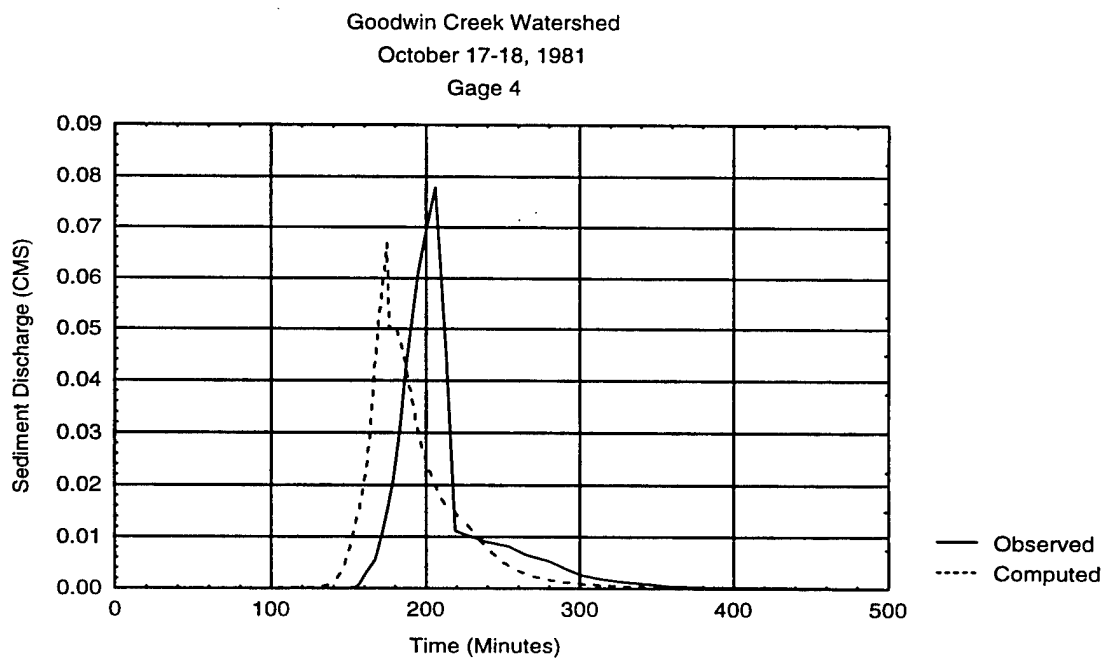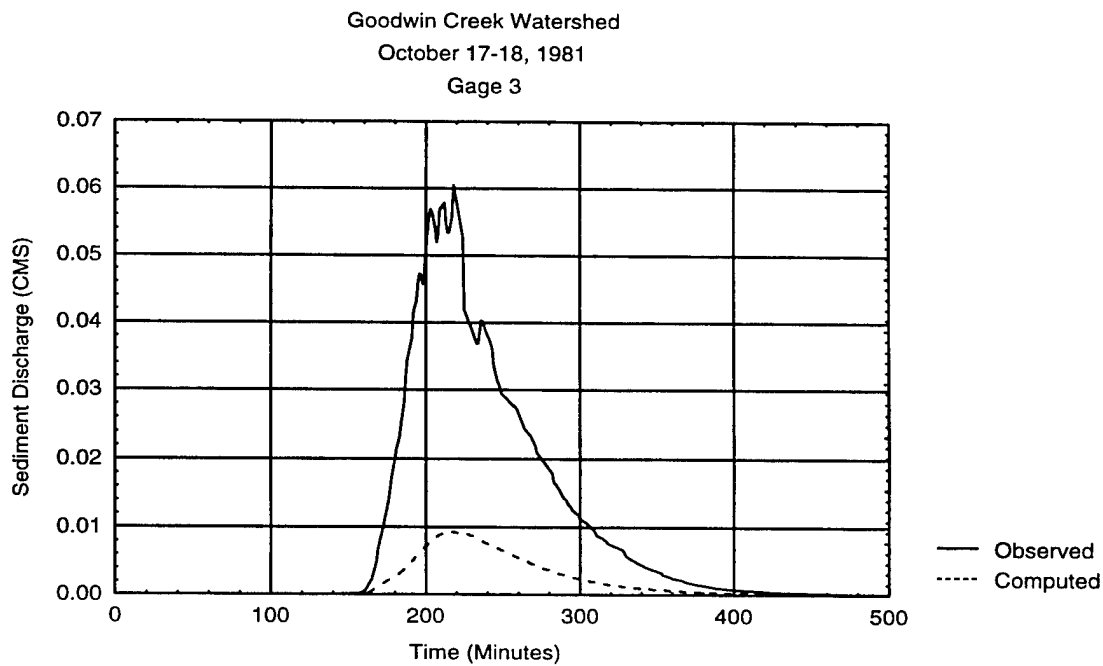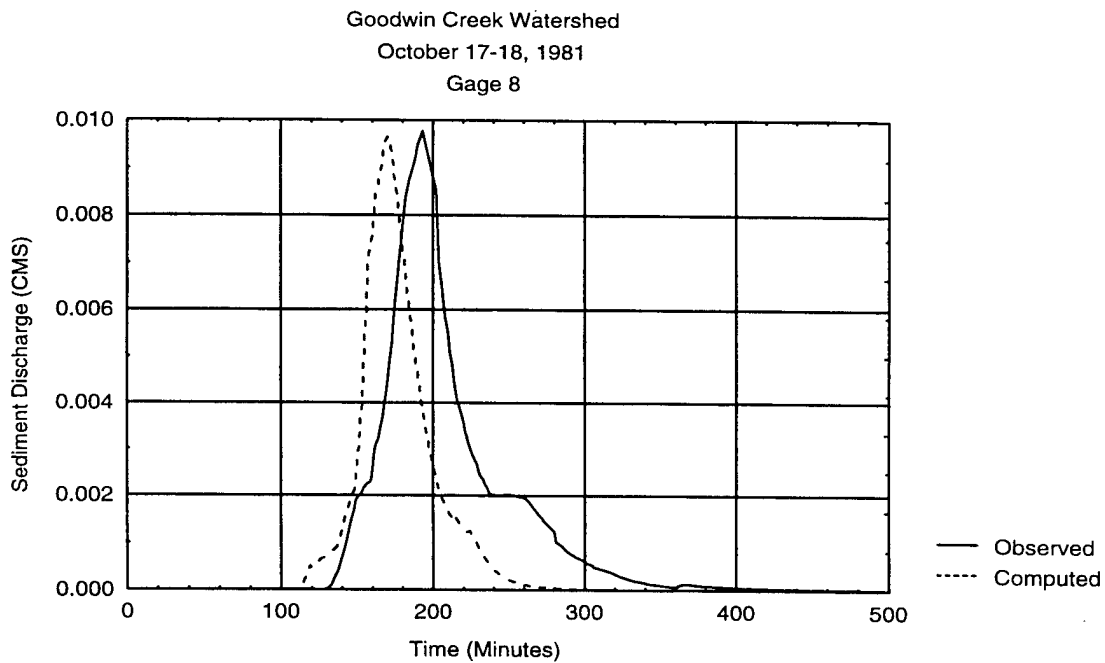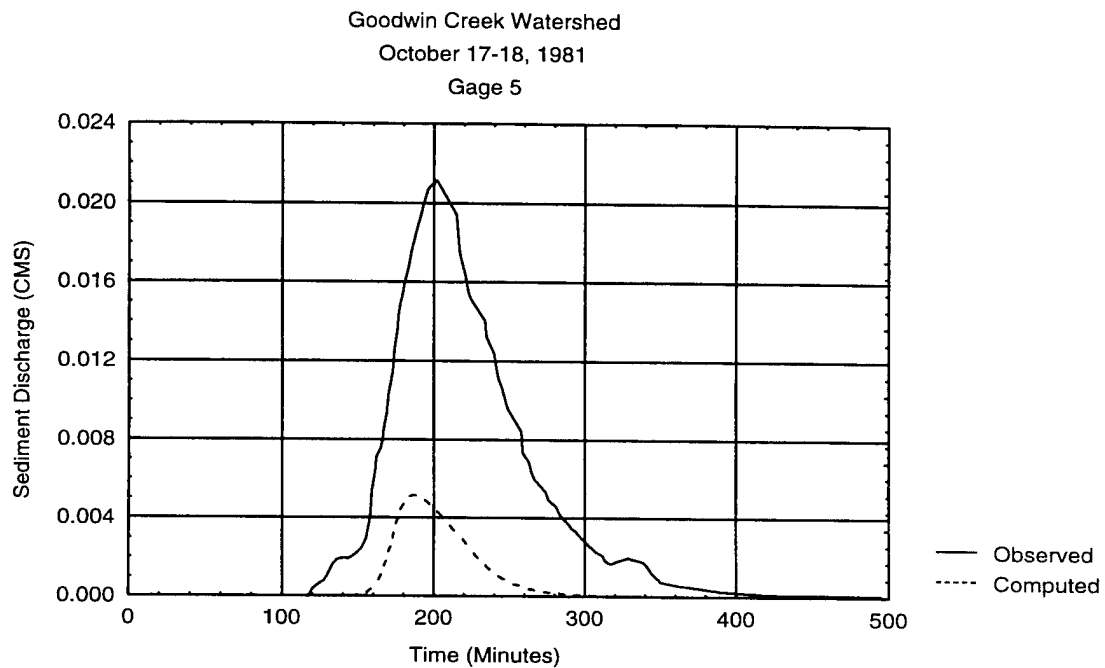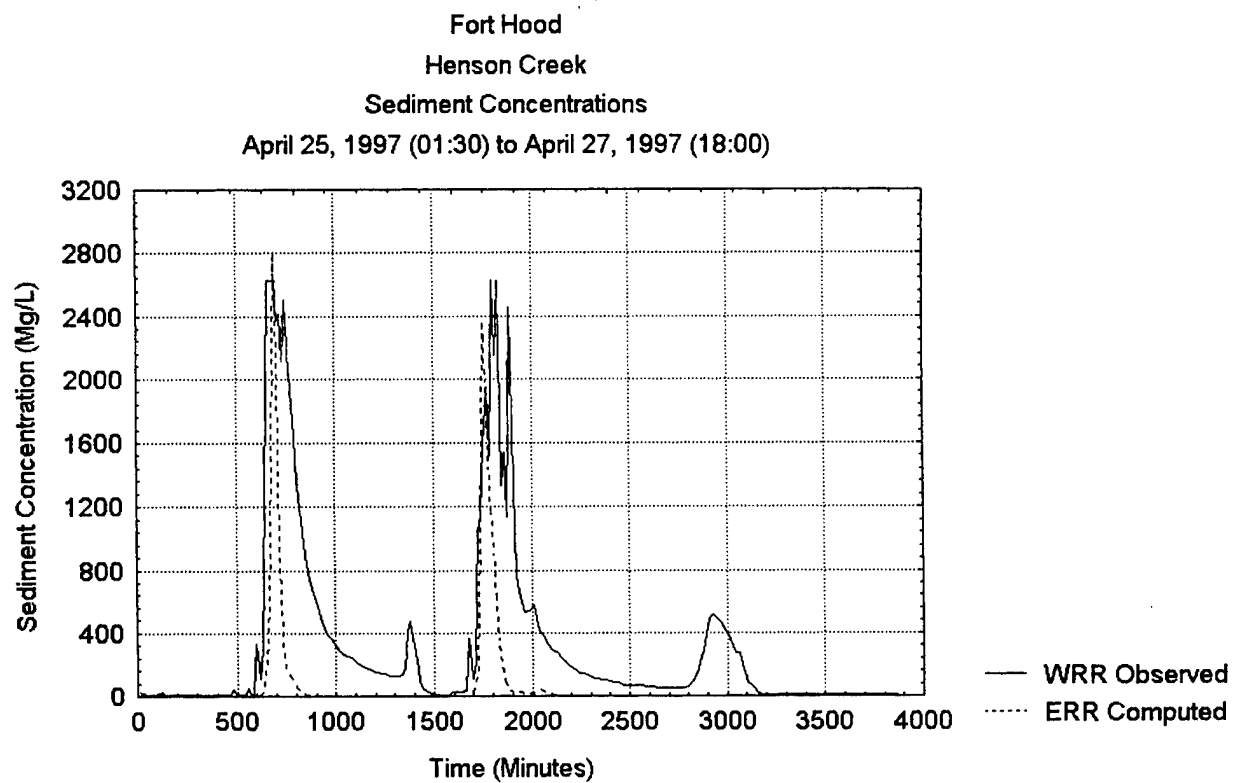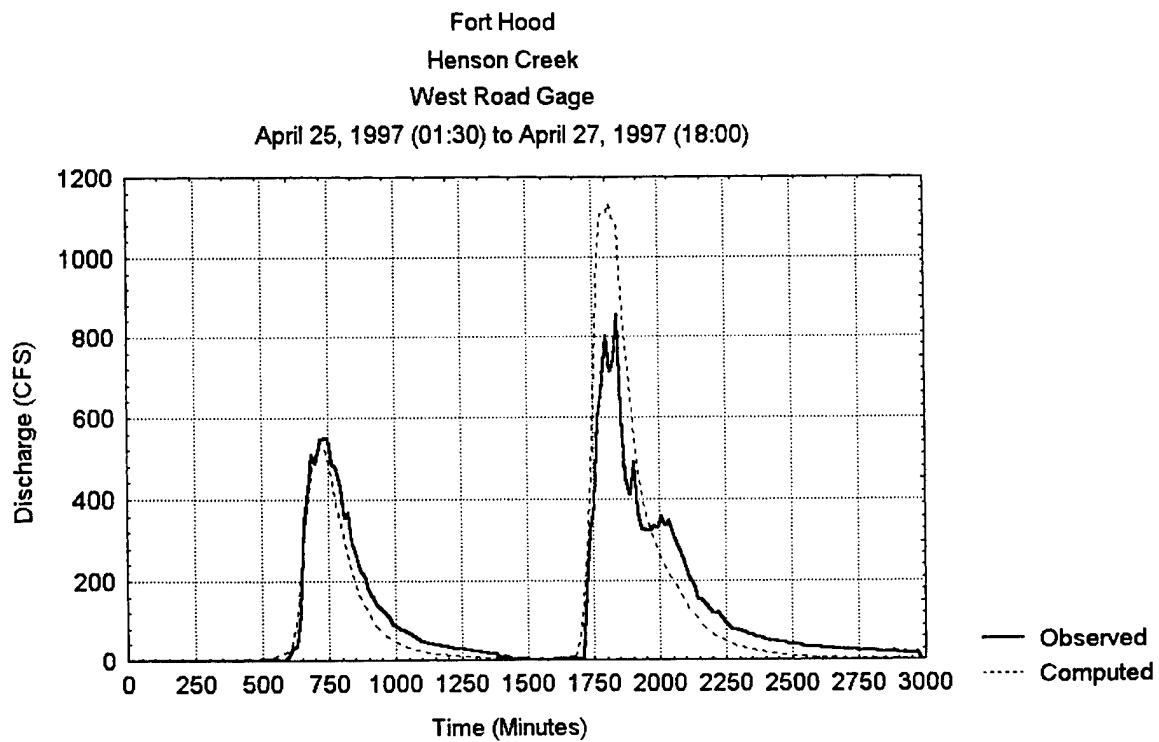
Figure 25. Actual and predicted runoff discharge and sediment concentration for April 25-27, 1997 for the Henson Creek watershed, Fort Hood, Texas.

placed by light deposition within the grassed waterways; net erosion was significantly reduced (Mitas and Mitasova 1998). It is interesting to note, that the land use design obtained by this rather simple computational procedure was potentially at least as effective in reducing erosion and sediment transport as a sustainable land use design proposed and implemented at the farm in 1993. Of importance to the farm manager, the optimized design removed less land from cultivation than the "best management" scenario developed without the aid of the erosion model.


7.7 Simulation of erosion/deposition at the Combat Maneuver Training Center, Germany

In order to compare the results of the enhanced USLE and USPED models, we computed average annual soil loss for the entire installation using a 10m DEM. The rainfall-runoff factor (R) was assumed to be uniform across the installation. The soil erodibility factor (K) varied spatially depending on the soil type. The cover factor (C) was based on the 1997 landcover map at CMTC. Given the absence of agricultural erosion control practices, the conservation practice factor (P) was assumed to be 1, such that it had no effect on the resulting erosion estimates. Figures 26 and 27 illustrate the distribution of soil erosion and deposition as estimated by the USLE and USPED models, respectively. The most obvious difference between the maps is the absence of areas of sediment deposition in the USLE soil loss map. As noted previously, due to the nature of the equation, the USLE is incapable of predicting deposition in its standard format. The spatial distribution of zones of high erosion (>8 t ac^{-1} yr^{-1}) are similar for both models. Quantitatively, the models predict a similar percent of the area experiencing higher levels of net erosion (Table 1). However, the USPED model results suggest that a significant portion of the area predicted by the USLE to experience light to moderate erosion (<8 t ac^{-1} yr^{-1}) is more likely experiencing deposition of sediments. Hence, the USLE will tend to overpredict net erosion.

Table 1. Quantitative comparison of the results of erosion and deposition estimation by the USLE and USPED models at Combat Maneuver Training Center, Hohenfels, Germany.

Erosion/Deposition Estimate	USLE	USPED
>0 t ac^{-1} yr^{-1} deposition	0%	25%
0-4 t ac^{-1} yr^{-1} erosion	79%	64%
4-8 t ac^{-1} yr^{-1} erosion	12%	4%
8-12 t ac^{-1} yr^{-1} erosion	4%	2%
12-16 t ac^{-1} yr^{-1} erosion	2%	1%
>16 t ac^{-1} yr^{-1} erosion	3%	5%

The SIMWE model is computationally more demanding than the USPED model. Accordingly, we applied both models at 10m resolution for single watershed. For the USPED model, we used the same parameters as discussed above. For the SIMWE model, we performed the simulations for the current land cover considering two different conditions: (a) fully saturated soil with all rainfall contributing to surface runoff, and (b) spatially variable rainfall excess with high portion of rainfall infiltrated in the undisturbed areas covered mostly by forest and with reduced infiltration in the disturbed areas. The latter condition involves more complex modeling with spatially variable rainfall excess which had not previously been tested. The
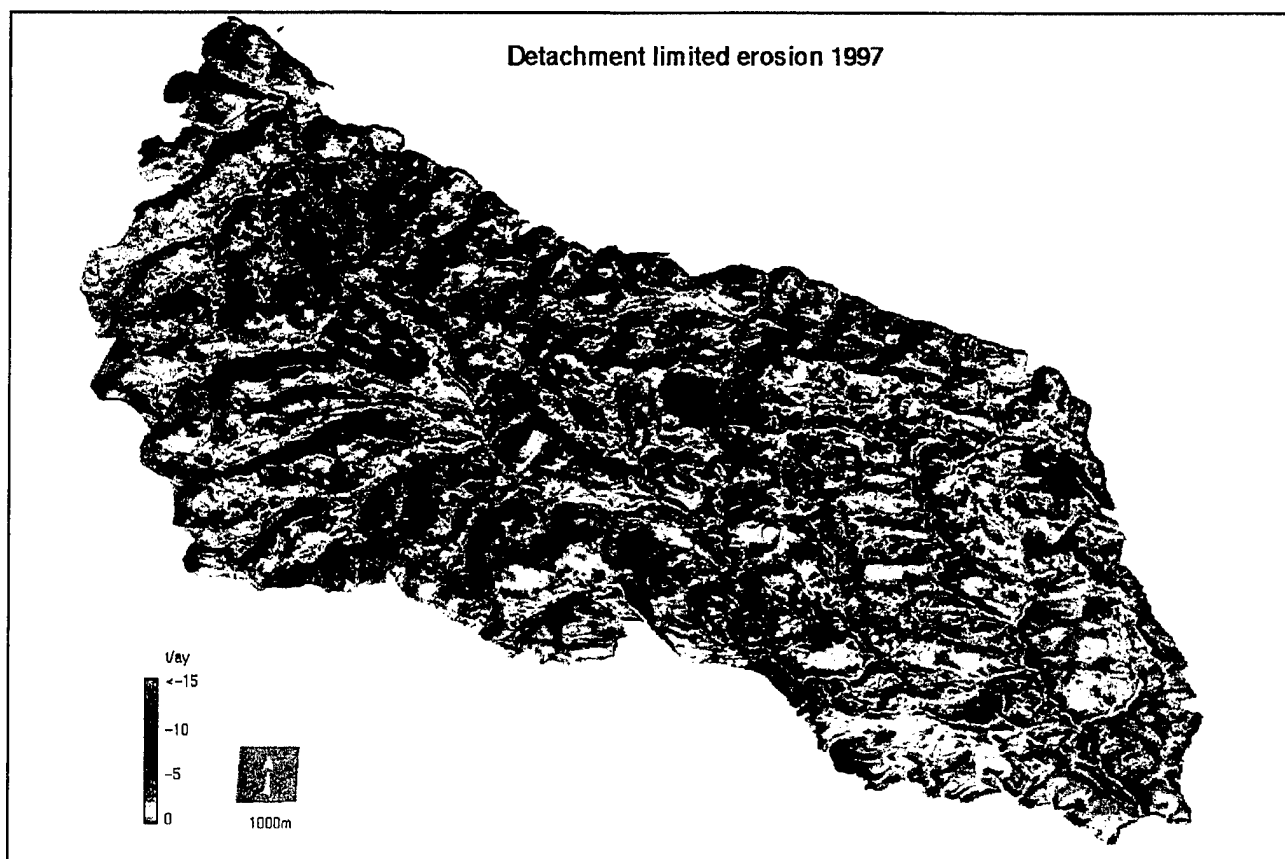
Figure 26. Soil erosion estimated by the enhanced USLE model at the Combat Maneuver Training Center, Germany.
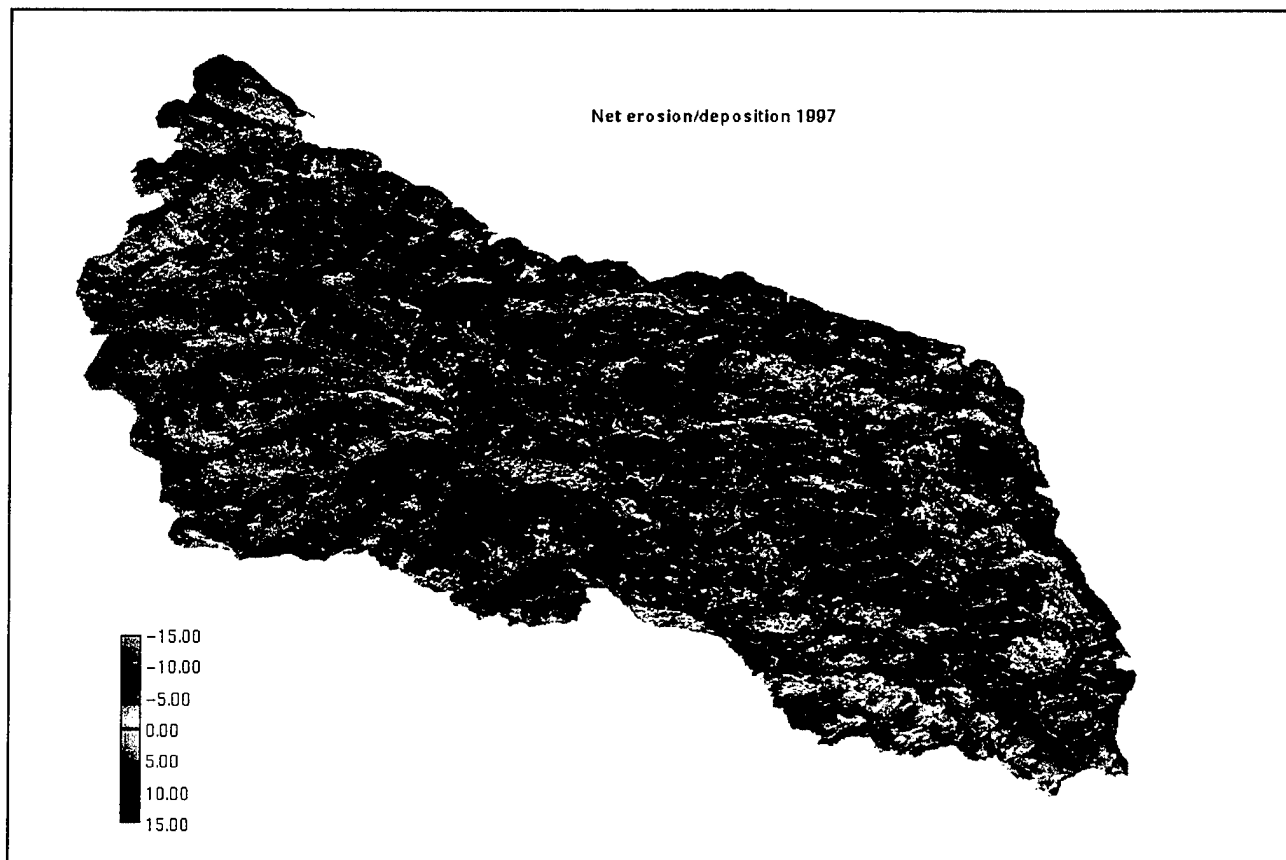
Figure 27. Soil erosion/deposition estimated by the USPED model at the Combat Maneuver Training Center, Germany.

input parameters (elevation gradient, rainfall excess, erodibility, transportability, roughness [Manning's n], critical shear stress) were estimated using the elevation, C-factor and K-factor data, as well as the information about the land cover and soils from the report by Warren and Kowalski 1989. The modeling results for the USPED (Figure 28) and SIMWE (Figure 29) models were similar, with the notable exception that the SIMWE model predicted greater risk for erosion in hollows and centers of valleys and on disturbed ridges. The SIMWE model predicted severe erosion risk over 5.9% of the watershed with uniformly saturated soil conditions. Spatially variable infiltration increased the difference between sediment loads from disturbed and undisturbed areas, with undisturbed areas being much more stable and producing very little sediment compared to disturbed areas (Figure 29). The impact of higher infiltration rates in undisturbed areas reduced the spatial extent of areas with severe erosion to 3.9%.

This application reveals several issues relevant to land management: (a) the importance of erosion prevention measures in areas of concentrated flow and on disturbed ridges, (b) the reduction of actual sediment delivery to streams due to deposition, and (c) the stabilizing effect of high infiltration in undisturbed areas.
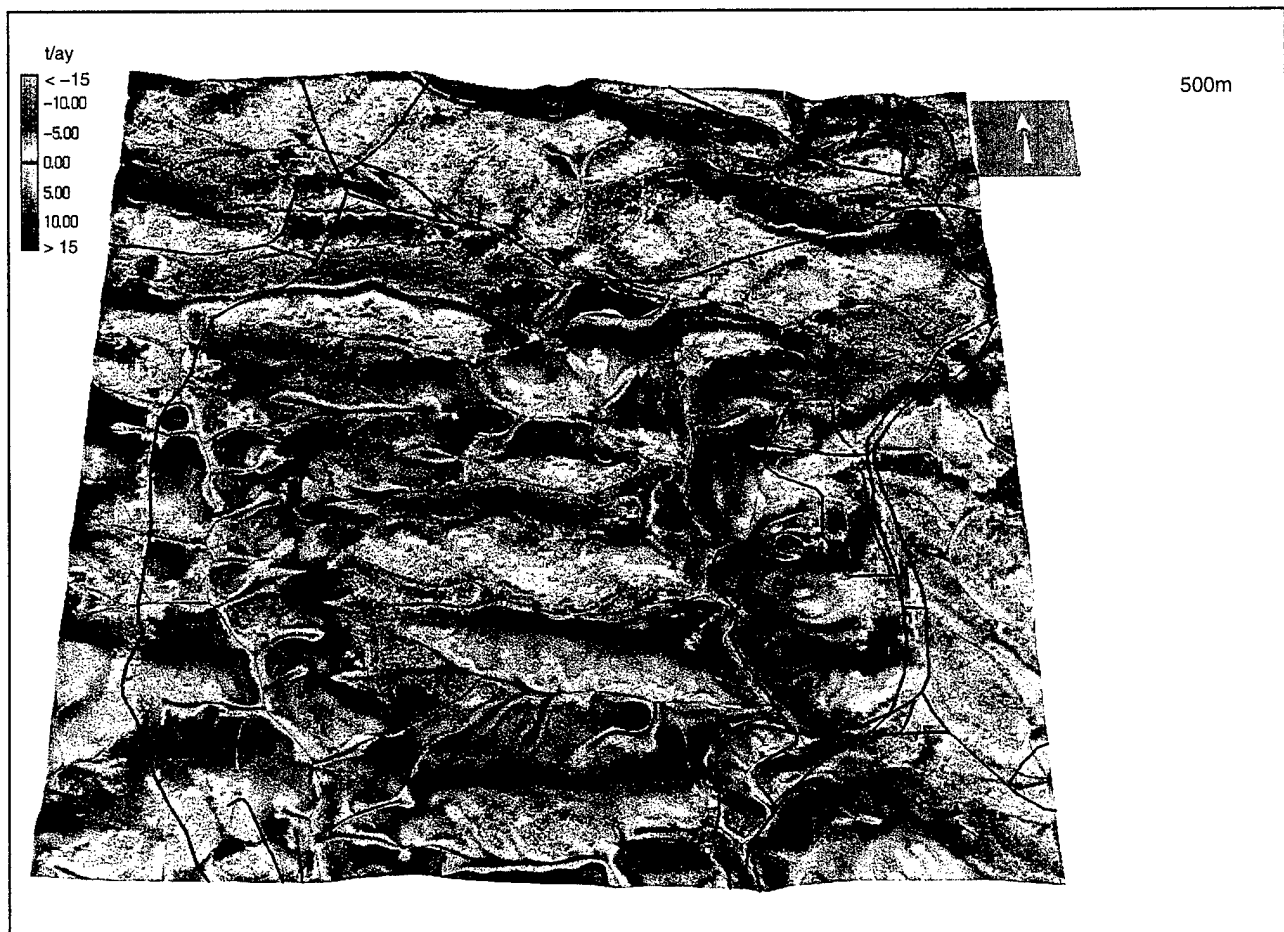
Figure 28. Soil erosion/deposition estimated by the USPED model for an area in the eastern half of the Combat Maneuver Training Center, Germany.
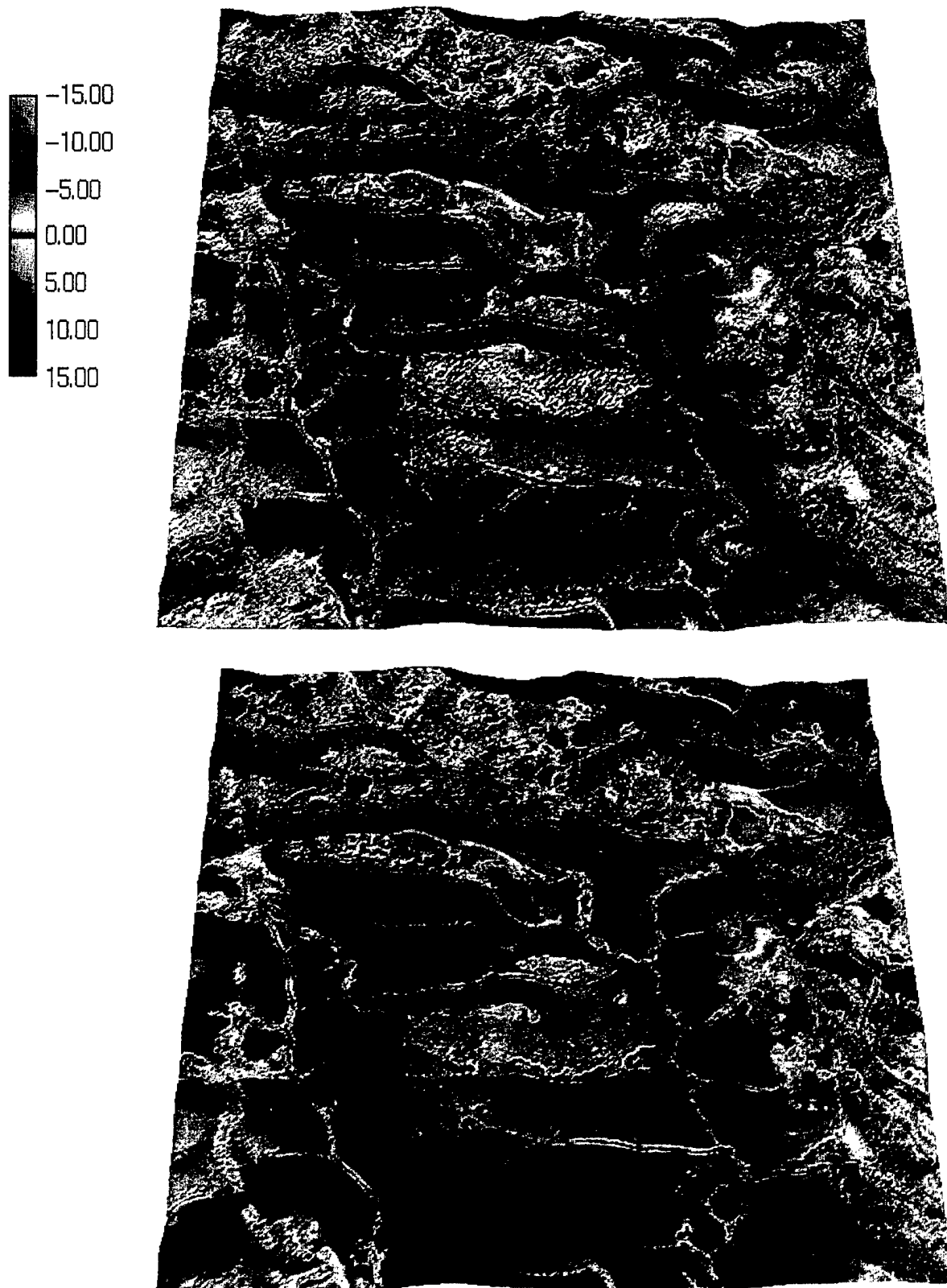
Figure 29. Soil erosion/deposition estimated by the SIMWE model for an area in the eastern half of the Combat Maneuver Training Center, Germany assuming uniformly saturated soil conditions (a) and spatially variable infiltration (b) based on land use patterns.

8. CONCLUSIONS

Integration of topographic analysis and erosion modeling with a GIS provides an environment for effective evaluation of various approaches to erosion/deposition risk assessment for landscape scale applications. This SERDP project has produced three erosion/deposition models that are applicable to a wide range of needs. The USPED model is a significant enhancement to the USLE. It is relatively simple to use and requires the least amount of data. It is a semi-empirical model that produces estimates of long-term average annual erosion and deposition in complex landscapes. The CASC2D-SED is an enhancement to the CASC2D rainfall-runoff model. It is also semi-empirical, but provides estimates of erosion and deposition for individual rainfall events. The SIMWE model is a physically-based model that can provide estimates of erosion, sediment transport and deposition for single rainfall events. Long-term estimates of erosion and deposition can be generated by the CASC2D-SED and SIMWE models by simulating a realistic series of rainfall events. The SIMWE model requires much more data input than the other models. In addition, it is computationally demanding. All three models represent significant improvements to the field of erosion/deposition modeling. For any given application, the choice of the model be determined by the proposed goals and the quantity and quality of data to drive the models.

During the process of developing and applying the USPED, CASC2D-SED and SIMWE models, we have made numerous contributions to the general understanding of erosion and deposition processes as well as the mechanisms to include these and other phenomena in multidimensional modeling. These include:

▶ Curvature of the slope profile along a downhill gradient (profile curvature) and curvature of the slope perpendicular to the downhill gradient (tangential curvature) are both important in determining net erosion and deposition. Profile curvature controls the velocity of runoff, while tangential curvature controls convergence and divergence of flow, thus affecting both the volume and velocity of runoff. Both curvatures must be considered in areas of complex topography. We have introduced methods to calculate both forms of curvature from digital elevation models.

▶ For areas of complex topography, 'upslope contributing area' is a more appropriate parameter than 'slope length' for capturing the influence of accumulated flow of runoff. We have developed a simple, continuous equation for the computation of 'upslope contributing area' in complex terrain.

▶ The Universal Soil Loss Equation predicts soil erosion for situations where erosion is controlled primarily by the ability of flowing water to detach soil particles (detachment limited erosion). Field studies tend to indicate that landscape patterns of erosion/deposition are better related to situations where erosion is limited primarily by the ability of runoff to transport detached soil particles (transport limited erosion). Hence, the results of the USPED model more closely represent real-world conditions.

▶ Soil erodibility or detachability (K_d) is determined largely by soil qualities. It significantly influences the spatial patterns of erosion and deposition, but has only minimal influence on the amount of sediment load in a stream. Hence, the common practice of using of in-stream sediment loads for making land rehabilitation and management decisions is questionable.

▶ Soil transportability (K_t) is determined by soil properties and vegetation. It influences both sediment loads and the spatial patterns of erosion and deposition.

▶ Surface roughness, while having minimal impact on soil erosion, significantly affects both the pattern and magnitude of sediment deposition.

▶ Rainfall excess, or the rainfall intensity minus infiltration rate per unit time, affects the magnitude of erosion and deposition, but has minimal impact on the spatial patterns of erosion and deposition.

▶ The ability of the soil to resist the critical shearing forces of flowing water (critical shear stress) primarily affects the patterns of erosion and deposition. However, on steep slopes and in areas of concentrated flow, the ability of the soil to resist shearing in an upslope position may increase the magnitude of erosion downslope because clean water has a greater potential to suspend sediment than dirty water.

▶ The various parameters of the physically-based SIMWE model do not act independently. It is the interplay of the various parameters that ultimately determines the magnitude and spatial distribution of erosion and deposition.

Based on our applications and case studies, we are able to make the following conclusions and recommendations:

▶ For effective modeling of erosion and deposition in complex terrain, a digital elevation model with a horizontal resolution of 20 m or less and a vertical resolution of less than 1 m is required.

▶ For the purposes of erosion/deposition modeling, areas of flat terrain are more susceptible to noise and systematic errors in elevation data than steeper terrain.

▶ New-generation erosion/deposition models can be valuable planning tools to effectively predict the consequences of proposed land-use changes.

▶ New-generation erosion/deposition models can be used to effectively plan erosion and sediment control practices.

In support of the new generation of erosion and deposition models we have developed a number of geographic information system tools for data processing and graphic display.

9. REFERENCES

Abramowitz, M. and I.A. Stegun. 1964. Handbook of Mathematical Functions. Dover, New York, NY

Andrulis Research Corporation. 1994. U.S. Army research & development requirements. Arlington, VA

Auerswald, K., A. Eicher, J. Filser, A. Kammerer, M. Kainz, R. Rackwitz, J. Schulein, H. Wommer, S. Weigland and K. Weinfurtner. 1996. Development and implementation of soil conservation strategies for sustainable land use - the Scheyern project of the FAM. Pages 25-68. In: H. Stanjek (ed), Tour Guide, Development and Implementation of Soil Conservation Strategies for Sustainable Land Use, International Congress of the European Society for Soil Conservation. Technische Universität München, Freising-Weihenstephan, Germany

Bennet, J.P. 1974. Concepts of mathematical modeling of sediment yield. Water Resources Research 10:485-496

Brown, W.M. and D.P. Gerdes. 1992. SG3d - supporting information. U.S. Army Corps of Engineers, Construction Engineering Research Laboratories, Champaign, Illinois. http://www.cecer.army.mil/grass/viz/sg3d.html

Brown, W.M. and M. Astley. 1995. NVIZ tutorial. Geographic Modeling and Systems Laboratory, University of Illinois at Urbana-Champaign

Brown, W.M., M. Astley, T. Baker and H. Mitasova. 1995. GRASS as an integrated GIS and visualization environment for spatio-temporal modeling. Pages 89-99. In: D.J. Peuquet (ed), Proceedings of the Auto Carto 12. ACSM/ ASPRS, Charlotte, NC

Busacca, A.J., C.A. Cook and D.J. Mulla. 1993. Comparing landscape scale estimation of soil erosion in the Palouse using Cs-137 and RUSLE. Journal of Soil and Water Conservation 48:361-67

Desmet, P.J. and G. Govers. 1995. GIS-based simulation of erosion and deposition patterns in an agricultural landscape: a comparison of model results with soil map information. Catena 25:389-401

Desmet, P.J. and G. Govers. 1996. A GIS procedure for automatically calculating the USLE LS factor on topographically complex landscape units. Journal of Soil and Water Conservation 51:427-433

Dikau, R. 1990. The application of a digital relief model to landform analysis in geomorphology. Pages 51-77. In: J. Raper (ed), Three dimensional applications in Geographic Information Systems. Taylor & Francis, London

Ehlschlaeger, C. and M. Goodchild. 1994. Uncertainty in spatial data: defining, visualizing, and managing data errors. Pages 246-253. In: Proceedings, GIS/LIS'94, Phoenix, AZ

Fairfield, J. and P. Leymarie. 1991. Drainage networks from grid digital elevation models. Water Resources Research 27:709-717

Finkner, S.C., M.A. Nearing, G.R. Foster and J.E. Gilley. 1989. A simplified equation for modeling sediment transport capacity. Transactions of the American Society of Agricultural Engineers 32:1545-1550

Flanagan, D.C. and M.A. Nearing (eds), 1995. USDA-Water Erosion Prediction Project. National Soil Erosion Research Laboratory Report No. 10. U.S. Department of Agriculture, Agricultural Research Service, Lafayette, IN

Foster, G.R. 1994. Comment on "Length-slope factors for the Revised Universal Soil Loss Equation: Simplified method of estimation." Journal of Soil and Water Conservation 49:171-173

Foster, G.R. and L.D. Meyer. 1972. A closed-form erosion equation for upland areas. Pages 12.1 - 12.19. In: H.W. Shen (ed), Sedimentation: Symposium to Honor Prof. H.A. Einstein. Colorado State University, Ft. Collins, CO

H.W. Shen (ed), Sedimentation: Symposium to Honor Prof. H.A. Einstein.Colorado State University, Ft. Collins, CO

Foster, G.R. and W.H. Wischmeier. 1974. Evaluating irregular slopes for soil loss prediction. Transactions of the American Society of Agricultural Engineers 12:305-309

Freeman, T.G. 1991. Calculating catchment area with divergent flow based on regular grid. Computers and Geosciences 17:413-422

Franke, R. 1982. Smooth interpolation of scattered data by local thin plate splines. Computers and Mathematics with Applications 8:273-281

Gardiner, C.W. 1985. Handbook of Stochastic Methods for Physics, Chemistry, and the Natural Sciences. Springer, Berlin.

Govers, G. 1991. Rill erosion on arable land in central Belgium: rates, controls and predictability. Catena 18:133-155

Govindaraju, R.S. and M.L. Kavvas. 1991. Modeling the erosion process over steep slopes: approximate analytical solutions. Journal of Hydrology 127:279-305

Guy, B. T., Rudra, R. P. Rudra and W. T. Dickinson 1991, Process-oriented research on soil erosion and overland flow. Pages 225-242. In: A.J. Parsons and A.D. Abrahams (eds), Overland Flow Hydraulics and Mechanics. Chapman and Hall, New York

Haan, C.T., B.J. Barfield and J.C. Hayes. 1994. Design Hydrology and Sedimentology for Small Catchments. Academic Press.

Hairsine, P.B. and C.W. Rose. 1992. Modeling water erosion due to overland flow using physical principles 1. Sheet flow. Water Resources Research 28:237-243

Hammond, B.L., W.A. Lester, Jr. and P.J. Reynolds. 1994. Monte Carlo Methods in Ab Initio Quantum Chemistry. World Scientific, Singapore

Hutchinson, M.F. 1989. A new procedure for gridding elevation and stream line data with automatic removal of spurious pits. Journal of Hydrology 106:211-232

Jenson, S.K. and J.O. Domingue. 1988. Extracting topographic structure from digital elevation data for geographic information system analysis. Photogrammetric Engineering and Remote Sensing 54:1593-1600

Julien, P.Y. and D.B. Simons. 1985. Sediment transport capacity of overland flow. Transactions of the American Society of Agricultural Engineers 28:755-762

Julien, P.Y., B. Saghafian and F.L. Ogden. 1995. Raster-based hydrologic modeling of spatially varied surface runoff. Water Resources Bulletin 31:523-536

Kilinc, M. and E.V. Richardson. 1973. Mechanics of soil erosion from overland flow generated by simulated rainfall. Hydrology Papers No. 63, Colorado State University.

Krcho, J. 1991. Georelief as a subsystem of landscape and the influence of morphometric parameters of georelief on spatial differentiation of landscape-ecological processes. Ecology /CSFR/10:115-157

Lettenmaier, D.P. and E.F. Wood. 1992. Hydrologic forecasting. Pages 26.1-26.30. In: D.R. Maidment (ed), Handbook of Hydrology. McGraw-Hill, NY

McCauley, J.D. and B.A. Engel. 1995. Approximation of noisy bivariate traverse data: tests of splines, natural neighbor, kriging and Shephard's method. Department of Agricultural Engineering, Purdue University. West Lafayette, IN

Mitas, L. 1996. Electronic structure by Quantum Monte Carlo: atoms, molecules and solids. Computer Physics Communications 97:107-117

Mitas, L. and H. Mitasova. 1988. General variational approach to the interpolation problem. Computers and Mathematics with Applications 16:983-992

Mitas, L. and H. Mitasova. 1998. Distributed soil erosion simulation for effective erosion prevention. Water Resources Research 34:505-516

Mitas, L. and H. Mitasova. 1999. Spatial Interpolation. Pages 481-492. In: P. Longley, M.F. Goodchild, D.J. Maguire and D.W. Rhind (eds.), Geographical Information Systems: Principles, Techniques, Management and Applications. GeoInformation International, Wiley Press

Mitas, L., W.M. Brown and H. Mitasova. 1999. Role of dynamic cartography in simulations of landscape processes based on multi-variate fields. Computers and Geosciences 23:437-446

Mitasova, H. and L. Mitas. 1993. Interpolation by regularized spline with tension: I. Theory and implementation. Mathematical Geology 25:641-655

Mitasova, H. and J. Hofierka. 1993. Interpolation by regularized spline with tension: II. Application to terrain modeling and surface geometry analysis. Mathematical Geology 25:657-669

Mitasova, H., W.M. Brown and J. Hofierka. 1994. Multidimensional dynamic cartography. Kartograficke listy 2:37-50

Mitasova, H., L. Mitas, W.M. Brown, D.P. Gerdes and I. Kosinovsky. 1995. Modeling spatially and temporally distributed phenomena: New methods and tools for GRASS GIS. International Journal of GIS 9:443-446.

Mitasova, H., J. Hofierka, M. Zlocha and R.L. Iverson. 1996. Modeling topographic potential for erosion and deposition using GIS. International Journal of Geographical Information Science 10:629-641

Moore, I.D. and G.J. Burch. 1986. Physical basis of the length-slope factor in the Universal Soil Loss Equation. Soil Science Society America Journal 50:1294-1298

Moore, I.D., R.B. Grayson and A.R. Ladson. 1991. Digital terrain modeling: a review of hydrological, geomorphological and biological applications. Hydrological Processes 5:3-30

Moore, I.D. and J.P. Wilson. 1992. Length-slope factors for the Revised Universal Soil Loss Equation: Simplified method of estimation. Journal of Soil and Water Conservation 47:423-428

Nearing, M.A., L.D. Norton, D.A. Bulgakov, G.A. Larionov, L.T. West and K.M. Dontsova. 1997. Hydraulics and erosion in eroding rills. Water Resources Research 33:865-876

Quine, T.A., P.J.J. Desmet, G. Govers, K. Vandaele and D.E. Walling. 1994. A comparison of the roles of tillage and water erosion in landform development and sediment export on agricultural land near Leuven, Belgium. Pages 77-86. In: L.J. Olive, R.J. Loughran and J.A. Kesby (eds), Variability in Stream Erosion and Sediment Transport. IAHS Publication No. 224

Renard, G.K., G.R. Foster, G.A. Weesies, D.K. McCool and D.C. Yoder. 1997. Predicting soil erosion by water: A guide to conservation planning with the Revised Universal Soil Loss Equation (RUSLE). U.S. Department of Agriculture, Agriculture Handbook No. 703

Renard, G.K., G.R. Foster, G.A. Weesies and J.P. Porter. 1991. RUSLE - Revised Universal Soil Loss Equation. Journal of Soil and Water Conservation 46:30-33

Rohling, R.N., A.H. Gee and L. Berman. 1998. Radial basis function interpolation for 3D ultrasound. Cambridge University Engineering Department Technical Report 327

Rouhi, A. and J. Wright. 1995. Spectral implementation of a new operator splitting method for solving partial differential equations. Computers in Physics 9:554-563

Sutherland, R.A. 1991. Caesium-137 and sediment budgeting within a partially closed drainage basin. Zeitschrift fur Geomorphologie N.F. 35:47-63

Talmi, A. and G. Gilat. 1977. Method for smooth approximation of data. Journal of Computational Physics 23:93-123

Wahba, G. 1990. Spline models for observational data. CNMS-NSF Regional Conference Series in Applied Mathematics 59, SIAM, Philadelphia, PA

Warren, S.D. and D.G. Kowalski. 1989. Land condition-trend analysis at Hohenfels Training Area, Germany 1986-1989. Report to Hohenfels Training Area. US Army Construction Engineering Research Laboratory, Champaign, IL.

Wischmeier, W.H. and D.D. Smith. 1978. Predicting rainfall erosion losses, a guide to conservation planning. Agriculture Handbook No. 537, US Department of Agriculture, Washington D.C.

Zevenbergen, L.W. and C.R. Thorne. 1987. Quantitative analysis of surface topography. Earth Surface Processes and Landforms 12:47-56

Zhang, W. and D.R. Montgomery. 1994. Digital elevation model grid size, landscape representation and hydrologic simulations. Water Resources Research 30:1019-1028

APPENDIX A - Publications

The following is a list of publications and presentations have all resulted from this SERDP project.

Peer reviewed publications

Mitas, L. and H. Mitasova. 1998. Distributed soil erosion simulation for effective erosion prevention. Water Resources Research 34:505-516.

Mitas L., W.M. Brown and H. Mitasova. 1997. Role of dynamic cartography in simulations of landscape processes based on multi-variate fields. Computers and Geosciences 23:437-446. (http://www.elsevier.nl/inca/homepage/miss/cageo/mitas/mitas.htm)

Mitasova, H., J. Hofierka, M. Zlocha and R. L. Iverson. 1997. Reply to Comment by Desmet and Govers. International Journal of Geographical Information Systems 11:611-618.

Mitasova, H., J. Hofierka, M. Zlocha and R. L. Iverson. 1996. Modeling topographic potential for erosion and deposition using GIS. International Journal of Geographical Information Systems 10:629-641.

Mitasova, H., L. Mitas, W.M. Brown, D.P. Gerdes and I. Kosinovsky. 1995. Modeling spatially and temporally distributed phenomena: New methods and tools for GRASS GIS. International Journal of Geographical Information Systems 9:443-446.

Saghafian, B., P. Y. Julien and F. L. Ogden. 1995. Similarity in catchment response 1. Stationary rainstorms. Water Resources Research 31:1533-1541.

Julien, P.Y., B. Saghafian and F.L. Ogden. 1995. Raster-based hydrologic modeling for spatially-varied surface runoff. Water Resources Bulletin 31:523-536.

Mitasova, H., W.M. Brown and J. Hofierka. 1994. Multidimensional dynamic cartography. Kartograficke listy (Cartographic Letters) 2:37-50.

Chapters in Books:

Mitas, L. and H. Mitasova. 1998. Multi-scale Green's function Monte Carlo approach to erosion modeling and its application to land-use optimization. Pages 81-90. In: W. Summer, E. Klaghofer and W. Zhang (eds), Modeling Soil Erosion, Sediment Transport and Closely Related Hydrological Processes. IAHS Publication No. 249.

Mitas, L. and H. Mitasova. 1999. Spatial Interpolation. Pages 481-492. In: P. Longley, M.F. Goodchild, D.J. Maguire and D.W. Rhind (eds), Geographical Information Systems: Principles, Techniques, Management and Applications. Geo Information International, Wiley Press.

Saghafian, B. 1996. Implementation of a Distributed Hydrologic Model within GRASS. Pages 205-208. In: M.F Goodchild, L.T. Steyaert and B.O. Parks (eds), GIS and Environmental Modeling: Progress and Research Issues. GIS World, Inc., Ft. Collins, CO.

Mitasova, H., L. Mitas, W.M. Brown, D.P. Gerdes, I. Kosinovsky and T. Baker. 1996. Modeling spatially and temporally distributed phenomena: New methods and tools for Open GIS. Pages 345-352. In: M.F. Goodchild, L.T. Steyaert and B.O. Parks (eds), GIS and Environmental Modeling: Progress and Research Issues, GIS World, Inc., Ft. Collins, CO.

Proceedings, reports and other publications:

Warren, S.D. 1998. Digital terrain modeling and distributed soil erosion simulation/measurement for minimizing environmental impacts of military training. US Army Construction Engineering Research Laboratory Interim Report 99/12. Champaign, IL.

Mitas, L. and H. Mitasova. 1997. Green's function Monte Carlo approach to erosion modeling in complex terrain. Paper 973066. American Society of Agricultural Engineers annual meeting. St. Joseph, MI.

Brown, W.M., H. Mitasova and L. Mitas. 1997. Design, development and enhancement of dynamic multidimensional tools in a fully integrated fashion with the GRASS GIS. Report to US Army Construction Engineering Research Laboratory. University of Illinois, Urbana-Champaign, IL.

Mitasova, H., W M Brown, L. Mitas and S.D. Warren. 1997. Multi-dimensional GIS environment for simulation and analysis of landscape processes. Paper 973034. American Society of Agricultural Engineers annual meeting. St. Joseph, MI

Mitasova, H., L. Mitas, W.M. Brown and D. Johnston. 1996. Multidimensional soil erosion/ deposition modeling. III. Process based erosion simulation. Report to US Army Construction Engineering Research Laboratory. University of Illinois, Urbana-Champaign, IL.

Mitasova, H., W.M. Brown, D. Johnston and L. Mitas. 1996. GIS tools for erosion/deposition modeling and multidimensional visualization. II. Unit stream power-based erosion/deposition modeling and enhanced dynamic visualization. Report to US Army Construction Engineering Research Laboratory. University of Illinois, Urbana-Champaign, IL.

Mitas, L., H. Mitasova, W.M. Brown and M. Astley. 1996. Interacting fields approach for evolving spatial phenomena: application to erosion simulation for optimized land use. In: M.F. Goodchild, L.T. Steyaert and B.O. Parks (eds), Proceedings of the III International Conference on Integration of Environmental Modeling and GIS. Santa Fe, NM. National Center for Geographic Information and Analysis, Santa Barbara, CA. Available on CDROM and WWW.

Mitasova, H., W.M. Brown, D. Johnston, B. Saghafian, L. Mitas and M. Astley. 1995. GIS tools for erosion/ deposition modeling and multidimensional visualization. Part I: Interpolation, rainfall-runoff, visualization. Report to US Army Construction Engineering Research Laboratory. University of Illinois, Urbana-Champaign, IL.

Brown, W.M., M. Astley, T. Baker and H. Mitasova. 1995. GRASS as an integrated GIS and visualization environment for spatio-temporal modeling. Pages 89-99. In: Proc. Auto-Carto XII, February 12 - March 2, Charlotte, NC. American Congress on Surveying and Mapping and American Society for Photogrammetry and Remote Sensing.

Professional presentations :

Warren, S.D., M.R. Jourdan, R. Larson, H. Mitasova, L. Mitas, W.M. Brown and B.E. Johnson. 1998. Soil erosion simulation for minimizing environmental impacts from military training. Partners in Environmental Technology Technical Symposium and Workshop, 1-3 December, Arlington, VA. Strategic Environmental Research and Development Program and Environmental Security Technology Certification Program.

Johnson, B.E., P.Y. Julien and C.C. Watson. 1998. Development of a storm-event based two-dimensional upland erosion model (CASC2D-SED). First Federal Interagency Hydrologic Modeling Conference, April 21 - April 25, Las Vegas, NV.

Warren, S.D., H. Mitasova and L. Mitas. 1998. Advanced erosion and sediment modeling for land use optimization. 51st Annual meeting of the Society for Range Management, Feb 8-12, Guadalajara, Mexico.

Mitas, L., H. Mitasova and W.M. Brown. 1997. Multi-variate fields and process based landscape simulations: Application to erosion modeling and land use optimization. Illinois GIS Association Conference, April 15-16, Champaign, IL.

Warren, S.D. and W.D. Goran. 1997. Erosion and sediment modeling. Department of Defense Environmental Security Modeling and Simulation Technical Workshop, Mar 19, Washington, D.C.

Mitas, L., H. Mitasova and W.M. Brown. 1996. Multi-variate fields and process based landscape simulations: Application to erosion modeling and land use optimization. Geographic Modeling Systems (GMS) Lab and USACERL GIS Colloquium Series, December 18, Champaign, IL.

Mitas,L., H. Mitasova, W. Brown and M. Astley. 1996. Interacting fields approach for evolving spatial phenomena: application to erosion simulation for optimized land use. Third International Conference on Integration of Environmental Modeling and GIS, January 21-25, Santa Fe, NM.

Mitas, L., H. Mitasova and S.D. Warren. 1996. Distributed, process-based erosion simulations for optimization of land rehabilitation measures. 5th Annual Land Rehabilitation and Maintenance Workshop, August 26-29, LaCrosse, WI.

Warren, S.D., K. Auerswald, H. Mitasova and L. Mitas. 1996. Advanced tools for predicting soil erosion and deposition. Second International Congress of the European Society of Soil Conservation, Sep 1-7, Munich, Germany.

Warren, S.D., L. Mitas and H. Mitasova. 1996. Terrain modeling and soil erosion simulation. Second Annual Strategic Environmental Research and Development Program Symposium, Nov 20-22, Vienna, VA.

Mitasova, H., L. Mitas and W.M. Brown. 1995. Digital elevation modeling and soil erosion simulation. First Annual Strategic Environmental Research and Development Program Symposium, April 12-14, Washington D.C.

Mitasova, H., L. Mitas, W.M. Brown, S.D. Warren and K. Auerswald. 1995. Multidimensional GIS tools for spatially distributed phenomena: Application to soil erosion prediction. American Society of Agricultural Engineers Annual Meeting, June 18-23, Chicago, IL.

Brown,W.M., M. Astley, T. Baker and H. Mitasova. 1995. GRASS as an integrated GIS and visualization environment for spatio-temporal modeling. Auto-Carto 12, February 27 - March 2, Charlotte, NC. American Congress on Surveying and Mapping and American Society for Photogrammetry and Remote Sensing.

Saghafian, B. and F. L. Ogden. 1994. Two-dimensional hydrologic modeling CASC2D workshop. Memphis State University, Memphis, TN. June 9-10.

Ogden, F.L., B. Saghafian and W. F. Krajewski. 1994. GIS-based channel extraction and smoothing algorithm for distributed hydrologic modeling. Annual American Society of Civil Engineers National Conference on Hydraulic Engineering, Buffalo, NY.

Kosinovsky, I., H. Mitasova and D.P. Gerdes. 1994. Library for Multidimensional Surface Modeling and Analysis in GRASS. 9th Annual GRASS/GIS Conference, Reston, VA.

Brown, W.M. 1994. Multi-Dimensional Visualization using GRASS. 9th Annual GRASS/GIS Conference, Reston, VA.

Mitasova, H., L. Mitas and I. Kosinovsky. 1994. Surface modeling. USDA, Soil Conservation Service, Midwest GIS meeting, Champaign, IL.

Mitasova, H. 1994. Surface modeling: Analysis and visualization with applications to environmental modeling. Lectures at the National Center for Geographic Information and Analysis, March 9-11, Santa Barbara, CA.

Trade journal articles:

Mitasova, H., L. Mitas, W.M. Brown and S.D. Warren. 1997. GIS environment for simulation and analysis of landscape processes. Mapnotes 15:7-14. Illinois GIS Association.

APPENDIX B - Manuals and Tutorials

The following GRASS GIS tools were developed during the course of this project. Please use the following web address to access the manuals and tutorials:

http://www2.gis.uiuc.edu:2280/modviz/reports/cerl98/aman98.html

1. **gsurf** library overview http://www2.gis.uiuc.edu:2280/modviz/reports/cerl98/gsurf/gsurf.html

2. **gsurf** library prototypes and selected include files

    1.1. public function prototypes http://www2.gis.uiuc.edu:2280/modviz/reports/cerl98/gsurf/protos.html

    1.2. public include file gsurf.h http://www2.gis.uiuc.edu:2280/modviz/reports/cerl98/gsurf/gsurf_h.html

    1.3. public include file keyframe.h http://www2.gis.uiuc.edu:2280/modviz/reports/cerl98/gsurf/keyframe_h.html

    1.4. public color packing utility macros rgbpack.h http://www2.gis.uiuc.edu:2280/modviz/reports/cerl98/gsurf/rgbpack_h.html

    1.5. private types and defines gstypes.h http://www2.gis.uiuc.edu:2280/modviz/reports/cerl98/gsurf/gstypes_h.html

    1.6. private utilities gsget.h http://www2.gis.uiuc.edu:2280/modviz/reports/cerl98/gsurf/gsget_h.html

3. **nviz** tutorial http://www2.gis.uiuc.edu:2280/modviz/reports/cerl98/nviz_tut.html

4. **sg3d** updated features http://www2.gis.uiuc.edu:2280/modviz/reports/cerl98/sg3d42.html

5. **xganim** user's manual page http://www2.gis.uiuc.edu:2280/modviz/reports/cerl98/xganim_man.html

6. **r.out.mpeg** user's manual page http://www2.gis.uiuc.edu:2280/modviz/reports/cerl98/r.out.mpegman.html

7. **d.siter** user's manual page http://www2.gis.uiuc.edu:2280/modviz/reports/cerl98/dsiter.html

8. **d.sites.qual** user's manual page http://www2.gis.uiuc.edu:2280/modviz/reports/cerl98/dsites_qual.html

9. **s.info** user's manual page http://www2.gis.uiuc.edu:2280/modviz/reports/cerl98/sinfo.html

10. **p.vrml** user's manual page http://www2.gis.uiuc.edu:2280/modviz/reports/cerl98/pvrml.html

11. **r3.mkdspf** user's manual page http://www2.gis.uiuc.edu:2280/modviz/reports/cerl98/r3.mkdspf.html

12. **r3.showdspf** user's manual page http://www2.gis.uiuc.edu:2280/modviz/reports/cerl98/r3.showdspf.html

13. **s.surf.rst** user's manual page http://www2.gis.uiuc.edu:2280/modviz/reports/cerl98/ssurfrst.html

14. **r.flow** user's manual page http://www2.gis.uiuc.edu:2280/modviz/reports/cerl98/rflow42.html

15. **r.slope.aspect** user's manual page http://www2.gis.uiuc.edu:2280/modviz/reports/cerl98/rslopeasp.html